Method for analysis of sleep parameters based on ultra-wideband communication channel impulse response measurement

Čuljak, Ivana

University of Zagreb
FACULTY OF ELECTRICAL ENGINEERING AND COMPUTING

Ivana Čuljak

METHOD FOR ANALYSIS OF SLEEP PARAMETERS BASED ON ULTRA-WIDEBAND COMMUNICATION CHANNEL IMPULSE RESPONSE MEASUREMENT

DOCTORAL THESIS

Zagreb, 2023

University of Zagreb
FACULTY OF ELECTRICAL ENGINEERING AND COMPUTING

Ivana Čuljak

METHOD FOR ANALYSIS OF SLEEP PARAMETERS BASED ON ULTRA-WIDEBAND COMMUNICATION CHANNEL IMPULSE RESPONSE MEASUREMENT

DOCTORAL THESIS

Supervisor: Professor Mario Cifrek, Ph.D.

Zagreb, 2023

Sveučilište u Zagrebu
FAKULTET ELEKTROTEHNIKE I RAČUNARSTVA

Ivana Čuljak

METODA ANALIZE PARAMETARA SPAVANJA ZASNOVANA NA MJERENJU IMPULSNOGA ODZIVA ULTRAŠIROKOPOJASNOGA KOMUNIKACIJSKOG KANALA

DOKTORSKI RAD

Mentor: prof. dr. sc. Mario Cifrek

Zagreb, 2023.

This doctoral thesis has been done at the University of Zagreb, Faculty of Electrical Engineering and Computing, Department of Electronic Systems and Information Processing.

Supervisor: Professor Mario Cifrek, Ph.D.

The doctoral thesis contains: 177 pages

Doctoral thesis number: _____

About the supervisor

Mario Cifrek was born in Varaždin in 1964. He received Dipl. Eng., M.Sc. and Ph.D. degrees in electrical engineering from the University of Zagreb, Faculty of Electrical Engineering and Computing (FER), Zagreb, Croatia, in 1987, 1992, and 1997, respectively.

Since December 1987 he has worked in the Department of Electronic Systems and Information Processing, FER. In December 2012 he was promoted to Tenured Full Professor. During his work at FER, he participated in numerous Faculty working committees and served two terms as Vice Dean for Education from 2006 to 2010. From 2013 to 2017, he was a member of the Accreditation Council of the Agency for Science and Higher Education, and since 2017 he has been a member of the Committee of the Accreditation Council for Follow-up within Reaccreditation Processes. Since 2013, he has been a member of the Scientific Field Committee for the Field of Electrical Engineering and Computing.

He participated in seven scientific projects financed by the Ministry of Science, Education and Sports of the Republic of Croatia and in three projects of the Croatian Science Foundation. He led three bilateral Croatian-Chinese scientific and technological projects, two Proof-of-Concept (PoC) projects of the BICRO agency, one Horizon 2020 EIT Health RIS Innovation project, and one project under the call Strengthening capacities for research, development and innovation (STRIP). He is a researcher on the project DATACROSS of the Centre of Research Excellence for Data Science and Advanced Cooperative Systems and has participated in the project “Application of Croatian Qualification Framework in the area of biomedical engineering”. He has led or participated in a number of collaborative projects with industry.

He is a co-author of two books, 15 chapters in scientific books, more than 40 journal papers, 31 of them CC with more than 800 citations in WoS, and more than 180 conference papers in the field of biomedical engineering, sensors and electronic instrumentation. He participated in scientific or program committees at international conferences and also serves as a reviewer for various international journals. He received awards in national and international innovation exhibitions, and he is also active in science popularization.

He is a member of professional associations IEEE (senior member), IFMBE, ESEM, Croatian Biomedical Engineering and Medical Physics Society and Croatian Society for Communications, Computing, Electronics, Measurement & Control. He is a member of the Croatian Academy of Engineering (HATZ), where he is a secretary of the Department of Systems and Cybernetics. He is a member of the Scientific Council for Technological Development of the Croatian Academy of Science and Arts (HAZU).

He was awarded the bronze "Josip Lončar" medal (1988) for the graduate student score, silver “Josip Lončar” medals for outstanding master of science thesis (1992) and the doctoral dissertation (1997), gold “Josip Lončar” medal (2019) for a significant contribution to the Faculty by establishing procedures to assess, assure and improve the quality of education, and for raising the profile of the Faculty through their scholarly research and professional work, Annual Award “Rikard Podhorsky” of the Croatian Academy of Engineering in 2014, the Annual award of the City of Zagreb in 2014, and a State award for science for the year 2020 in the field of technical sciences.

O mentoru

Mario Cifrek je rođen 1964. godine u Varaždinu. Diplomirao je, magistrirao i doktorirao u polju elektrotehnike na Sveučilištu u Zagrebu Fakultetu elektrotehnike i računarstva (FER), 1987., 1992., odnosno 1997. godine.

Od prosinca 1987. godine radi na Zavodu za elektroničke sustave i obradbu informacija FER a. U prosincu 2012. godine izabran je u zvanje redovitog profesora u trajnom zvanju. Tijekom rada na FER-u sudjelovao je u radu brojnih radnih tijela Fakulteta, a od 2006. do 2010. godine bio je prodekan za nastavu u dva mandata. Bio je član Akreditacijskog savjeta Agencije za znanost i visoko obrazovanje od 2013. do 2017. godine, a od 2017. godine je član Povjerenstva Akreditacijskog savjeta za naknadno praćenje u postupcima reakreditacije. Od 2013. godine član je Matičnog odbora za područje tehničkih znanosti, polja elektrotehnike i računarstva.

Sudjelovao je na sedam znanstvenih projekata Ministarstva znanosti, obrazovanja i sporta Republike Hrvatske te na tri projekta Hrvatske zaklade za znanost, te tri međunarodna projekta. Vodio je tri bilateralna projekta znanstveno-tehnološke suradnje s NR Kinom, dva projekta iz Programa provjere inovativnog koncepta za znanstvenike i istraživače (PoC PUBLIC) agencije BICRO, projekt iz programa EIT Heath RIS Innovation te projekt iz programa Jačanje kapaciteta za istraživanje, razvoj i inovacije (IRI). Istraživač je na projektu DATACROSS Znanstvenog centra izvrsnosti za znanost o podatcima i kooperativne sustave te je sudjelovao u projektu Primjena hrvatskog kvalifikacijskog okvira u području biomedicinskog inženjerstva. Vodio je ili je bio suradnik na većem broju projekata suradnje s gospodarstvom.

Suautor je dvije knjige, 15 poglavlja u znanstvenim knjigama, objavio je više od 40 radova u časopisima od čega 31 CC sa više od 800 citata u bazi WoS, te više od 180 radova na međunarodnim i domaćim znanstvenim skupovima u području biomedicinskog inženjerstva, senzora i elektroničke instrumentacije. Sudjelovao je u organizaciji međunarodnih znanstvenih skupova kao član znanstvenog ili programskog odbora. Recenzent je u većem broju međunarodnih znanstvenih časopisa. Dobitnik je nagrada na domaćim i međunarodnim izložbama inovacija i aktivan je u popularizaciji znanosti.

Član je stručnih udruga IEEE (seniorski status), IFMBE, Hrvatskog društva za biomedicinsko inženjerstvo i medicinsku fiziku i Hrvatskog društva za komunikacije, računarstvo, elektroniku, mjerenja i automatiku. Redoviti je član Akademije tehničkih znanosti Hrvatske (HATZ) gdje je tajnik Odjela sustava i kibernetike. Član je Znanstvenog vijeća za tehnološki razvoj Hrvatske akademije znanost i umjetnosti (HAZU).

Dodijeljena mu je brončana plaketa „Josip Lončar“ za uspjeh tijekom studija 1988. godine, srebrne plakete „Josip Lončar“ za značajan i uspješan magistarski rad, te za posebno uspješnu doktorsku disertaciju 1992., odnosno 1997. godine, zlatna plaketa „Josip Lončar“ za značajan doprinos Fakultetu uvođenjem postupaka vrednovanja, osiguravanja i unapređenja kvalitete nastave te za podizanje prepoznatljivosti Fakulteta svojim znanstvenoistraživačkim i stručnim radom, godišnja nagrada „Rikard Podhorsky“ Akademije tehničkih znanosti Hrvatske za 2014. godinu, Nagrada grada Zagreba u 2014. godini te Državna nagrada za znanost za 2020. godinu za područje tehničkih znanosti.

Acknowledgments

The journey of being a PhD student has brought various people into my life, and I am grateful to all of them. They taught, answered my questions, supported, and strengthened me.

Firstly, I am thankful to my supervisor, Mario Cifrek, who gave me an opportunity and believed in me from day one of our journey. From our first talk in the last year of my undergrad studies until the conversations and support through the last days of my PhD journey, he was always there to push me further than I thought I could achieve. Thank you for educating me on how to become an independent researcher. I am enormously grateful that you have been my supervisor.

Moreover, I would like to express my gratitude to associate professor Željka Lučev Vasić for all the help and knowledge she shared with me throughout my work. Thanks to professor Darko Vasić for all your advice and help during my work on ZESOI.

Thanks to professor Hrvoje Džapo for his guidance and leadership through all the projects I worked on under your supervision. I learned a lot from you, and I will never forget all the tips and tricks I learned by observing your work. But most of all, I will never forget your review of my papers.

Thanks to assistant professor Domagoj Vidović, MD, for allowing me to be part of his team during the clinical study conducted at the University Psychiatric Hospital "Vrapče".

I would also like to thank the sleep technicians, Katarina, Mila, and Tomislav, for all their help during the measurements.

A big "Thank you!" goes to Mirta for her invaluable help and conversations. I am grateful to have her in my life.

Thanks to my best work buddy, Karla – you are amazing!

Thanks to Sara, Džaja, Krešo, Pavić, and Šeketa – the D-135 room crew. It was a blessing to have you as part of my PhD journey. Special thanks to Krešo for listening to all my problems throughout the years.

Thanks to Dorijan for his smart pieces of advice!

Thanks to Zrinka, Luka, Antonio, and all others who helped and talked about how tough PhD life is. Special thanks to Luka for all the help during the last year of my PhD.

Thanks to all my friends, for all the understanding and support. Special thanks to Matea Žilak to always be there.

In addition, I would like to express my deepest appreciation and love to my family for their unwavering support, encouragement, and understanding. Thank you for always being there for me, no matter how tough things got. Your love and support gave me the strength to keep going, and I couldn't have done it without you...

I dedicate this work to my mother.

Summary

Existing breathing monitoring solutions are based on wearable devices that involve physical contact with the subjects when providing information and thus may impair measurement results and quality. Therefore, a contactless breathing measurement system was investigated in the proposed thesis. The most common contactless approach is camera-based, where the vital signs signals can be extracted using video image processing algorithms. However, several drawbacks include an inability to capture accurately when the patient is covered with a blanket, high deployment costs, and privacy problems due to camera monitoring. Therefore, a contactless approach based on radio-frequency (RF) signals could be an adequate alternative because it is already presented in the monitored environment. The RF-based approach is based on the fact that the RF propagation channel is continuously changing by the breathing and movement of the person, thus modulating the received signal. Most RF-based contactless devices use Wi-Fi signals, but in recent years there has been rising interest for use of ultra-wideband (UWB) technology. The main advantage is higher bandwidth and, thus, lower spectral power density than the Wi-Fi signals. Recently, UWB technology has been increasingly applied in systems for the contactless measurement of vital-sign parameters, primarily obtained in ideal and controlled conditions. Thus, this thesis brings realistic scenarios data in the clinical environment, which are much more complex than the controlled one. It contains a lot of unpredictable situations, such as body movement, sleep postural transitions, body jerks, and many other specific factors for each patient. Consequently, signal processing methods and machine learning or combinations of these improve the stability and accuracy of each measurement.

Moreover, most of the existing UWB RF-based solutions are based on the radar approach, where they monitor a reflected signal from the person's chest and calculate the

change in the received distance or time of arrival. Unlike the common UWB radar approach, this research presents a non-radar solution, where movements and breathing are extracted from the channel impulse response (CIR) based on the commercial, low-cost UWB transceivers. Regardless of the breathing patterns and body movements coming from different multipath components, they are successfully detected, as they are presented as statistically independent components in channel propagation. Therefore, that leads to the assumption that the proposed system can be used in various environments and observed patterns can be extracted regardless of the multiple new obstacles found in new environments.

A custom-designed data acquisition (DAQ) system based on low complexity and low-cost UWB transceivers was developed in the first phase. The experiment consisted of placing UWB transmitters (Tx) and receivers (Rx) in predetermined positions on the left and right sides of the subject's bed, where the transmitters generated an ultra-short UWB pulse with a minimum bandwidth of 500 MHz. Information on the chest movement caused by breathing is extracted from the CIR. The proposed approach is based on the assumption that the chest movement caused by breathing continuously changes the parameter of the communication channel and thus modulates the observed parameters on the receiver side; assuming that the transmitter signal level and the relative position of the receiver and transmitter unit do not change their relative position over time.

The second phase involved implementing the methods for feature extraction of sleep breathing patterns and postural transitions based on ultra-wideband communication CIR measurement. The possibility of the combinations of different standard feature extraction methods from UWB signals and selection methods of the optimal number of features for further classification was implemented.

The third phase included implementing a statistical model for sleep parameters analysis based on the statistical output data of the previously mentioned variables, subjective information gathered from the sleep questionaries, and demographics and anthropometric data. More precisely, the influence of each parameter on the AHI value in a certain time interval was investigated. AHI is a primary diagnostic metric for sleep apnea severity but it was represented as a single scalar value. Therefore, there is a necessity of finding some more descriptive predictions compared to AHI that is still concise and straightforward.

The dataset for sleep analysis measurement based on the proposed system was gathered in collaboration with the University Psychiatric Hospital Vrapče, Department of Clinical

Psychophysiology and Organically conditioned mental disorders, Center for Sleep and Wake Disorders. Participants received all necessary information about the research before the recording and signed a consent to participate in the research. The study respected the privacy of the participant's data. It was conducted following all applicable guidelines based on the Helsinki declaration and its revisions, which ensured the proper implementation of procedures and the safety of persons who participated in this research.

Keywords: UWB, contactless device, sleep medicine, breathing patterns, sleep postural transitions patterns, sleep parameters, sleep breathing disorders, machine learning, feature engineering

Sažetak

Metoda analize parametara spavanja zasnovana na mjerenju impulsnog odziva ultraširokopojasnoga komunikacijskog kanala

Polisomnografija (PSG) je zlatni standard pri analizi spavanja i dijagnozi kvalitete spavanja. PSG prikuplja informacije o bioelektričnoj aktivnosti tijekom spavanja putem više zasebnih mjernih uređaja, a svi su oni u direktnom kontaktu s kožom spavača. Osim PSG, osmišljena su i druga rješenja koja pružaju manje biolektričnihi podataka iz manje mjernih uređaja. Svaki od navedenih nosivih uređaja uključuje fizički kontakt s ispitanikom prilikom pružanja informacija o spavanju, što u nekim slučajevima može narušiti kvalitetu spavanja i tako utjecati na mjerenje. Zbog navedenih razloga pojavila su se istraživanja beskontaktnih sustava za mjerenje disanja kako bi se uklonili nedostatci nosivih uređaja. Najčešće se koriste akustični senzori, senzor tlaka i infracrvena termografija. Za precizno mjerenje korištenjem senzora pritiska potrebno je više istih senzora, a za uspješnu detekciju ispitanik mora leći u predodređeni položaj prema postavljenim senzorima u madracu kreveta. Infracrvena termografija ima veliku točnost prilikom detekcije promjene disanja i u uvjetima pokreta i mogućih poremećaja disanja, ali ova pretraga je relativno skupa i ne može pružiti informacije o disanju ako je lice ispitanika prekriveno pokrivačem.

U posljednje vrijeme, ultra-širokopojasna (UWB) tehnologija se sve više primjenjuje u sustavima za beskontaktno mjerenje vitalnih fizioloških parametara, najčešće koristeći radarsko načelo. UWB komunikacija temelji se na slanju vrlo kratkih impulsa u trajanju od 100 ps do 1 ns uz zauzimanje minimalno 500 MHz širine pojasa u frekvencijskom području od 3,1 do 10,6 GHz. Velika širina pojasa omogućuje propagiranje kroz prepreke, uključujući i propagiranje kroz biološka tkiva.

Cilj ovog istraživanja je iskoristiti radiofrekvencijsku (RF) tehnologiju, točnije UWB tehnologiju, za beskontaktno mjerenje parametara spavanja i njihovu analizu korištenjem algoritama strojnog učenja i obradbe signala. Razvijena je UWB platforma za praćenje parametara spavanja (*Sleep-UWB Platform*) te je validirana provođenjem cjelonoćnog kliničkog istraživanja u Klinici za psihijatriju "Vrapče", Zavoda za psihofiziologiju i organski uvjetovane psihičke poremećaje, Centra za poremećaje spavanja i budnosti. Analiza dobivenih podataka prikupljenih platformom *Sleep-UWB Platform* uspoređena je s referentnim mjerenjima polisomnografijom (PSG). Prikupljeno je 20 cjelonoćnih mjerenja, od kojih je 17 uzeto u obzir. Istražena je analiza obrazaca disanja i promjena položaja tijela tijekom spavanja i sveukupna analiza parametara spavanja. Rezultati istraživanja pokazali su da se predloženim pristupom postižu bolji rezultati u odnosu na postojeće slične metode.

U prvom poglavlju opisana je motivacija i ciljevi istraživanja. Nepravilni obrasci disanja i promjena položaja tijela tijekom spavanja snažno su povezani s kvalitetom spavanja. Jedan od najčešćih primjera je spavanje u položaju polegnutom na leđa što može povećati rizik od opstrukcije gornjih dišnih putova i može dovesti do opstruktivne apneje za vrijeme spavanja. Postojeća rješenja za praćenje disanja temelje se na nosivim uređajima koji uključuju fizički kontakt s ispitanicima pri mjerenju i stoga mogu narušiti kvalitetu mjerenja i rezultate. Kako bi se riješili navedeni nedostatci nosivih uređaja, istražuju se sustavi za beskontaktno mjerenje disanja. Najčešći beskontaktni pristup je mjerenje kamerom, gdje se signali vitalnih funkcija mogu izdvojiti pomoću algoritama za obradbu video snimaka. Međutim, postoji nekoliko nedostataka koji uključuju nemogućnost preciznog snimanja kada je pacijent prekriven pokrivačem, kao i visoke troškove postavljanja kamere te probleme s privatnošću zbog nadzora kamerom. Stoga beskontaktni pristup temeljen na RF signalima može biti adekvatan zbog sve veće rasprostranjenosti RF signala. Pristup temeljen na RF-u temelji se na činjenici da se kanal širenja RF-a kontinuirano mijenja tijekom disanjem i pokreta, modulirajući tako primljeni signal. Većina beskontaktnih uređaja koji se temelje na RF-u koriste Wi-Fi signale, no posljednjih godina postoji veliko zanimanje za korištenje ultraširokopojasne tehnologije. Glavna prednost je veća širina pojasa, a time i niža gustoća spektra snage od Wi-Fi signala. UWB tehnologija se u posljednje vrijeme sve više primjenjuje u sustavima za beskontaktno mjerenje parametara vitalnih funkcija, prvenstveno dobivenih u kontroliranim laboratorijskom uvjetima. Ovo doktorsko istraživanje se provodi u realnom, kliničkom, okruženju koje je mnogo složenije od laboratorijskog okruženja. Sadrži mnogo nepredvidivih situacija kao što su pokreti tijela, promjene položaja tijela, trzaji tijela i mnogi

drugi specifični čimbenici za svakog pacijenta. Nadalje, primjenom metoda strojnog učenja poboljšava se stabilnost i točnost mjerenja s platformom Sleep-UWB Platform. Štoviše, većina UWB sustava temelji se na radarskom načelu, gdje se prate reflektirani signali od prsnog koša ispitanika i izračunavaju promjenu udaljenosti na temelju vremena dolaska signala. Za razliku od uobičajenog UWB radarskog pristupa, ovo istraživanje predstavlja ne-radarsko rješenje, gdje će se pokreti i disanje izdvojiti iz impulsnog odziva kanala (engl. channel impulse response, CIR) komercijalnih UWB primopredajnika.

Drugo poglavlje opisuje medicinsku pozadinu obrazaca disanja tijekom spavanja, položaja tijela i parametara kvalitete spavanja. Osim toga, opisani su poremećaji disanja tijekom spavanja (engl. sleep-disordered breathing, SDB), kao što je apneja za vrijeme spavanja. Najčešći oblik apneje za vrijeme spavanja je opstruktivna apneja za vrijeme spavanja (OSA). Simptomi OSA-a uključuju glasno hrkanje, prekide disanja tijekom sna, buđenje s osjećajem nedostatka daha ili gušenja, umor tijekom dana i smanjenje koncentracije.

U trećem poglavlju dan je pregled relevantnih znanstvenih radova i metoda za detekciju i analizu obrazaca disanja i promjene položaja tijela tijekom spavanja u vremensko-frekvencijskoj domeni. Uz to, opisane su osnove tehnologije i širenja UWB signala, zajedno s njihovim utjecajem na ljudska tkiva.

Četvrto poglavlje opisuje razvijene platforme *UWB platform* i *Sleep-UWB Platform*. Predloženi pristup temelji se na pretpostavci da pomak tijela uzorkovan disanjem i pokretom tijela kontinuirano mijenja parametre komunikacijskog kanala i na taj način modulira promatranu snagu signala na strani prijamnika, pod pretpostavkom da snaga odašiljačkog signala i međusobni položaj jedinica prijamnika i odašiljača ne mijenjaju međusobni položaj tijekom vremena. Istraživanje koristi dva čvora temeljena na komercijalno dostupnim DW1000 802.15.4a UWB primopredajnicima. Konfiguracija temeljena na dva para čvorova odabrana je radi povećanja prostorne razlučivosti kod detekcije promjene položaja tijela ispitanika.

U petom poglavlju detaljno je opisano kliničko istraživanje. Također je opisan prikupljeni skup podataka te je provedena analiza prikupljenih signala. Prikupljanje podataka provedeno je u suradnji s Klinikom za psihijatriju "Vrapče", Zavod za psihofiziologiju i organski uvjetovane psihičke poremećaje, Centar za poremećaje spavanja i budnosti. Sudionici su prije snimanja dobili sve potrebne informacije o istraživanju i potpisali suglasnost za sudjelovanje u istraživanju. Provedeno istraživanje poštovalo je privatnost

podataka sudionika istraživanja. Provedeno je prema svim važećim smjernicama temeljenim na Helsinškoj deklaraciji i njezinim revizijama, čime je osigurana pravilna provedba procedura i sigurnost osoba koje su sudjelovale u ovom istraživanju. Također, prikupljeni su relevantni upitnici o spavanju, poput Epworthove ljestvice pospanosti (engl. *Epworth Sleepiness Scale*, ESS) i Pittsburgh indeks kvalitete spavanja (engl. *Pittsburgh Sleep Quality Index*, PSQI). Referentno mjerenje provedeno je PSG uređajem (Alice 6, Respironics, Philips). PSG i UWB mjerenja trajala su približno osam sati po pacijentu. Provedena je analiza obrazaca disanja i promjene položaja tijela iz signala CIR-a s dvaju čvorova te su dobiveni rezultati uspoređeni s PSG mjerenjima. Prikazan je utjecaj pretilosti svakog pacijenta na detekciju obrazaca disanja i analize promjene položaja tijela tijekom spavanja. Pretilost je procijenjena putem podataka o visini, težini, te izmjerenim opsezima pojedinih segmenata tijela. Nakon toga, prikazan je utjecaj nepravilnih obrazaca disanja i promjena položaja tijela tijekom spavanja na uspješnost analize respiratornih događaja. Također je provedena analiza obrazaca disanja i promjena položaja tijela temeljena na metodama strojnog učenja.

Šesto poglavlje opisuje stohastički model temeljen na statističkim podacima UWB i PSG mjerenja i subjektivnim informacijama prikupljenim upitnicima o spavanju i antropometrijskih podataka izmjerenih prije i nakon spavanja. Poremećaji disanja za vrijeme spavanja, kao što je apneja za vrijeme spavanja, dolaze s brojnim komorbiditetima. Ljudi provedu otprilike jednu trećinu svog života spavajući ili pokušavajući spavati. Stoga se pravodobnim i svakodnevno dostupnim praćenjem može smanjiti neliječeni SBD i podići svijest o spavanju kod šire populacije. Parametar koji pokazuje ozbiljnost apneje za vrijeme spavanja je indeks apneje-hipopneje (AHI). AHI je ukupan broj epizoda apneja i hipopneja tijekom ukupnog vremena spavanja (engl. *total sleep time*, TST). Prema rezultatima AHI indeksa, doktori medicine postavljanju dijagnozu i liječenje, kao što je korištenje uređaja za kontinuirani pozitivni tlak u dišnim putovima (engl. *continuous positive airway pressure*, CPAP). Jedan od nedostataka AHI indeksa je što ne daje informaciju o distribuciji apneja i hipopneja tijekom spavanja kao i utjecaj položaja tijela, faze spavanja u odnosu na respiratorne događaje. Slijedom toga, u ovom istraživanju, razvijen je stohastički model koji uključuje podatke o položaju i fazi spavanja te antropometrijske mjere uzete prije i nakon spavanja, kao i podatke dobivene subjektivnim upitnicima i karakteristike ponašanja pacijenata na dan mjerenja, pokrivajući nedostatak informacija dan AHI indeksom. Analiza dobrote prilagodbe modela pokazuje da ovaj pristup može donijeti nove percepcije i poboljšanja u praćenju respiratornih događaja.

U sedmom poglavlju doneseni su zaključci o postignutim ciljevima te su predloženi potencijalni smjerovi za buduća istraživanja.

Ključne riječi: UWB, beskontaktna metoda, medicina spavanja, obrasci disanja, obrasci promjena položaja tijela tijekom spavanja, parametri spavanja, poremećaji disanja tijekom spavanja, strojno učenje, inženjerstvo značajki

Contents

Chapter 1
Introduction

1.1 Research motivation

"**There is a time for many words, and there is also a time for sleep**."

(Homer, The Odyssey)

From the time of Homer, sleep analysis has intrigued researchers from various fields. Many of them have endeavored to explain the physiological basis of sleep and dreams [1]. However, with new technologies, daily habits, and ways of life, people have inadvertently created several new disorders. Consequently, sleep disorders are more pervasive in society but most people are unaware of them [2]. Sleep analysis solutions are mainly based on wearable devices that could disturb sleep and deteriorate the measurement results. Therefore, the motivation for the research was to investigate a solution that would be minimally intrusive and without a contact with patients. Moreover, the population's interest in sleep sensing is increasing due to the development of smart gadget devices in recent years [3].

Polysomnography (PSG) is the current gold standard for sleep analysis [4]. PSG gathers information on bioelectrical activities during sleep via several separate measuring devices (pulse oximeter, thermistor, pressure transducer, ECG, EMG, EOG), and all of them are in direct contact with the sleeper's skin. Besides PSG, other solutions have been designed but they provide less bioelectrical activity data from a reduced number of measuring devices (see Subchapter 2.2). Each of the above mentioned wearable devices involves physical contact with the subject. Therefore, contactless breathing measurement systems were investigated to address the disadvantages of wearable devices. Most common contactless breathing

measurement systems in sleep medicine are based on acoustic, pressure, and infrared thermography [5]–[10]. Albeit, each of them has certain drawbacks. Several of the same sensors are required for accurate measurement using pressure sensors. Moreover, for successful detection, the subject must lie in a predetermined position according to the sensors placed in the bed mattress. Infrared thermography accurately detects respiratory changes during body movement and possible respiratory disorders. Still, this system is relatively expensive and cannot provide information about respiration if the subject's face is covered with a blanket.

UWB technology has recently been increasingly applied in systems for contactless measurement of vital-sign parameters, most commonly as UWB radar [11]–[14]. UWB communication is based on sending very short pulses in the duration of 100 ps up to 1 ns with a minimum of 500 MHz bandwidth in the frequency range from 3.1 up to 10.6 GHz [15]. A wide bandwidth allows propagation through obstacles, including propagation through biological tissues [11]. One of the first studies in the field of sleep breathing monitoring using UWB radar was by Javaid et al. [16]. The accuracy of sleep apnea detection was approximately 76%, and it was stated that there is a possibility of improvement in the detection method. A pilot study of the sleep quality measurement performance based on UWB radar was also proposed by Pallesen et al. [17] in 2018. The study was conducted on 12 subjects using commercial Novelda XeThru radar, and the results were compared with the PSG. According to the pilot study, it can be concluded that UWB radar is a promising tool for practical sleep parameters analysis, with accuracy, sensitivity, specificity, and Cohen kappa 0.931, 0.961, 0.695, and 0.670, respectively. The study did not consider the influence of body position during sleep; more precisely, the time interval in which the movement of patients occurs was excluded from the performance measurement of the proposed system. C. Li et al. [18] proposed breathing and heart rate measurement during sleep from four sides of the body but did not consider the influence of the interval of sleep postural transition on the measurement results.

With the enhancement of processing power, applying algorithms based on artificial intelligence methods become possible. Authors [12], [19] presented a system for breathing pattern classification using deep learning methods. The research results showed an increase in detection accuracy from 3% to 13% compared to the common machine-learning methods. The disadvantage is that the measurements were performed on the subjects while they were awake and in a predetermined short time interval of measurements. Furthermore, research

[20] presents sleep status measurement using three features: movements in bed during sleep, leaving the bed, and sleep breathing measurement. The most recent overview of all previous deep learning algorithms for monitoring human activities using RF signals was provided by Nirmal et al. [17].

Additionally, authors [21] present a method for classifying sleep stages based on detecting sleep breathing and body position using radar but with controlled and short-term experiments. Therefore, it was shown that apneas and hypopneas are more common when people sleep in a supine position, in both the REM (rapid eye movement) and NREM (non-rapid eye movement) sleep stages than those who sleep in a prone position [22].

Besides radar, channel state information (CSI) between transmitter and receiver was used in some recent research [23]. So far, most of the research that uses CSI has been based its research on the usage of Wi-Fi technology [25]. Unlike Wi-Fi technology, UWB technology uses channel impulse response (CIR) [27]. The CIR provides information on the multipath propagation characteristics of a wireless communication channel between a transmitter and a receiver. This method improves the signal-to-noise ratio (SNR) in comparison to the weak reflected wave from radar, and it is to be expected that the change in lung volume during breathing, as well as macro-movements that occur during sleep postural transition during sleep, will be better monitored [28], [29]. Wang et al. [30] presented similar research in this direction, where they measured UWB impulse penetration for respiration monitoring through the human body during car driving.

Therefore, unlike the common UWB radar approach, this research presents a non-radar solution in which movements and breathing are extracted from the CIR based on the UWB transceivers. The *Sleep-UWB platform* was developed for the experimental testing.

Moreover, this thesis contains the results of experiments performed under realistic conditions and scenarios for acquiring relevant data in the clinical environment, which was much more complex to achieve than under the controlled lab conditions. Experiments contains valueable data with lots of unpredictable situations, such as body movements, sleep postural transitions, body jerks, and many other specific factors for each patient that are present in data collected under realistic measurement conditions.

Furthermore, the thesis includes an investigation of temporal changes in the apnea-hypopnea index (AHI) and the influence of each parameter (sleep stage, body position, snoring, body movement variability, etc.) on the AHI value in a certain time interval.

The dataset for sleep analysis measurement based on the proposed system was gathered in collaboration with the University Psychiatric Hospital Vrapče, Department of Clinical Psychophysiology and Organically conditioned mental disorders, Center for Sleep and Wake Disorders. Participants received all necessary information about the research before the recording and signed a consent to participate in the research. The study respected the privacy of the participants' data. It was conducted by all applicable guidelines based on the Helsinki declaration and its revisions, which ensured the proper implementation of procedures and the safety of persons who participated in this research.

1.2 Research questions and contributions

Through the thesis following research questions will be addressed:

Research Question 1. What are sleep breathing patterns? Is there any optimal solution which can gather data from sleep and not impair sleep quality by placing the sensors on the body?

Research Question 2. What optimal features from collected sensor data can represent specific sleep breathing patterns and postural transition information?

Research Question 3. Is there a possibility to leverage information about respiratory events in some descriptive, upgraded form compared with the currently used AHI index?

The expected original scientific contributions of the proposed research are:

1) Method for measurement of sleep breathing patterns and sleep postural transitions based on ultra-wideband communication channel impulse response measurement;
2) Method for feature extraction of breathing patterns and postural transitions during sleep based on ultra-wideband communication channel impulse response measurement;
3) Method for analysis of sleep parameters from extracted features of breathing patterns and postural transitions.

1.3 Outline of the thesis

In the first chapter, the general motivation and the research objectives are described. Existing breathing monitoring solutions are based on wearable devices that involve physical contact with the subjects when providing information and thus may impair measurement results and quality. Hence, contactless breathing measurement systems are investigated to address the

disadvantages of wearable devices. The most common contactless approach is camera-based, where the vital signs signals can be extracted using video image processing algorithms. However, several drawbacks include an inability to capture accurately when the patient is covered with a blanket, high deployment costs and privacy problems due to camera monitoring. Therefore, a contactless approach based on RF signals can be an adequate alternative. The RF-based approach is based on the fact that the RF propagation channel is continuously changing by the breathing and movement of the person, thus modulating the received signal. Most of the currently investigated RF-based contactless solutions for this goal use Wi-Fi signals but in recent years there has been an interest in using UWB technology. The main advantage is higher bandwidth and, thus, lower spectral power density than the Wi-Fi signals. Recently, UWB technology has been increasingly applied in systems for the contactless measurement of vital-sign parameters, primarily obtained in controlled laboratory conditions. Thus, this research brings more realistic scenarios where data were collected in the clinical environment, which was much more complex to obtain compared to the controlled lab condiotions. Realistic data contains valuable data related to many possible unpredictable situations and sources of non-idealities in sensor data, such as body movements, sleep postural transitions, body jerks, and other factors that may be specific for each patient.

Furthermore, applying machine learning methods improves the measurements' stability and accuracy with the *Sleep-UWB Platform*, custom designed sensor solution capable of acquiring UWB CIR measurements for monitoring sleep parameters. Moreover, most of the UWB RF-based solutions investigated in the literature up to date are based on the radar approach, where a reflected signal from the person's chest is monitored and the distance obtained from the change in the time of arrival is calculated. Unlike such already established UWB radar approach, this research presents completely different a non-radar solution, where movements and breathing are extracted from the CIR obtained by transmitting signal through the human body as a propagation media, instead of monitoring reflected signals.

The proposed non-radar solution can be an attractive alternative to traditional radar-based methods for detecting movement and measuring distances by involving the measurement of the CIR. This method has several advantages over radar-based methods, including lower complexity, lower power consumption, and higher data rates. Furthermore, UWB CIR measurements are immune to multipath fading and can operate in environments where traditional radar systems may encounter difficulties.

The second chapter presents and describes the medical background of sleep breathing patterns, body positions and sleep quality parameters. In addition, sleep-disordered breathing (SDB) diagnoses, such as sleep apnea, have been described.

Furthermore, the third chapter presents an overview of the relevant scientific papers and the methods related to detecting and analyzing sleep breathing patterns and postural transition in the time-frequency domain. Moreover, the fundamentals of UWB technology and UWB signal propagation are described and their influence on human tissues.

The fourth chapter describes the custom developed *Sleep-UWB Platform*. The designed system is based on low complexity and low-cost commercially available UWB transceivers. UWB transmitters (Tx) and receivers (Rx) are placed at predetermined positions on the left and right sides of the subject's bed. The transmitters generates an ultra-short UWB pulse with a minimum bandwidth of 500 MHz. From the UWB channel impulse response (CIR), information about the micro-displacement of the body caused by breathing and body movement are extracted. Afterwards, a method of detecting breathing and sleep postural transitions was implemented. The proposed approach is based on the assumption that the chest movements caused by breathing and body movements continuously change the parameters of the communication channel and thus modulates the observed parameters on the receiver side, assuming that the transmitter signal level and the relative position of the receiver and transmitter unit do not change their relative position over time. The research uses two UWB nodes based on the commercially available DW1000 802.15.4a UWB transceivers. It was decided to use two nodes to leverage spatial resolution, regardless of the body position of the participants.

The fifth chapter describes in details the procedure of the conducted clinical study. Thereafter, the gathered dataset was described, and signal analysis was provided along with a detailed evaluation of the obtained results. The dataset was gathered in collaboration with the University Psychiatric Hospital Vrapče, Department of Clinical Psychophysiology and Organically conditioned mental disorders, Center for Sleep and Wake Disorders. Participants received all necessary information about the research before the recording and signed a consent to participate in the research. The study respected the privacy of the participant's data. It was conducted by all applicable guidelines based on the Helsinki declaration and its revisions, which ensured the proper implementation of procedures and the safety of persons who participated in this research. Also, relevant sleep questionnaires, such as the Epworth

Sleepiness Scale (ESS) and Pittsburgh Sleep Quality Index (PSQI), were gathered. The reference measurement was performed using a PSG device (Alice 6, Respironics, Philips). PSG and UWB data were recorded for approximately eight hours per patient. An analysis of breathing and sleep postural transitions of the CIR from the two nodes have been evaluated and compared with the PSG measurements. The influence of each patient's obesity on the detection of breathing and the analysis of sleep postural transitions are presented. Human obesity was estimated using the information on the height, weight, and circumference of specific body segments. Afterward, the influence of the sleep breathing patterns irregularity and sleep postural transitions on the success of the analysis of the respiratory events were depicted.

The sixth chapter describes the implementation of a model for sleep parameters analysis based on the statistical UWB and PSG data, subjective information gathered from the sleep questionnaires, and demographic and anthropometric data taken before and after sleeping. Sleep breathing disorders, such as sleep apnea, come with plentiful comorbidity. People spend about one-third of their life either sleeping or aiming to sleep. Therefore, timely and daily accessible monitoring of it can decrease untreated SDB and increase awareness among the wider population. Commonly, the parameter showing the severity of sleep apnea is the apnea-hypopnea index (AHI). AHI represents the total number of apnea and hypopnea episodes over a total sleep time (TST). According to the AHI index results, medical doctors establish a diagnosis and treatment, such as using a device for continuous positive airway pressure (CPAP). One of the disadvantages is that the AHI index does not cover the temporal changes of the apneas and hypopneas over time and its relative dependency on the relevant events that happened along with respiration events.

Consequently, the model was developed, including information about the body position, snoring, body movement variability and sleep stage, along with anthropometric measures taken before and after sleep, as well as the subjective questionnaires and behavioral characteristics of the patients on the day of the measurements, covering the lack of information given by the scalar AHI index. The goodness-of-fit analysis shows that this approach can bring new perceptions and improvements in monitoring respiratory events.

The seventh chapter of the dissertation provides summaries of conclusions from the conducted research and potential directions for further research, along with the limitation observed during the research.

Chapter 2
Medical background

2.1 Physiology of sleep

We spend almost one-third of our life sleeping; therefore, it plays an important role in the overall health state of the individual and significantly influences our daily performance [1], [2], [30], [31]. It is essential to understand the physiological changes in our body during sleep to understand sleep [4]. Roughly, sleep can be divided into two main stages:

1) **rapid eye movement (REM)** (mixed-frequency activity in EEG, rapid eye movement, muscle atonia), and
2) **non-rapid eye movement (NREM),**
    a. **N1 sleep** (theta waves in EEG, slow eye movement, diminution of muscle tone),
    b. **N2 sleep** (theta waves, sleep spindles, K complex in EEG, low muscle tone, absent eye movement),
    c. **N3 sleep** (more than 20% of the epoch has delta waves, observed from EEG),

according to the eye movements, EEG waveforms and muscle tone [4]. The NREM-REM interval alternates every 90-120 minutes in a healthy adult person, whereas an average healthy person has about 4-5 cycles [4]. Hence, several physiological changes happen inside the body through sleep, from wakefulness up through different sleep stages, and most of them can be monitored using polysomnography (PSG). Some of them are summarized in Table 2.1.

Table 2.1 Sleep physiological changes [4]

Changes	Wakefulness		NREM			REM
	Active	**Quiet**	**N1**	**N2**	**N3**	
Respiration	Irregular rate; variable of breathing amplitude	Regular rate; uniform breathing amplitude	Regular with a slowing rate; uniform breathing amplitude			Erratic rate and amplitude
Muscle tone	Increased		Reduced			Minimal (atonia)
Cardiac activity	Variable within a range		Regular beats (slowing of rate)			Irregular heart beats
Spontaneous movement	High	Reduced	Occasional			Absent
Brain electrical activity	Beta or gamma rhythm with occasional theta rhythm	Alpha rhythm	Theta rhythm	Theta rhythm with delta	Delta rhythm	Low voltage mixed frequency activity (similar to wakefulness)

2.2 Sleep sensing

Sleep sensing devices can measure physiological changes through the different sleep stages. The quantification of sleep, qualitative study of sleep and the diagnosis of sleep disorders can be performed using it [32]. Sleep sensing includes in-sleep center polysomnography (PSG) and out-of-center sleep testing (OCST), where OCST can be used for home sleep testing, such as for sleep apnea [2]. For OCST, the diagnostic metric for apnea severity is described as the number of apneas and hypopneas per hour of monitoring time or the so-called *respiratory event index* [2]. For PSG, the diagnostic metric for apnea severity is AHI and based on the last AASM scoring manual, it is defined as the number of apneas and hypopneas per hour of sleep [2], [33].

The PSG system is a gold standard for sleep monitoring. Still, this method has a lot of disadvantages, such as complexity, on-body devices and cables and unavailability to the broader population.

Regarding the channel number (correlated with a sensor number) and the number of physiological parameters observed, sleep studies can be divided into four levels [4]. **Level IV**

includes one or two channels. Usually, it is used for recording respiratory monitoring through the night (recording oxygen saturation, respiratory flow, or both) [4]. **Level III** includes at least four channels, such as a pulse oximeter, nasal airflow, chest or abdominal movements, and electrocardiogram (ECG) [4]. An example of the Level III commercial device is presented in Figure 2.1. **Level II** includes all the devices as **Level I** but without video recording and does not include observation of a sleep technician as it is done from the patient's home [4]. Therefore, it includes the following [4]:

- pulse oximeter,
- nasal airflow (thermistor, pressure transducer or both),
- chest and abdominal movements (respiratory inductance plethysmography (RIP) belts),
- electrocardiogram (minimum two electrodes that can record Leads I or II, or III),
- electroencephalogram (minimum two channels of EEG are present, where active electrodes are placed at some of these positions: frontal, central, and occipital on both sides of the head—right side and left side; Table 2.2),
- the electrooculogram (right eye and left eye),
- electromyogram (chin electromyogram; anterior tibialis muscles of each leg)
- body position.

Level I includes all the devices used in the Level II study. Still, it was done in a sleep laboratory with a sleep technologist presented throughout the study, and video and audio recordings were taken and synchronized with the other sensors [4]. An example of a Level I commercial device is presented in Figure 2.2.

Respiratory data from the PSG measurements are obtained using airflow or chest and abdomen sensors. An airflow is recorded using a thermocouple or thermistor and pressure transducer [4]. With the respiratory inductance plethysmography (RIP) belts, the volume of the chest and abdomen changes are monitored. Using two belts, one for the chest and the other for the abdomen, can distinguish obstructive sleep apnea from central sleep apnea [4].

Figure 2.1 Alice NightOne (Philips Respironics) home sleep testing device - Level III device.
Figure was taken from: [34]

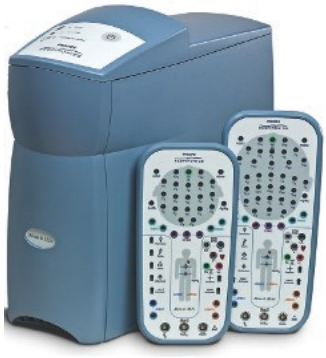

Figure 2.2 Alice 6 (Philips Respironics) - Level I device.
Figure was taken from: [35]

Table 2.2 Recommended and acceptable EEG derivation for PSG study based on AASM rules [4], [33]

Recommended	
Primary	**Backup**
F4-M1	F3-M2
C4-M1	C3-M2
O2-M1	O1-M2
Acceptable	
Primary	**Backup**
Fz-Cz	Fpz-C3
Cz-Oz	C3-O1
C4-M1	C3-M2

2.3 Sleep breathing patterns

Sleep-disordered breathing (SDB) is identified as an abnormalities of respiration during sleep [33], [36] [37]. They are grouped into [36]:

1) obstructive sleep apnea (OSA) disorders,
2) central sleep apnea (CSA) disorders,
3) sleep-related hypoventilation disorders, and
4) sleep-related hypoxemia disorder.

Some of the patients will have a combination of more than one SDB. Usually, there is a combination of obstructive and central sleep apnea [36]. The reference guideline for scoring sleep and associated events are given by the American Academy of Sleep Medicine (AASM), which includes a different set of rules for adult and pediatric individuals, as well as definitions of SDB events [33], [38].

Apnea in adults is defined as attenuation of the peak signal excursion by 90% in a minimum duration of 10 s [39]. Hypopnea is defined as a reduction in airflow more than or equal to 30% from baseline in a duration of more than or equal to 10 seconds, as well as a decrease in saturation of at least 4% from baseline SpO_2% before the event [39]. In clinical observation, hypopneas are defined along with apneas. One of the most common types of sleep apnea is obstructive sleep apnea (OSA) [40], [41]. OSA is characterized as a recurrent episode of apnea and/or hypopnea by a partial or complete collapse of the pharyngeal airway [42]. In addition, it is shown that OSA is related to many heart diseases, such as coronary artery disease, atrial fibrillation (AF) and chronic heart failure (CHF) [43]. The apnea severity is defined by the AHI index. The AHI index represents the sum of apnea (hypopnea) through an hour of sleep [44]. OSA is diagnosed if AHI is ≥ 5, and it is divided into three stages: mild OSA ($5 \leq AHI < 15$), moderate OSA ($15 \leq AHI < 30$), and severe OSA ($AHI \geq 30$) [38]. In addition to the AHI index, there is also the RDI (Respiratory Disturbance Index), which is defined by a number of respiratory effort- related arousal (RERA) events [30]. RERA is characterized by obstructive upper airway airflow reduction that does not meet the criteria of apnea or hypopnea but in duration for a minimum of 10 s. It is associated with increased respiratory effort (arousal) [39].

In more detail, according to the [39], subcategories of the abovementioned SDB groups are:

1. **Central apnea syndromes**
    a. Primary central apnea
    b. Cheyne - Stokes respiration
    c. Periodic respiration of high altitude
    d. Central apneas without Cheyne-Stokes respiration secondary to other disorders (vascular, malignant, degenerative, or traumatic disorders of the central nervous system, cardiac/renal disorders)
    e. Central apneas caused by medicine or other substances
    f. Primary sleep apnea of newborn
2. **Obstructive sleep apnea syndrome**
    a. Obstructive apnea in adults
    b. Obstructive apnea in children
3. **Hypoventilation/hypoxemia syndromes associated with sleep**
    a. Non-obstructive alveolar hypoventilation, idiopathic
    b. Congenital central hypoventilation
    c. Hypoventilation/hypoxemia secondary to other disorders: lung parenchymal, airway (e.g., chronic obstructive pulmonary disease (COPD)), or vascular (e.g., pulmonary hypertension) disorders; neuromuscular disorders; thoracic wall abnormalities; obesity.
4. **Undefined/non-specific sleep disorders**
    Disorders without specific characteristics to allow their classification in any of the above categories require further investigation.

Based on a respiratory effort, the three main apneas can be distinguished [39]:

- Obstructive sleep apnea (OSA),
- Central apnea (CA),
- Mixed apnea (MA).

In the case of OSA, the respiratory effort is recorded throughout the event. Still, on the other side, the absence of respiratory effort throughout the event is presented in the case of CA. Additionally, in the case of MA, the absence of respiratory effort at the beginning of the event is usually followed by increasing respiratory effort during the other half [39].

Furthermore, from the above mentioned, a Cheyne-Stokes respiration is set by recording at least three crescendo-decrescendo fluctuations in respiration and one of the following [39]:

- five or more central apneas or hypopneas per hour of sleep,
- duration of crescendo-decrescendo fluctuations in respiration at least ten continuous minutes.

The symptoms of Cheyne-Stokes respiration are sleepiness or insomnia and arousal (with or without dyspnea) [39].

2.3.1 Obstructive sleep apnea

Obstructive sleep apnea (OSA) is classified as a disorder according to ICSD3[1] [2], [33].

Diagnostic criteria for an OSA are at least one of the following [39]:

- Sleepiness, hypersomnolence, exhaustion or insomnia.
- Arousals with a feeling of asphyxiation/ suffocation.
- Snoring and breathing pauses are witnessed by a sleep partner.
- Apnea, hypopnea, or RERAs ≥ 5 per hour of sleep.
- Recording of respiratory effort during part of the whole event.

Severity criteria: The severity of OSA is a combination of the severity of daytime sleepiness and the value of the AHI [39].

- The severity assessment of daytime sleepiness can be subjective and objective. Subjective assessment is obtained with questionnaires. Epworth Sleepiness Scale (ESS) is the most commonly used, with a range of 0-24 and a minimum normal value of 10.
- Apnea-Hypopnea Index (AHI) or Respiratory Disturbance Index (RDI):
  - Mild: 5-15 events per hour.
  - Moderate: 15-30 events per hour.
  - Severe: more than 30 events per hour.

[1] International Classification of Sleep Disorders (ICSD) is a fully revised version of the American Academy of Sleep Medicine's manual of sleep disorders nosology.

Apnea signals representation from several sensors are given in Figure 2.3, and hypopnea in Figure 2.4. Moreover, Table 2.3 summarizes the American Academy of Sleep Medicine's (AASM) scoring rules for apneic events.

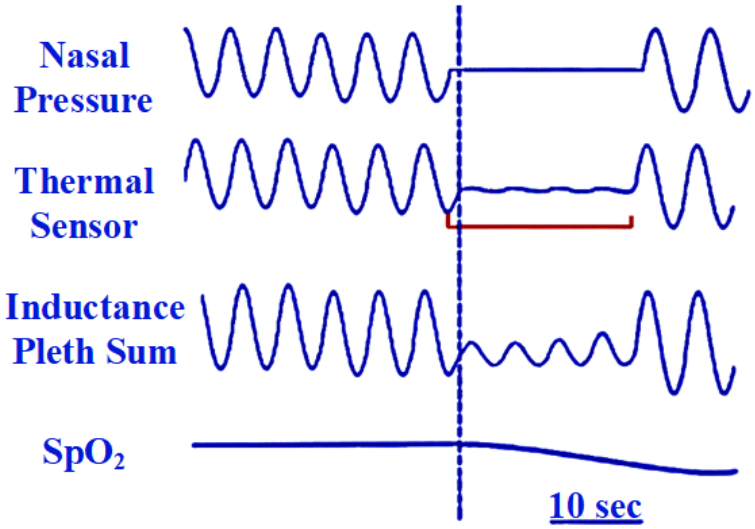

Figure 2.3 Apnea from the different sensors.
Figure adjusted from [33]

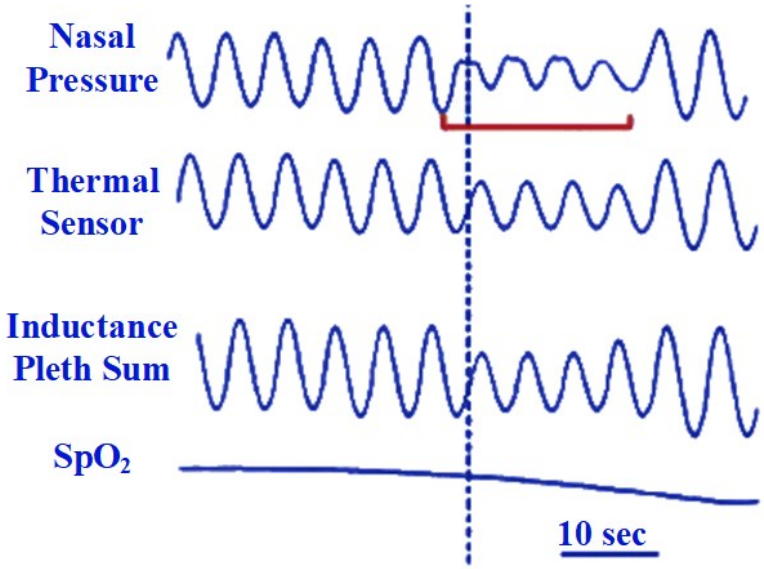

Figure 2.4 Hypopnea from different sensors.
Figure adjusted from [33]

Table 2.3 AASM Manual for scoring apneic events (adults) [38]

<table>
<tr><th colspan="5">Scoring Rules</th></tr>
<tr><td>Apnea Rules</td><td colspan="4">i. Peak drop in thermal sensor excursion by > 90% of pre-event signal baseline
ii. Duration of event > 10 seconds</td></tr>
<tr><td rowspan="4"></td><td colspan="4">Types of apneas:</td></tr>
<tr><td>Obstructive</td><td colspan="3">Respiratory effort during the event</td></tr>
<tr><td>Central</td><td colspan="3">Absence of respiratory effort during the event</td></tr>
<tr><td>Mixed</td><td colspan="3">Absence of respiratory effort at the beginning of the event but followed by respiratory effort during the second half</td></tr>
<tr><td>Hypopnea Rules</td><td colspan="4">i. Nasal pressure signal peak drop by > 30% of airflow pre-event signal baseline
ii. Duration of event > 10 seconds
iii. Occurs with an ≥ 3% arterial oxygen desaturation or an arousal</td></tr>
<tr><td rowspan="4">Severity criteria</td><td colspan="2" rowspan="4">AHI</td><td>Normal</td><td>< 5</td></tr>
<tr><td>Mild</td><td>5 - 15</td></tr>
<tr><td>Moderate</td><td>15 - 30</td></tr>
<tr><td>Severe</td><td>> 30</td></tr>
</table>

2.3.1.1 Demographics

OSA can be developed in all age groups, although the prevalence of OSA patients increases with age [36]. Moreover, the ratio of OSA between women and men is roughly one to two, but in the middle to older age after menopause in women, the difference is usually smaller [36].

2.3.1.2 Pathophysiology

Usually, OSA patients have reduced cross-sectional area of the upper airway lumen because of either soft tissues (tongue, soft palate, and lateral pharyngeal walls) or craniofacial anatomy, or in some situations, due to the reduction in both of them [36], as mentioned in the previous subchapter.

In the lumen of the upper airway during inspiration, a negative pressure is generated, promoting closure; but pharyngeal dilating muscles maintain patency [36]. During sleep, the activity of the aforementioned muscles decreases but sufficient to maintain an open airway [36]. Opposite, in OSA patients, pharyngeal dilating muscle activities become insufficient to maintain the open upper airway, and therefore narrowing the upper airway occurs [36].

As it is shown in Figure 2.5, the MRI shows three factors that are associated with OSA severity [2]:

- increased tongue size,
- increased size of lateral pharyngeal walls,
- increased total soft tissue volume.

During REM sleep, there is a further reduction in tone and phasic activity of pharyngeal dilating muscles, mainly in phasic REM, which contributes to more prolonged and more pronounced apneas and hypopneas [36].

The patient becomes more hypoxemic with the progress of the apneas and hypopneas events, where the degree of oxygen desaturation is dependent on the duration of the event, the patient's baseline oxygen saturation, lung volume, and the presence of comorbid lung conditions [36].

According to the performed longitudinal population studies, the severity of untreated OSA measured by the AHI index has the propensity to progress slowly over time [36].

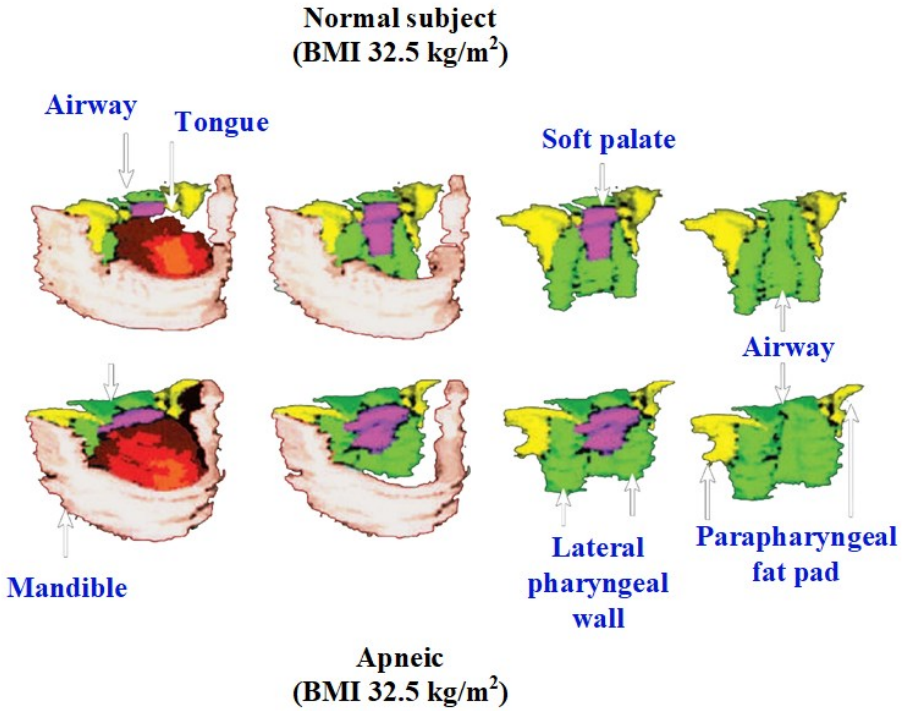

Figure 2.5 Representation of a volumetric reconstruction of axial magnetic resonance images in a normal subject and an apneic patient with the same body mass index (BMI) value.
It was shown that the airway is larger in the normal subject than in the apneic subject, and the tongue, soft palate, and lateral pharyngeal walls are larger in the patient with sleep apnea [2].
Figure adjusted from [45]

One of the earliest signs of OSA is snoring [46]. It is caused by the vibration of anatomical formation in the pharyngeal airway [47]. Thus, it can reveal the upper airway obstruction's location, site, and degree [47]. The pitch of the snoring sound caused by palate vibration is located in the low-frequency range, below 500 Hz, while the snoring caused by other sources is noisier and occupies the spectral sub-region above 500 Hz [47].

A high percentage of people are affected by snoring [48]. Snoring is caused by rapid reopening or obstruction in the upper airway [49]. Therefore, numerous snoring cases are leading to OSA syndrome. The upper airway is generally uniform for every human, where air can simultaneously enter through the mouth, nose, or both. After the mouth and nose, air enters the pharynx up to the larynx, the trachea, and the lungs. At the upper end of the pharynx, there is a soft palate responsible for closing off the nasal airway during swallowing and regulating the amount of air entering the nose during a speech, acting as a flap or valve [48].

The upper airway can be represented as a tube with upper and lower-end openings, where the tube is rigid at both ends but flexible in its mid-section [48].

The leading cause of snoring in a human adult is the soft palate flapping backward and forwards in the airway [48], [50]. More rarely, snoring can be caused by a collapse of the pharyngeal air between the soft palate and larynx [48]. The most effective technique for upper airway collapse treatment, except the surgical procedure (uvulopalatopharyngoplasty), is nasal CPAP. At the beginning of the snoring analysis investigation, in the paper, authors [48] explored the snoring caused by the soft palate's flutter and the pharyngeal airway's collapse and vibration. Comparing the snoring spectrum of the OSA subject and the simple snoring subject shows an evident difference in their spectrum (subject size: 17 male patients) [51]. For the OSA subject, the snoring sound is characterized by a low peak frequency, and the sound energy was scattered on a narrower band of frequencies; on the other side, for the simple snorer, the spectrum was characterized by the presence of fundamental frequency and several harmonics [51]. Healthy snorers' fundamental snore sound frequency is around 110 – 190 Hz, and for OSA patients is commonly higher than 800 Hz [51]. As they concluded in the paper, the maximum energy for OSA snorers is around the fundamental frequency, where maximum energy is defined as the upper frequency containing 90% of the total power of the spectrum. Moreover, their results show no identifiable harmonics for the OSA snorers.

One of the topics of the investigation was a comparison of the snoring sound-induced during nasendoscopy and natural sleep using snoring frequency spectra (subject size: 16) [52]. The palatal snoring obtained by nasendoscopy had a median frequency of 137 Hz, tongue-base snoring had 1243 Hz, and concurrent palate and tongue snore sound median frequency was 190 Hz. Furthermore, epiglottic snores had a peak frequency of 490 Hz. They have shown the tonsil vibration at the lower peak frequency – 170 Hz. Comparing the sample size of the 118 induced snores and 300 natural snore samples of the 12 palatal snorers indicated a significant difference in the power ratio and center frequencies (P=0.031 and P=0.049) of the induced and natural snore sounds. However, the peak frequency position was similar in both (P=0.34). As a result, they showed the existence of the higher frequency component of the sound during induced snores, compared with natural snoring, which is probably related to tongue-base snoring [52].

For surgical treatment to be successful, it is necessary to classify the vibrating tissue that affects the severity of snoring from the rest of it in the upper respiratory system. Therefore, there is a need for more profound research, as stated in the paper [53]. Mainly, there are four different excitation locations [53]. Despite the drug-induced sleep endoscopy (DISE) successfully classifying the vibration's location during sleep, it has several disadvantages. The first and foremost disadvantage is that it is performed during artificial sleep, which does not necessarily follow natural sleep [53].

Furthermore, DISE is invasive, time-consuming and expensive to use. Therefore, in recent years, the monitoring of acoustic properties during snoring has been investigated in many papers. It has been shown to detect and classify the snoring excitation location [53]. In general, several acoustic features are usually used to extract information from snoring sound for snoring detection and classification regarding excitation location, such as average power, spectral entropy, and power spectrum density [53]. Regarding the snoring excitation location classification, the [53] presented an overview of leading papers from 2002 to 2019 that successfully performed a classification task over several vibration locations caused by snoring. Usually, four classes were taken into account for the classification, called VOTE (velum-oropharyngeal-tongue-epiglottis). According to them, up to 2019, the best results regarding unweighted average recall (UAR) on four types of snoring (VOTE classification) was 74.19% [54]. Usually, snoring happens during inspiration, where the pressure in the collapsed upper airway increases as the degree of collapse increases; therefore, some soft tissues can vibrate and produce snores regarding the narrowed upper airway. Accordingly,

snoring can vary depending on the soft tissue vibration's degree of collapse and localization [53].

Early snore sound classification was based on palatal and non-palatal snoring, but today, researchers use the VOTE scheme classification [46]. [55] presented a five class-scheme entitled ACLTE-scheme with the 1115 snore sound samples from 343 subjects., where: A, V level, anterior-posterior vibration; C, V or O level, concentric vibration; L, O level, lateral vibration; T, T level, any vibration orientation; E, E level, any vibration orientation. They concluded that velum snoring is relatively common, while isolated tongue-base snoring is rare.

Sun et al. [53] proposed a new feature called trend-based MFFC (TTC) that, as they stand, outperformed the MFCC feature. The unweighted average recall (UAR) was 87.7% on the classification of 4 excitation locations applied on the Munich Passau Snore Sound Corpus (MPSSC) [56]. Furthermore, [53] directly applied the smooth-varying trend (adaptive and robust) to the amplitude spectrum for its “low-frequency component” approximation. Regarding the VOTE classes, the V type had 93% accuracy, the E class 96%, the O class 83%, and the T class 74%. Furthermore, they conclude that the V class can be easily distinguished from T or E and class E from classes V or O. But, on the other side, the difference between T and O and O and V can be challenging to distinguish. The reason for this lay in the physiological position of the individual types of snores. They took 484 V class, 216 O class, 39 T class, and 89 E class snore samples for method testing.

Qian et al. [46] bring an overview of the machine learning methods for assisting snoring sound excitation location. As they mentioned, snore sound analysis can be divided into three trends; where first was from 1990 to 2012 and included basic acoustic features calculation and analysis with statistical methods. The second trend was from 2013 to 2016 and included human-crafted features with the conventional machine learning models. Finally, the current and third trend was from 2017 up to today. It includes using deep learning models for extracting higher representation from snore sound or end-to-end learning from row snore sound signals (without human expert knowledge). Huang et al. [57] give a systematic overview of the investigation of the connection between snoring sound parameters and obstruction sites and analyze the prediction models methodology reported in recent papers. As they said, the prediction models were usually based on snoring sound parameters in the frequency domain. The systematic review took 28 eligible studies from 1016 retrieved

references. Xie et al. [58] introduce a snore detection method based on deep learning methods on the subject size of 38 patients. The study used five microphones placed around the bed in predetermined positions and investigated the algorithm's performance depending on the microphone placement. They achieved an accuracy of 95.3 ± 0.5%, with a 92.2 ± 0.9% sensitivity and specificity of 97.7 ± 0.4% (data set = 18412 sound events). According to them, comparisons of audio recordings with high accuracy and microphone placement do not significantly impact snore detection performance.

Gürpinar et al. [59] investigated the site of obstruction using DISE (subject size: 55). Subjects of the studies were divided into three groups regarding the level of obstruction: retopalatal (RP) obstructions, retolingual (RL) obstructions, and multilevel (ML) obstructions. They used mean pitch frequency, peak sound frequency, and fundamental frequency (F_o). According to their results, the difference between the features mentioned above was statistically different between all obstructions sites except RP and ML.

Sebastian et al. [60] presented an original work where they investigated a correlation between individual acoustic features and individual sites of collapse events (subject size = 58) by manually determining the site of collapse by analysis of the shape of the airflow signal during hypopnea events and corresponding snore sound segments from the audio signal. For each hypopnea event, they developed an ML algorithm that automatically annotated three sites of collapse: lateral wall, palate, and tongue-base. Performance was estimated using cross-validation, and the predominant site of collapse was determined from individual hypopnea annotations. For tongue/non-tongue collapse, the cluster analysis showed a mean silhouette coefficient of 0.79 and an accuracy of 68% for the classification task (non-tongue/tongue). However, the classification model based on linear discriminants achieved an accuracy of 81% for non-tongue/tongue and 64% for all collapse sites. Their results showed that snore signals during hypopnea could provide information regarding the predominant site of collapse in the upper airway.

Sebastian et al. [61] used an unsupervised algorithm for predominant site-of-collapse identification of the upper airway during natural sleep using nocturnal audio recordings. They have done simultaneous recording with PSG and ceiling microphones and extracted various snoring signal features during hypopnea events. Furthermore, they developed a feature extraction algorithm that combines silhouette analysis with the Laplacian score algorithm.

2.3.1.3 Comorbidities

One of the common findings within OSA is systemic hypertension [36]. Moreover, OSA is observed in patients with coronary artery disease, stroke, atrial fibrillation and type 2 diabetes, where a significant amount of accumulating data indicates that OSA is a risk factor for developing type 2 diabetes [36]. Furthermore, patients with a severe stage of OSA may have a substantial risk for pulmonary hypertension and cor pulmonale developing. Still, it is mainly daytime hypercapnia patients due to comorbid conditions such as chronic obstructive pulmonary disease (COPD) or severe obesity [36]. COPD and OSA regularly exist side-by-side, regardless of no typical pathophysiologic relationship [36]. However, patients with both disorders have significant nocturnal oxygen desaturation and daytime hypercapnia for the same degree of bronchial airflow obstruction, with a more significant risk of pulmonary hypertension and right heart failure development [36].

In addition, some OSA patients can have gastroesophageal reflux symptoms, nocturia, mood disturbance, and erectile dysfunction [36]. Further, the disorder can be related to some following motor parasomnias [36]:

- OSA-induced arousals from NREM sleep mimic a primary disorder of arousal;
- OSA-induced arousals from REM sleep mimicking REM sleep behavior disorder;
- OSA-induced arousals linked with a sleep-related eating disorder.

2.3.1.4 Obstructive sleep apnea features

Usually, apneic and hypopneas events occur in the N1, N2 and REM stages and less in the N3 stage [36]. Moreover, the more extended events by duration and association with a more severe decrease in oxygen saturation usually occur in the REM stage and when the subject sleeps in the supine position [36].

Furthermore, snoring that occurs between the apneas events is usually reported by bed partners and is defined as episodes of choking or hasping and body movements [36]. Usually, the patients feel tired in the morning regardless of sleep duration [36]. The apneas, hypopneas and snoring episodes can be worsened by the consumption of alcohol, usage of sedating medication before sleep or more considerable body weight [36].

The main predisposition of OSA development is obesity, with around 60% of moderate to severe OSA associated with obesity [36]. With increasing weight, the severity of OSA is

also increasing, with a high prevalence of OSA patients with morbid obesity [36]. Usually, OSA patients with normal or below-normal body mass index (BMI) have upper airway obstruction because of a localized structural abnormality (maxillomandibular malformation or adenotonsillar enlargement) [36]. Therefore, the neck circumference is commonly taken into account as the increase of it predicts higher AHIs [36].

In a nutshell, according to the [33], for scoring an event as an apnea, it must contain the following:

- peak signal excursion drops by ≥ 90% of the pre-event baseline,
- for scoring as OSA, it needs to be associated with continued or increased inspiratory effort during an entire period of absent airflow,
- for scoring as CA, it needs to be associated with absent inspiratory effort during the whole period of absent airflow,
- for scoring as MA, it needs to be related to the absence of inspiratory effort during the beginning of the event, but it resumes in the second portion of the event.

Additionally, there are a few more points regarding apnea scoring [33]:

- for scoring the apnea, it does not need to have a desaturation in the signal,
- if a part of the respiratory event that meets the criteria of hypopnea meets the criteria for apnea, the whole event needs to be scored as apnea,
- the event is computed in AHI if apnea or hypopnea begins or ends in an epoch scored as sleep, while if apnea or hypopnea occurs in an epoch scored as wake, it does not compute in AHI.

2.4 Sleep body positions

Sleep body posture categorization has been shown to help diagnose sleep disease and subsequent treatment. The best-known example is avoiding the supine position in a patient with sleep apnea syndrome, which can reduce the risk of disease progression [43].

According to the AASM, the most common sleep positions are [38]:

1) **Supine** (on your back): This position can help maintain a healthy spine and prevent wrinkles but it may be difficult for people who snore or have sleep apnea.

2) **On the side** (left or right): This position can help reduce snoring and sleep apnea and cause wrinkles and pressure on the muscles and joints.

3) **Prone** (on the stomach): Sleeping on the stomach is the least common position. This position can cause strain on the neck and back and may lead to wrinkles but it can also make breathing difficult and worsen snoring and sleep apnea.

However, the people in most cases are not strictly in a prone, supine, or side position; they are more in positions like those provided in Figure 2.6, such as foetus, log, yearner, and soldier positions, where [26]:

- **Foetus:** Sleeping all curled up into a ball with knees drawn up and chin tilted down;
- **Log:** On the side, arms at the sides;
- **Yearner:** On the side, arms out;
- **Soldier:** On the back, arms at sides;
- **Freefaller:** Face down;
- **Starfish:** On the back, arms up.

Moreover, it is worth mentioning that the positional effect persists in REM sleep but the frequency of the apneic events, according to the study [22], increases with REM sleep. The study was conducted on 60 male patients with sleep apnea syndrome.

Figure 2.6 Most common sleep positions.
Figure adjusted from [26]

2.5 Sleep quality parameters

The often-used sleep quality term is not clearly defined. In a narrower sense, it can be defined through the events that disturb sleep, such as spontaneous awakenings or apneas. Sleep quality is sometimes viewed as an aspect of sleep that is orthogonal to sleep quantity. In a broader sense, sleep quality can be defined through quantitative aspects of sleep and subjective aspects of sleep, or more precisely, variations in the experience of sleep itself, regardless of its quantitative aspects.

Objective **sleep quality parameters** derived from polysomnography include [62]:

- **total sleep time** (TST) – the overall duration of sleep stages when concatenated,
- **sleep latency** (SL) – the elapsed time to falling asleep from lying in bed,
- **sleep efficiency** (SE) – the ratio between TST and total time in bed,
- **wake-time after sleep onset** (WASO) – the summation of all awakening episodes during sleep,
- **awakening index** (AI) – the average awakening per hour.

Moreover, it is worth mentioning a **hypnogram**. It describes the sleep stages concerning time, as represented in Figure 2.7 [4]. Where sleep stage terminology in [33] is defined as:

- stage W – Wakefulness,
- stage N1 – NREM 1,
- stage N2 – NREM 2,
- stage N3 – NREM 3,
- stage R – REM.

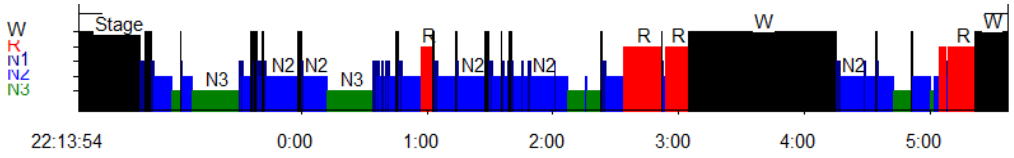

Figure 2.7 The representation of the hypnogram.
Figure was taken from a clinical report (Neuro PSG Report (Philips Respironics)

Regarding subjective sleep quality parameters, there are defined through the sleep questionnaires, such as:

- specific individual questions,
- sleep diaries,
- standardized sleep questionnaires.

Standardized sleep questionnaires, such as Pittsburgh Sleep Quality Index (PSQI), are the most commonly used. The PSQI measures seven components of sleep quality:

1. subjective quality of sleep,
2. latency of falling asleep,
3. duration of sleep,
4. usual sleep efficiency,
5. sleep disturbances,
6. use of pharmacological agents,
7. daily functioning.

Furthermore, Epworth Sleepiness Scale is usually taken during overnight sleep studies [36]. Moreover, the introspection of the own sleep condition can be conducted [2]:

- mood scales,
- fatigue scales,
- visual analog scales,
- Stanford sleepiness scale,
- Karolinska sleepiness scale.

In addition, it is good to be aware of sleep hygiene to understand sleep better. Sleep hygiene can depend on the surrounding sleep environment, the physiological state and the individual's behavior [63].

Chapter 3

Human body as a part of a communication propagation channel

Body-centric wireless networks (BCWN) have become one of the most prominent communication systems today, given their versatile applications across various fields [64]–[67]. Personal health care is the dominant field of application of BCWN communication systems, which examples include fitness tracking, vital signs detection, monitoring in daily life etc. [64]. Body-centric communications channels can be divided into on-body, off-body, body-to-body, and in-body, as shown in Figure 3.1.

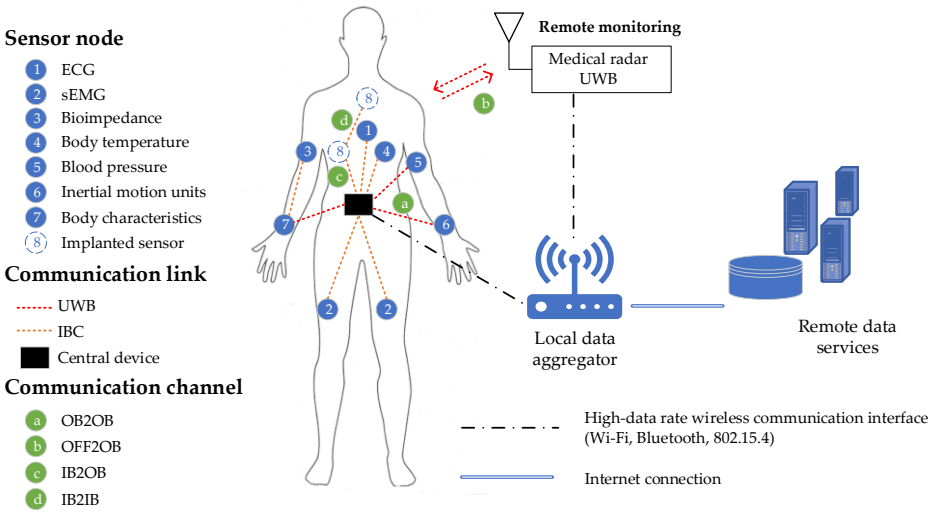

Figure 3.1 Body-centric wireless sensor networks topology of UWB and intra-body communication (IBC) wireless body area networks (WBAN) [68]

3.1 Ultra-wideband technology

In recent years, UWB technology has emerged as an alternative for short-range wireless communication to other widely used standard and protocols, such as Wi-Fi, Bluetooth, ZigBee etc. Its use is governed by IEEE 802.15.4a and IEEE 802.15.6 standards, as shown in Table **3.1** and Table 3.2. The primary difference and advantage of UWB technology compared to existing wireless technologies is its ability to transmit and receive data over a very large frequency range with very low power consumption, and with a low maximum effective isotropic radiated power (EIRP) spectral density of -41.3 dBm/MHz, as shown in Figure 3.2. This allows for high data rates and a high level of accuracy in measuring distances and detecting movements. In addition, UWB technology is less susceptible to interference from other wireless signals and is capable of penetrating through walls and other obstacles, which makes it well-suited for indoor positioning, motion tracking, and other applications where high accuracy and reliable connectivity are required. UWB technology is also known for its ability to operate in harsh or noisy environments, where traditional wireless technologies may struggle to maintain a reliable connection [69].

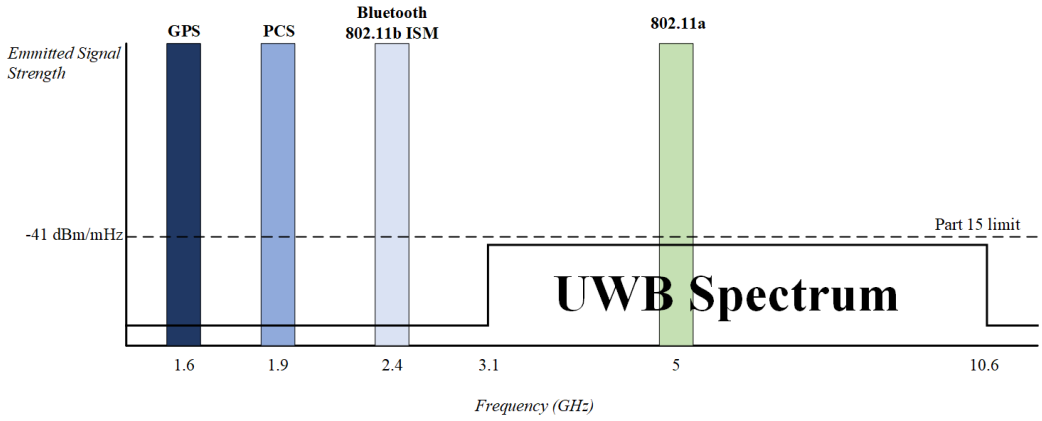

Figure 3.2 UWB spectrum and the FCC requirements

Moreover, UWB communication systems are of low complexity by design, low power consumption, and high data rate [64]. Therefore, it has a high resolution (typically in the range of centimeters or even millimeters), small antenna size (compared to other wireless technologies), and good penetration properties. Based on the above mentioned properties it can detect micromovement (such as breathing and heartbeat) and macro movements as a large human body movement [13].

Furthermore, experimental analysis in [70] showed that UWB systems do not affect human tissues and are not harmful to the human body, so that they can be used in various health clinical applications. In addition, it solves the effects of multipath fading, an essential feature in WBAN systems. Following all the aforementioned benefits of UWB technology, it proved to be a good candidate for wide use as a short radio communication solution for various medical and healthcare applications [68]. It is particularly suited for applications that require precise indoor localization, movement detection, vital signs detection, and capsule endoscopy to detect diseases. Besides healthcare application, the UWB technology can find practical applications in other fields, such as military applications, sports, security solutions, and entertainment sectors [64].

A wireless signal propagation channel can be described as a complex number with a real and an imaginary part. It characterizes changes in a radio signal, or more precisely, changes in magnitude and phase at different frequencies due to propagation from the transmitter to receiver over the specific wireless channel.

UWB signal is characterized by the property that it occupies bandwidth of 500 MHz or more and/or uses a bandwidth of 20% or larger than carrier frequency [71]. Some of the reasonss that UWB communication achieved great interest in academic research, as well as industry, are the following [71]:

- extremely low power transmission level,
- large bandwidth,
- high data-rate communications,
- low cost,
- ability to penetrate through various media (such as walls, biological tissues etc.).

The UWB communication can be considered in time domain or frequency domains. In this research the focus was on the use of UWB communication in time domain and the measurement of the UWB propagation channel impulse response (CIR), modulated by human body movements. CIR measurements made under such conditions, where human body is a part of the physical communication channel, are primary the quantity of interest to be measured to enable monitoring human subjects' parameters under test.

Table 3.1 IEEE 802.15.4a parameters and UWB PHY layer characteristics

Parameters	Typical Value
EIRP spectral density	– 41.3 dBm/MHz
Communication data rate	110 kbps, 850 kbps, 1.7 Mbps, 6.81 Mbps and 27.24 Mbps
Signal	Impulse radio UWB and CSS (chirp spread spectrum).
Pulse repetition frequency (PRF)	3.9 MHz, 15.6 MHz and 62.4 MH
Frequency range	3.1 up to 10.6 GHz
Number of communication channel	16

Table 3.2 IEEE 802.15.6 UWB PHY layer operating frequency bands

Band group	Channel number	Central frequency (MHz)	Bandwidth (MHz)	Channel attribute
Low band	1	3494.4	499.2	Optional
	2	3993.6	499.2	Mandatory
	3	4492.8	499.2	Optional
High band	4	6489.6	499.2	Optional
	5	6988.8	499.2	Optional
	6	7488.0	499.2	Optional
	7	7987.2	499.2	Mandatory
	8	8486.4	499.2	Optional
	9	8985.6	499.2	Optional
	10	9484.8	499.2	Optional
	11	9984.0	499.2	Optional

3.2 Fundamentals of ultra-wideband signal propagation

As stated in [71], the main constraints of UWB communications are determined by the propagation channel in which the system operates and by the complexity of the wireless propagation.

In the ideal situation, the signal is transmitted from Tx to Rx and back to Tx in a direct path called a **line of sight** (LOS). The total traveling time of the signal is called the time of flight (TOF). However, in the realistic scenario, the signal traveled from Tx to the Rx is composed of a direct path and additional signals reflected from different objects in the environment. The propagation of the RF signals during measurement is affected by **non-line-of-sight** (NLOS) conditions [72].

Therefore, the multipath propagation principle is defined as a signal propagation from the Tx antenna to the Rx antenna via different paths and interactions [71], as shown in Figure **3.3**. For example, the transmitter antenna sends a sum of components. Each component propagating to the receiver antenna might be reflected, diffracted, or scattered by objects in the communication channel [71]. As a result, each interaction with objects changes the direction of the propagating components. Furthermore, some interactions can split components into multiple new components, called **multipath components** (MPCs) [71]. The MPC can have a different path from Tx to Rx; depending on that, it has a specific delay, attenuation, and direction of arrival [71]. For the UWB channels, all the interactions with the objects are frequency-dependent, so the single MPC is not a Dirac δ function but a distorted pulse $\chi_i(\tau)$ [71]. Therefore, regarding [71], the channel impulse response (CIR) can be presented as:

$$\boldsymbol{h(\tau) = \sum_{i=1}^{N} a_i \chi_i(\tau) * \delta(\tau - \tau_i),} \qquad \textbf{(3.2.1)}$$

where a_i and τ_i are the gain and delay of the i-th MPCs, respectively.

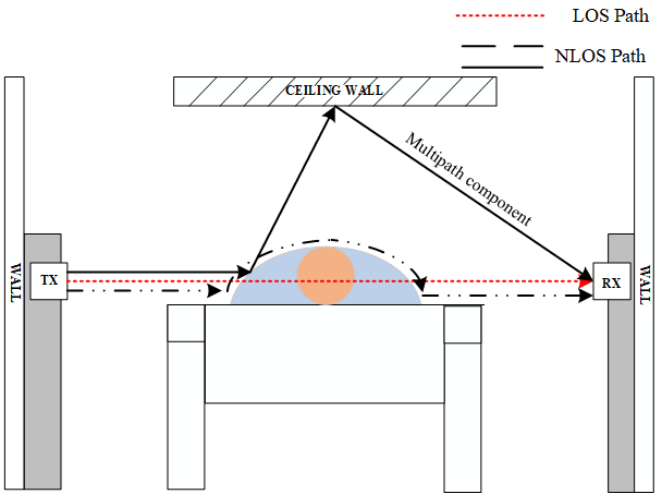

Figure 3.3 Multipath propagation principles in the indoor environment

The path of the UWB signals propagation, as well as other RF signals, can be divided into **static and dynamic paths**, where a static path is defined as a reflection and diffraction caused by stationary objects, and a dynamic path is caused by a reflection and diffraction with objects that are moving in an environment, such as people or smaller movements, such as chest movement [73].

Mostly, in the indoor environment, the objects are clustered in a group of individual objects separated in space and are not uniformly distributed. The clustering of the objects can be described as a clustering of the MPC, so the impulse response can be represented as shown [71]:

$$\boldsymbol{h(\tau) = \sum_{l=0}^{L} \sum_{k=0}^{K} a_{k,l} \cdot \delta(\tau - T_l - \tau_{k,l})}, \qquad \textbf{(3.2.2)}$$

and $a_{k,l}$ is the tap weight of the k-th components in the *l-th* cluster, and T_l is defined as a delay of the *l-th* cluster, and a $\tau_{k,l}$ is defined as a delay of the *k-th* MPC to the *l-th* cluster arrival of the T_l, L is the number of clusters and K is the number of MPCs in each cluster. Furthermore, the most popular model used in the UWB communications system, the **Saleh-Valenzuela (SV) model** [74], recommends that the T_l can be represented as a Poisson distributed variables, with interarrival rate Λ, where $1/\Lambda$ is in a range of 10-50 ns [71]. Afterward, the interarrival times are modeled within one cluster with an arrival rate β, as shown in Figure 3.4.

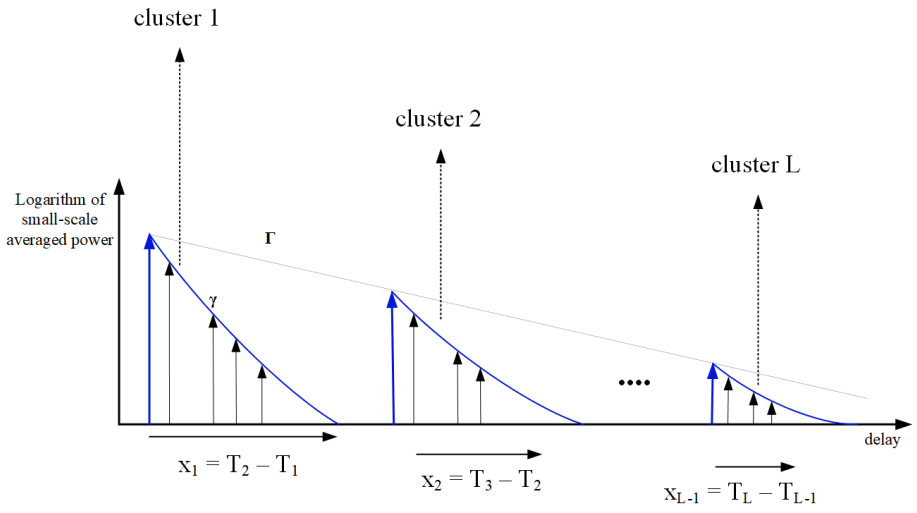

Figure 3.4 The representation of the Saleh-Valenzuela model.
Figure adjusted from [71]

In [75], the authors presented a multi-classification method to classify UWB signal propagation channels based on one-dimensional wavelet packet analysis (ODWPA) and

convolutional neural networks (CNN). They first decompose CIR into colored coefficients images employing a one-dimensional wavelet packet function. Then, they used images to train CNNs with different structures and selected CNN models with the best performance to identify the category of unknown UWB signal propagation channels. The experimental results for the various scenarios are always higher than 90% and up to 100%.

In [73], the combination of periodicity and variance features was used to select the projection coordinate axis to improve respiration monitoring robustness. Furthermore, it was stated that an accuracy of 97.25% was achieved for single-person respiration rate estimation in different sleeping positions under the NLOS scenario.

3.2.1 Dielectric properties of human tissues

The human body consists of different tissues with their own propagation characteristics. The main electrical properties of the human tissues are **electrical conductivity** (σ) and **relative permittivity** ($\mathcal{E}$). Relative permeability (μ) is equal to 1 because human tissues do not have magnetic properties; conversely, the electrical conductivity and relative permittivity are nonlinear, and frequency depends, which makes the human tissues propagation model more complex towards the detection of the respiration rate, the observed UWB signal propagated through four different tissue layers. The thickness of each tissue layer is different and affects the characteristics of the observed channel. The paper [70] provides the multilayer signal propagation model through the human body. It was concluded that along with the mentioned propagation characteristics, it is necessary to consider that the propagation velocity varies in different tissue layers, resulting in multiple reflections. This presents a significant challenge for analyzing signal propagation through the human body. In addition, it was mentioned that among the real part of the permittivity, loss materials (i.e., the human body) may have an imaginary part that significantly influences the calculation of propagation velocity, attenuation, reflection, and transmitting parameters. Consequently, most researchers consider the channel model homogeneous, without loss, to simplify the model calculation. The simulation results of the EM wave propagation through human tissues show that with higher frequency values, the value of the σ increases linearly, and Ɛ decreases linearly, as shown in Figure 3.6.

In the [76], results of the electromagnetic energy absorption in the two types of human tissue models are presented; the first one was homogeneous – consisting only of muscle tissues, and the second one was layered human body models consisting of the skin, fat and

muscle tissues at the frequencies of the 3,6 and 8 GHz. The distances between the human body and the antenna are 2, 5, and 10 mm. They concluded that the SAR ratio increases when the distance between the antenna and the human body increases. The maximum absorbed power is deposited in the skin layer when the fat thickness is around $\lambda/4$. The body surface between the air-skin boundary creates a large reflecting surface. As given in [77], the reflection coefficient is approximately 70 up to 80%, and blood, muscles, and bone tissue result in higher signal attenuation, unlike the spinal cord and bones. Human breathing causes chest movement in a range from 1 mm up to a few millimeters [78]. Figure 3.5 shows a 3D image of the chest anatomy and the two RF signal paths through the human body, depending on what is to be observed [11]. In the case of path selection shown with a green arrow, it will be easier to estimate heart rate (HR) because it minimizes the muscles' influence, increases the influence of bones, and propagates more energy to the heart, which has a larger permittivity [11]. The path shown by the white arrow decreases the distance between the radar and the lung. It improves the estimation of respiration rate (RR), thus, which is followed by changes in reflection coefficients during inhalation and exhalation [11].

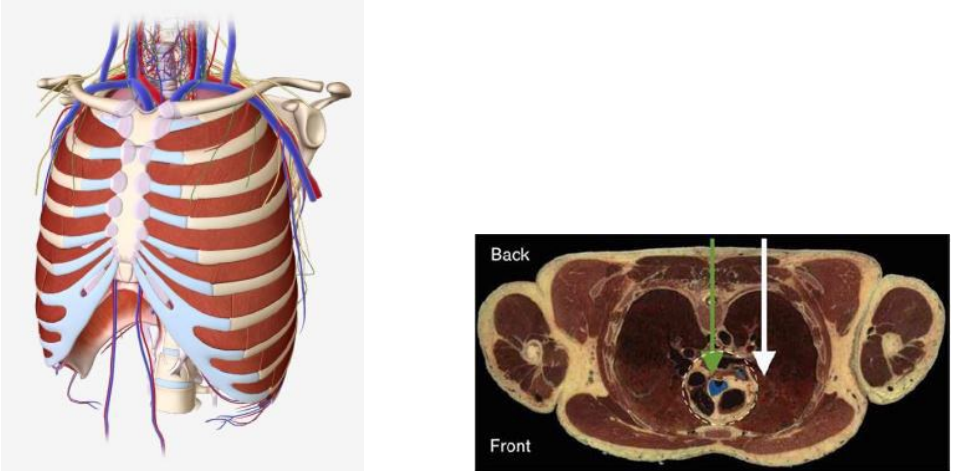

(a) (b)

Figure 3.5 (a) 3D view of the chest anatomy. Figure taken from [79];
b) Example of two RF signal paths through the human body. Figure taken from [11]

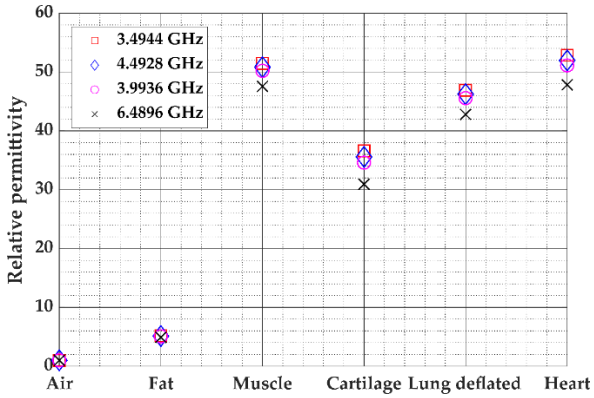

(a)

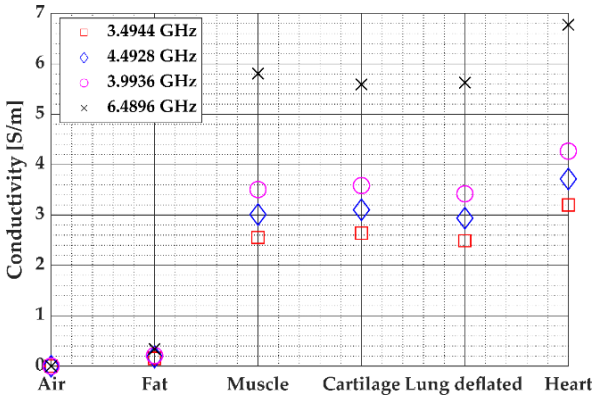

(b)

Figure 3.6 Relative permittivity (a) and conductivity (b) frequency dependence for different human body tissues [68]

Lazaro et al. [80] presented a mathematical formulation for breathing signal detection. Nguyen and Weitnauer [81] proposed a modeling framework for arbitrary periodic heart and lung motion. Furthermore, the mathematical model of vital signs by observing the changes in the propagating time delay and the echo signal was presented in [82].

3.3 Ultra-wideband technology in medicine

Applications of UWB technology in medicine can be divided into medical monitoring and imaging. Medical monitoring includes monitoring the patient's movements. This function can be applied in intensive care units, emergency departments, home care, pediatric clinics, or rescue operations after natural disasters and accidents.

In [83], a noncontact multiple targets vital sign detection method, using a variational mode decomposition (VMD) algorithm based on the UWB radar (NVA 6100) system, was

proposed. The respiration rates were tracked using a Hilbert transform, and the experiments successfully distinguished the vital signs of two targets.

Shen et al. [84] present a paper for a respiration and heartbeat rate measurement based on autocorrelation using an IR-UWB radar (PulsOn 410). The bandwidth of radar was 2.2 GHz, spanning a frequency range of 3.1 to 5.3 GHz and with a center frequency of 4.3 GHz. A subject was sitting on a chair facing the radar antenna, and the recording duration was 30 seconds.

Lee et al. [85] provided a system for heart rate monitoring using an impulse-radio ultra-wideband (IR-UWB) technology. They have used Novelda Xethru X4M06 radar to collect radar data.

UWB radar system for breathing and heart rate detection using feature time index with the first valley peak of the energy function of intrinsic mode functions (FVPIEF)-based two-layer EEMD was proposed in [86]. They have used a Time Domain UWB radar (4.3 GHz center frequency and a 2 GHz bandwidth). A participant was sitting in front of the radar in a stationary position.

In [12], a UWB radar system was presented for respiration rate detection and classification of the five types of respiration (eupnea, bradypnea, tachypnea, apnea, and during moving). They placed radar at 20 cm from the human chest while the person was lying on the bed in a normal state. The main limitations of the proposed study were the following: four of the breathing patterns were intentionally generated and collected within the range of a signal and during the awake state.

In [87], a person-specific heart rate estimation based on CNN using UWB radar was presented. They used a 79-GHz UWB multiple-input multiple-output (MIMO) radar system with 4 Tx antennas and 4 Rx antennas. The distance radar participant was 1.1 m.

Due to the high spatial resolution provided by the IR-UWB signal, it has been suggested for several medical applications [88], [89]. For increasing the SNR, the authors in [90] used range-bins weighted averaging (RBWA) of the targeted signal. Lauteslager et al. [91] used a Novelda X2 single chip radar.

In the literature most common radar used for contactless vital sign estimation are the following:

- CW Doppler radar,

- frequency-modulated continuous-wave (FMCW) radar,
- stepped-frequency continuous wave (SFCW) radar,
- impulse radio ultra-wideband (IR UWB) radar.
- millimeter wave radar [43] [92].

In [90], a low-cost, ultra-wideband radar system for detecting and monitoring respiratory motion during radiation therapy treatment delivery was presented. The authors presented an artificial neural network (ANN) model for recovering breathing motion patterns. A difficulty was that a gantry motion during recording causes substantial interference and affects the quality of the extracted respiration motion signal. Furthermore, they have used four breathing classes: no breathing, breath fold, free breathing, and deep inspiration. Additionally, they have got an excellent agreement with the reference data recorded with the respiratory motion phantom.

Table 3.3 gives the literature overview of the studies in the UWB vital signs monitoring application field.

Table 3.3 Literature Overview: UWB vital signs monitoring application

Ref., Year	Parameter	Algorithm	UWB system and Frequency	Experimental setup	Accuracy and Limitation
[93], 2008	HMT, RR	HHT	UWB noise radar 1–2 GHz	Through-wall detection of human movements	3 dB difference between breathing/no breathing
[94], 2010	HR, RR	Wiener filter	IR-UWB radar FCC compliant	Radar was directed toward the human	The subject was holding his breath
[95], 2012	HR, RR	Wavelet transform; filter banks	Generated UWB waves Central freq. 4.7 GHz	It was assumed that only thorax of the subject was dynamic part	The influence of the RBM was not investigated
[96], 2014	HR, RR	SHAPA algorithm	IR-UWB radar Central freq. 4.1 GHz	Eight subjects, lying on the top of a mattress	Practical for a real-time system
[97], 2014	RR	MA filter Time delay	NRM400 UWB radar Central freq. 4.3 GHz	Sleep apnea detection	The influence of the RBM was not investigated
[98], 2014	Human Heart Motion	Time-lapse imaging	Switched Array UWB r. 0.75–2.27 GHz	Antenna was aligned with the body	The subject was holding his breath
[99], 2015	HR	FFT	IR UWB CMOS radar Central freq. 5 GHz	Noninvasive heartbeat extraction	Under controlled conditions
[100], 2016	RR	VMD algorithm	NVA6100 chip CMOS r. 0.85 to 9.55 GHz	Through-wall multiple targets tracking	Investigation of the complex experiments
[101], 2016	HR, RR	EEMD;CWT	IR-UWB radar Central freq. 6.8 GHz	Sitting in a chair and breathing regularly	SNR of RR and HR improved by 7.59 dB and 4.82 dB
[102], 2016	HR	Phase-Based	UWB Impulse Doppler r. 1.5 – 4.5 GHz	Subject sat still in front of the radar system	CSD and AD heart rate deviation was 2.6% and operating rate was 0.8 m
[103], 2016	HR	Cascade convolutional neural network	NVA-R661 IR-UWB radar module	HR analysis by combination of the ECG and radar features	Results accuracy of 88.89% in the slight motion state

[104], 2017	HR, RR	Autocorr., FFT Kalman filter	NVA6201 IR-UWB Central freq. 6.8 GHz	Signal reflected from the chest and from the back	Retains the last valid measurement in stationary condition
[105], 2017	HR, RR	FFT	NVA6201 IR-UWB radar Central freq. 6.8 GHz	Human body motion while driving	single IR-UWB radar and the mobile phone usage
[11], 2018	HR, RR	Phase-based and freq. estimation	Ventricorder IR module 3.8 to 9 GHz	In-body monitoring of lungs and heart motion	Static and dynamic experiments
[106], 2018	HR, RR	FVPIEF based Two-Layer EEMD	UWB radar Central freq. 4.3GHz	Simultaneously analysis of RR and HR	Relatively accurately
[107], 2018	HR, RR Subject location	Autocorr. VMD; FFT	PulsOn410 UWB radar Center freq. 4.3 GHz	Vital signs monitoring	Potential implemention in integrated circuits and embedded systems
[108], 2019	HR Subject position	CFAR algorithm	XK300-MVI radar 7.29 – 8.748 GHz	Clinical application	Quantified index to clinically record
[109], 2019	RR	1D CNN model	UWB radar 3 – to 4 GHz	Eupnea, bradypnea, tachypnea, apnea, and motion classification	Average recognition rate of respiration patterns 93.9%
[110], 2022	Respiration	Spectrogram and CNN	UWB radar (Novelda X4) 4.1–10.3 GHz	Normal, speaking, apnea classification	F1-score 0.79, Specificity 0.9, Precision 0.86
[111], 2022	HR and RR	1D CNN	UWB radar (XeThru X4M03)	Vital signs monitoring	80-percentile HR/RR errors of 7.4/4.9 beat/breaths per minute (bpm)
[112], 2022	HR	CNN-SVM	UWB radar (Novelda X4) 4.1–10.3 GHz	Vital signs monitoring	Average HR error rate 2.32%

3.3.1 Ultra-wideband technology in sleep medicine

One of the pilot studies from 2018 regarding the use an impulse radio ultra-wideband radar technology as a sleep assessment was presented in [17]. They have used a Novelda Xethru radar on the 12 participants on the overnight seep. The radar placement was on the bedside table or a photo tripod placed along the head of the subject facing diagonally downwards to the feet [17]. According to the pilot study, it can be concluded that UWB radar is a promising tool for practical sleep parameters analysis, with accuracy, sensitivity, specificity, and Cohen kappa 0.931, 0.961, 0.695, and 0.670, respectively. The study did not consider the influence of body position during sleep; more precisely, the time interval in which the movement of patients occurs was excluded from the performance measurement of the proposed system.

One of the first clinically verified noncontact OSA screenings was proposed by Alekhin et al. [113]. In the paper, the bioradiolaocation signals breathing patterns (BSBP) were used for the OSA screening, employing a wavelet transform (WT) and neural network (NNW) applications. Furthermore, the three classes of breathing patterns, OSA, central sleep apnea (CSA), and normal calm sleeping (NCS) without sleep-disordered breathing episodes, were used.

Kagawa et al. [114] presented a non-contact screening system for OSA based on two Doppler radars and applied a time-varying baseline method with hypopnea-detecting techniques. In the paper, two Doppler radars were used to capture chest movement and the other for abdominal movements. Furthermore, the OSA was detected as paradoxical movements between the chest and abdominal radar signals.

Javaid et al. presented a non-contact system for OSA screening based on under-the-mattress IR-UWB radar [14]. Four subjects were included in the paper, 25 hours of data were obtained, and the proposed system was compared with the PSG. An accuracy of around 70% was obtained using cross-validation to detect apnea and normal epochs. Moreover, the 14 moment-based features and time-domain principal components-based features that exploit the start and stop times of apnea periods were used in the paper.

In [115], an adaptive segmentation algorithm for the breath sounds of patients with obstructive sleep apnea was presented. The proposed algorithm divides the breath sounds into segments with similar amplitude levels by creating an envelope of the signal. It then applies

the K-means clustering to detect the borders between different segments in the envelope signal and then uses it to segment and normalize the original signal.

In the [113], the discrete fast wavelet transform method (mean-squared values of WT detailed coefficients of each BRL signal quadrature) was used for the feature extraction method and classification of the patterns. Finally, the neural network classifier was applied to distinguish three breathing patterns: normal breathing, OSA, and CSA. One of the main contributions of the [113] was the proposed attribute vector, which was constructed from the BRL signal quadratures, and expressed as follows:

$$\boldsymbol{V_j = \sqrt{\left(d_j^Q\right)^2 + \left(d_j^I\right)^2},} \qquad \textbf{(3.3.1.1)}$$

where the V_j is the attribute vector of the BPBS resulting components, j is the current number of the V_j, d_j^Q and d_j^Q is the detailed wavelet coefficient for the Q and I quadrature of the BRL signal, respectively.

Hu and Jin [82] presented short-range vital signs sensing system based on IR-UWB radar. They used an improved ensemble empirical mode decomposition (EEMD) for a noise reduction method. For a vital sign separation (breathing and heart rate) method, they used a continuous wavelet transform (CWT).

In [116], the apnea detection method based on wavelet information entropy spectrum using a bio-radar was proposed. The bio-radar was placed at a distance of 2.5 m above the bed. They recorded 10 OSA patients in a controlled environment for one hour.

El-Barden et al. [117] used an IR-UWB radar (central frequency of 3.9 GHz) to continuously monitor a resting subject's respiration and heart rates.

Lin et al. [20] presented SleepSense, a noncontact sleep monitoring system for continuous recognition of sleep status (on-bed movement, bed exit, and breathing section). It consisted of the Doppler radar-based sensor, a robust automated radar demodulation module, and a sleep status recognition framework. They used short-term controlled experiments with an overall accuracy of 95.1% and a 75-minute sleep study in real life, where the breathing extraction rate was 6.65%. Regarding the features extraction for sleep status categorization, several features were used, including two statistical features, two frequency domain features, and a non-linear time-series feature, more precisely, root mean square (RMS), mean crossing rate (MCR), energy, mel-frequency cepstral coefficients-based coefficients (MFCC based

coefficients), and sample entropy. A detailed algorithm for vital sign monitoring on stationary and non-stationary humans based on IR-UWB was presented in [104].

In [118], an under-mattress bed sensor (UBMS) for capturing nocturnal body movement information was presented. The slow turn and higher intensity posture shifts are included in nocturnal movement information. The UBMS system consists of a grid of 24 fibre optic-based pressure sensors, or tactless, integrated into a lightweight 1 cm x 90 cm x 23 cm foam mat. The paper validates the algorithms regarding movement-related features (statistical, spatial, and spatiotemporal) extraction. Furthermore, the typical nocturnal bed movements were explained and separated into the following categories [118]:

1) Large body movements
    a. Postural shifts
        i. Quick postural shifts
        ii. Quick postural shifts with a corresponding mediolateral change in position
        iii. Slow rolling movement
    b. Movement-related arousals
2) Small body movements
    a. Breathing
    b. Heart rate

Lazaro et al. [80] presented a paper on sleep apnea detection and breathing rate signal processing technique based on an IR UWB radar system. The paper tried to solve the main problems of clutter suppression, body movement, and body orientation detection. Clutter suppression was solved by using a moving average filter to estimate it dynamically, and the body movement artifacts were removed using a threshold method before breathing signal analysis. In addition, the motion was detected using a time delay after clutter removal, maximizing the received signal. In the period of the signal where standard deviations of the time delay are above a threshold are considered macro-movements, and they are neglected. Sleep apnea intervals are detected if the signal was below the threshold for at least 10 seconds [80].

Additionally, the breathing rate was estimated using a Lomb periodogram algorithm from the spectrum. The proposed system in the [80] was compared with signals recorded by a microphone. The body–antenna distance was about 1 m, and the distance between the

transmitter and receiver is 65 cm. The central frequency was set at 4.3 GHz with 1.3 GHz bandwidth and a pulse repetition frequency (PRF) of 10 MHz. The experimental results were obtained one only one healthy patient, and the conditions and positions were simulated, like breathing continuously and holding the breath.

Long et al. analyzed the respiratory effort amplitude based on the PSG recording. They proposed a set of 12 features that reflect respiratory depth and volume that can help classify sleep stages. The 48 healthy subjects were included in the study, and a linear discriminant classifier was used within accuracy and Cohen's Kappa coefficient of agreement as evaluation methods. Using 10-fold cross-validation, it was shown that adding features set to an existing improved the results. For REM, light, and deep sleep stage, classification values of Kappa and accuracy were 0.38 and 63.8%, and in classifying wake, REM sleep, and NREM sleep, values of Kappa and accuracy were 0.45 and 76.2%, respectively. The 10th-order Butterworth low-pass filter with a cut-off frequency of 0.6 Hz was used for the preprocessing stage. In the time domain, Long et al. [119] calculated the mean and SD of breath lengths(L_m and L_{sd}) and the mean and SD of breath-by-breath correlations (C_m and C_{sd}).

Furthermore, from the frequency domain, features based on the respiratory effort spectrum for each epoch were estimated using a short-time Fourier transform (STFT) with a Hanning window. In addition, the dominant frequency (F_r) in the 0.05 – 0.5 Hz range, logarithm of its power (F_p), spectral power in the very low-frequency band between 0.01 and 0.05 Hz (VLF), low-frequency band between 0.05 and 0.15 Hz (LF), and high-frequency band from 0.15 to 0.5 Hz (HF) and the ratio between LF and HF spectral powers (LF/HF) were calculated. Also, the standard deviation of respiratory frequency over five epochs (F_{sd}) was computed. Regarding the non-linear features, self-similarity was measured between each period of interest. The other epochs used dynamic time and frequency warping (S_{dtw} and S_{dfw}), and signal regularity was estimated by sample entropy (R_{se}) was calculated. Moreover, the paper [119] observed that the envelopes formed by the peak and trough sequences of the signal during wake and REM sleep were more irregular and had a lower absolute mean or median and larger variance compared with those during light and deep sleep. Furthermore, the five depth-based features were extracted from the peak and trough sequences of the respiratory effort signal.

Set of the features set, f_k; $(k=1,..15)$, from time and frequency domains were presented in [14]. In the paper, the process of feature extraction was divided into two phases, where the

first phase was a first- and second-order moments of various quantities extracted directly from each episode, and the second phase consists of two features extracted after the application of principal component analysis and signal processing algorithm [14]:

1. f_1: mean absolute deviation (MAD) of a respiratory signal
2. f_2: mean absolute deviation of the maxima or peak values of a respiratory signal
3. f_3: number of times the signal crosses the mean
4. f_4: variance of the time duration (number of samples) between the points where the signal crosses the mean
5. f_5: variance of the number of samples between local maxima and the next local minima in an epoch
6. f_6: variance of the difference in amplitude of local maxima and next local minima in an epoch
7. f_7: inter-quartile range, i.e., the difference between the 75th and 25th percentiles of the number of samples between mean crossings in each epoch
8. f_8: sum of power spectral density (PSD) values in the frequency range [0-0.5 Hz] for each episode
9. f_9: Variance of $\sigma_{\varepsilon_i}^2$ (variance of the 10 second interval –i = 1,2,...,6)) values across the small epochs ε_i, i.e., $var\left(\left[\sigma_{\varepsilon_1}^2, \sigma_{\varepsilon_2}^2, \dots, \sigma_{\varepsilon_{i6}}^2\right]\right)$
10. f_{10}: Variance of absolute difference of $\sigma_{\varepsilon_i}^2$ across ε_i ,i.e., $var\left(\left[\left|\sigma_{\varepsilon_1}^2 - \sigma_{\varepsilon_2}^2\right|, \left|\sigma_{\varepsilon_2}^2 - \sigma_{\varepsilon_3}^2\right|, \dots, \left|\sigma_{\varepsilon_5}^2 - \sigma_{\varepsilon_6}^2\right|\right]\right)$
11. f_{10}: DFT calculated for the small epoch and frequency $f\varepsilon_i$ corresponding to the highest peak for each small epoch ε_i. Variance σ_f^2 of the highest frequency for each small epoch was represented as a $\sigma_f^2 = var([f\varepsilon_1, f\varepsilon_2, \dots, f\varepsilon_6])$

Furthermore, the following year, Javaid et al. presented a similar paper [16] where they added snore features and improved performance by around 5%, which was not sufficient to say that it improved a lot in comparison to taking only features from IR-UWB radar.

The autocorrelation function of the short-term energy sequence *XcorrPeaksSTE* feature was calculated using the coefficient of determination (R^2) achieved when applying a 0.3 Hz sine wave curve fitting to the autocorrelation function [120].

Tataraidze et al. [21] presented a bioradiolocation-based sleep stage classification (wakefulness, REM, light and deep sleep). It was validated using data from 32 subjects without sleep-disordered breathing who underwent a PSG study in a sleep clinic. The results showed Cohen's kappa coefficient of 0.49 in the wake-REM-light-deep sleep classification, 0.55 for the wake-REM-NREM classification and 0.57 for the sleep/wakefulness determination.

One of the most prominent research groups in the field of capturing nocturnal breathing signals using wireless signals is Dina Katabi's research group from the Department of Electrical Engineering and Computer Science, Massachusetts Institute of Technology (MIT). Their research interest can be divided into the following:

- RF-based fall monitoring [121]
- Pose estimation [122]
- Indoor Localization [123]–[125]
- Sleep monitoring [126]–[128]
- Insomnia Monitoring [129]
- Emotion recognition [130]

They have used FMCW and an antenna array in most of their research [127], [129]. Their last publications and research focus were on detecting and assessing Parkinson's disease (PD) using nocturnal breathing signals [131], [132]. In [131], they used two sources of a dataset (wireless signal and breathing belt). They developed an AI model that predicts PD severity based on e Movement Disorder Society Unified Parkinson's Disease Rating Scale (MDS-UPDRS) positive or negative answer for detecting PD. Moreover, several dataset sources have been used in research, containing an overall of 11,964 nights with over 120,000 h of nocturnal breathing signals from 757 PD subjects.

In [133], the feasibility of adapting RGB-based unsupervised representation learning for leveraging RF signals and through-wall pose estimation, action recognition, scene captioning, and human re-identification was presented. As they mentioned, the advantage of the RF signals in comparison with the RGB data was that they can traverse walls and occlusion and work in the daytime and the darkness. Moreover, they are not human-interpretable; that is, in the case of privacy preservation, great advantage [133].

One of the interesting research regarding contactless in-home monitoring of the respiratory and behavioral phenotypes in adults with COVID-19 was presented in [134]. They

have collected results from continuous monitoring of the three residents of an assisted living facility for three months (through the disease and recovery phase). Overall, 4.358 measurements of gait speed, 294 nights of sleep, and 3.056 hours of respiration were collected. They concluded that there was a difference between respiration signals between asymptomatic and symptomatic patients.

The DeepBreath system based on FMCW radio equipped with an antenna array was presented in [128]. As they stated, it was the first RF-based respiration monitoring system to recover respiration from more than one person. First, they synthetically modeled interference due to multiple reflected RF signals and demonstrated that they could recover individual breathing utilizing independent component analysis (ICA). Afterward, they conducted 21 nights of sleep and over 150 hours of data from 13 couples who shared the bed and applied the implemented model. They have conducted an evaluation performance, but with a lot of constraints taken into account, so the exact error rate cannot be distinguished.

Furthermore, the same research group from MIT presented a system called BodyCompass for sleep posture monitoring using a wireless signal [127]. They evaluated a system using over 200 nights of sleep data from 26 subjects in their own homes, with 94% accuracy for one week of the data, one night of the data with an accuracy of 87%, and 16 minutes of labeled data from the subject have 84% accuracy.

The research group that is very prominent in the field of using UWB technology for sleep monitoring is Sung Ho Cho's lab from the Hanynag University, Seoul, South Korea [13], [104], [135]–[137]. In [135], the comparison of the IR-UWB radar with the PSG results was presented. They collected data from 6 healthy volunteers and 15 patients with suspected OSA and measured the success of the heart rate (HR) and breathing rate (BR) detection. For the normal and mild OSA, the obtained BR and HR intraclass correlation coefficients R (ICCR) compared with the PSG were 0.959 and 0.957, and 0.927 and 0.926, respectively. The results were slightly worse for moderate and severe OSA; BR ICCR were 0.957 and 0.873; HRs ICCR was 0.907 and 0.799. They have used a single IR-UWB radar sensor, XK300-VSA, by placing it 0.5 m above the head side of the bed.

Furthermore, in [13], they presented a non-contact solution for diagnosing OSA based on the IR-UWB radar. Ninety-four subjects were included in this study, where 23 controls and 24, 14, and 33 with mild, moderate, and severe obstructive sleep apnea, respectively. They have defined an abnormal breathing index (ABI) as equivalent to an AHI index obtained from

the PSG ground truth device. As a result, an agreement between the ABI and AHI, a more precise intraclass correlation coefficient was 0.927. For mild OSA, it was 0.93; for moderate OSA, 0.91; and for severe OSA was 1.

Nevertheless, it is worth mentioning, that accuracy for respiratory events detection was 0.868, and the precision for a control group of a patient was 0.74, for mild 0.79, or moderate 0.78 and severe 1. Also, in this research, the single IR-UWB radar sensor, XK300-VSA, was used and placed 0.5 m above the head side of the bed. The benefit of the proposed research was the size of the dataset. However, they have done research with the radar on the fixed distance and did not go into details about the movements and respiratory events classifications.

One of the two radar solutions mainly used in non-contact vital signs monitoring is IR-UWB and FMCW (frequency modulation continuous wave) radars. As stated in [138], the main differences with the IR-UWB radars are that the FMCW requires phase information for vital signs estimation, and it is usually enhanced to multi-input multi-output (MIMO) antenna topologies. Moreover, as experimentally showed in [131], IR-UWB radars had better accuracy and higher SNR than FMCW radar.

In Table 3.4, an overview of the state-of-the-art sleep monitoring methods was provided.

Table 3.4 Overview of the state-of-the-art sleep monitoring methods

Authors	Year	Data Info	System	Parameters/Methods	Results
Walsh et al. [118]	2011	Two healthy adults with possible sleep disorders in a clinical setting	Under Mattress Bed Sensor	Extraction of the **bed restlessness**, spatial description of movement, and spatiotemporal description of each in-bed body movement	No quality accuracy – just quantity description of the individual features data
Lazaro et al. [80]	2014	1 healthy patient	NRM400 UWB radar from TimeDomain impulse-radio (IR) ultra-wideband radar center frequency of the radar was around 4.3 GHz and its bandwidth was 1.3 GHz	Breathing rate and sleep apnea detection Moving average filter Threshold methods Time delay method Lomb periodogram algorithm CFAR technique was used to estimate the decision threshold.	Results obtained show that this technique may be particularly suitable for overnight sleep apnea monitoring
Kagawa et al. [114]	2014	31 outpatients at a hospital	Two Doppler radar	Time-varying amplitude baseline method	Respiratory disturbance indexes obtained from radars correlated with 90% accuracy with those from PSG
Javaid et al. [14]	2015	4 patients with OSA (25 hours of data)	Under the mattress IR-UWB radar; 4.2 GHz central frequency, transmitted pulses are 13 ns long	Linear Discriminant classifier 14 moment-based features, with a time-domain PCA based feature	70% in detection of apnea and normal epoch
Qi et al. [116]	2017	10 OSA patient	Bio-radar (24 GHz)	Apnea detection method based on wavelet information entropy spectrum	Apnea detection accuracy for bio-radar signal was 93.1%, and for PSG signal reach 96.1%

Pallesen et al. [17]	2018	12 participants overnight study	Novelda XeThru model X2 IR-UWB pulse-Doppler radar		Mean values obtained for accuracy, sensitivity, specificity, and Cohen kappa were 0.931, 0.961, 0.695 and 0.670, respectively.
Kang et al. [13]	2020	94 subjects	IR-UWB radar	Abnormal breathing detection	intraclass correlation coefficient = 0.927
de Goederen et al. [139]	2021	32 children (clinical PSG data) from 2 months up to 14 years	Body movement and breathing rate based on the UWB radar X2M200 and X4M200 radar modules	38 features from the motion signals and breathing rate AdaBoost algorithm (estimation of sleep stages)	Cohen's Kappa coefficient of 0.67 with overall accuracy of 89.8% for wake and sleep classification; 0.47 and 72.9% for wake, REM sleep, and non-REM sleep, and 0.43 and 58.0% for wake, REM sleep, light sleep and deep sleep
Bin Kwon et al. [140]	2022	36 recordings	IR-UWB radar	Hybrid CNN -LSTM	Cohen's kappa coeffcient of 0.728, sensitivity of 0.781, specifcity of 0.956, and an accuracy of 0.930.

Chapter 4

Method for measurement of sleep breathing patterns and postural transitions based on UWB communication CIR measurements

Method for measurement of sleep breathing patterns and postural transition based on UWB communication CIR measurement was divided into two phases. To investigate the proof of concept of measuring respiration rate using information from the UWB CIR, short-term and laboratory-controlled respiration rate measurements were done with a pair of nodes of modified DWM1000 modules, detailed in Chapter 4.1. Afterward, a modified version based on two pairs of nodes of DWM1001 modules was used for a clinical study using a *Sleep-UWB platform*, detailed in Chapter 4.2. Moreover, additional details along with the measured parameters.are described in Chapter 5.

The DWM1000 and DWM1001, shown in Figure 4.1 and Figure 4.2, are both UWB transceiver modules with similar capabilities, but there are some key differences between the two models. One major difference is that the DWM1001 includes an integrated Nordic Semiconductor nRF52832 Bluetooth Low Energy (BLE) chip, which provides Bluetooth connectivity [141]. Another difference is that the DWM1001 operates at a lower power level compared to the DWM1000, which makes it well-suited for battery-powered applications. Despite these differences, both models are capable of transmitting and receiving data over a wide frequency range with high accuracy.

The core of both developed platform was Decawave DW1000, a single-chip wireless transceiver based on UWB technology which is compliant with the IEEE802.15.4-2011 standard [141]. Some of the main characteristics of DW1000 integrated circuit are: high data rate communications (up to 6.8 Mbps), immunity to multipath fading, and low power consumption (can range from 4.9 mA to 27.2 mA in different operating modes). The Decawave DW1000 supports six frequency bands with central frequencies from 3.5 GHz up to 6.5 GHz. In the both measurement setup only the channel 4 was used (Table 4.1), with a central frequency of 3.9936 GHz and bandwidth of 499.2 MHz, as the channel with the highest bandwidth and the lowest central frequency. Moreover, the same communication protocol was employed for both of the measurement setup to ensure consistency across the measurements. Furthermore, in the measurement setup, the maximum peak power limit of 0 dBm/50 MHz and the maximum allowed transmit power of - 41.3 dBm/MHz was set, based on the regulations set by the FCC.

Table 4.1 DW1000 - UWB PHY channel frequencies [142]

Channel Number	Center frequency (MHz)	Bandwidth (MHz)
1	3493.4	500
2	3993.6	500
3	4492.8	500
4	**3993.6**	**900**
5	6489.6	500
7	6489.6	900

It is important to note that DW1000 implements in hardware an estimate of the channel impulse response (CIR), which is available at the Rx side. CIR is a sum of the delayed multipath components (MCPs) of the observed radio channel. The output of the radio channel can be calculated as a convolution of the transmitted signal *x(t)* and channel impulse response *h(t)*, and transmitted noise *n(t)* [143]:

$$\boldsymbol{y(t) = x(t) * h(t) + n(t)}, \tag{4.1.1}$$

where CIR is [144] in three-dimensional environmental was presented as:

$$\boldsymbol{h(t) = \sum_{k=0}^{N-1} a_k e^{j\theta_k} \delta(t - \tau_k)}, \tag{4.1.2}$$

where N is the number of multipath components, the a_k is amplitude, τ_k is propagation delay, θ_k is the signal phase of the *k-th* MCPs and δ are Dirac delta function.

The CIR is a key concept in UWB technology that refers to the response of the communication channel to a short pulse. When a UWB pulse is transmitted from a source, it propagates through the communication channel and interacts with the channel's characteristics, such as reflections, scattering, and other phenomena. The CIR is a mathematical function (Eq. (4.1.2)) that describes the channel's response to this pulse and provides information on the time-varying channel behavior, including delay spread, multipath components, and other propagation effects. The CIR is obtained by correlating the received signal with the transmitted pulse, and it is used to extract relevant information about the transmission medium and its impact on the signal.

In DW1000 on the receiver side the signal was continuously conditioned by the filter via an integrated antenna. Then, by analog to digital converter (ADC), the conditioned signal was periodically digitized as a series of ternary samples [145].

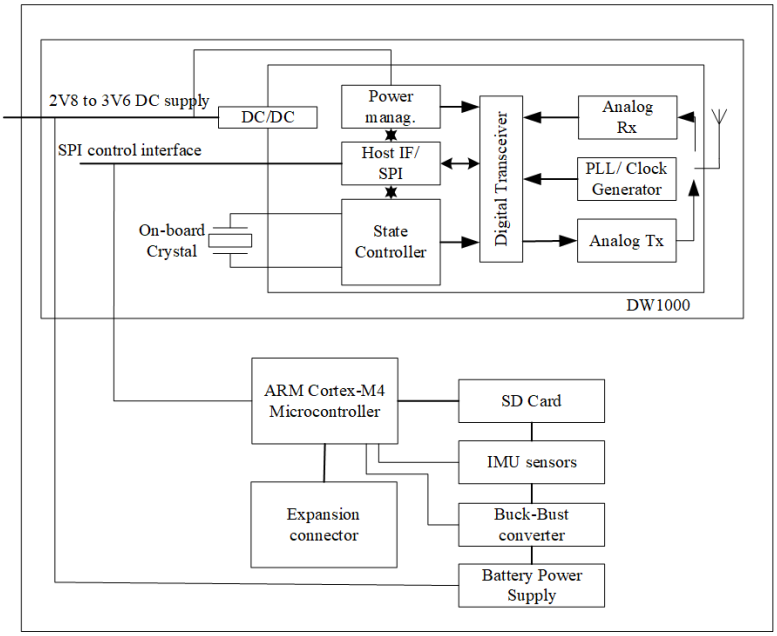

Figure 4.1 *UWB platform*: DWM1000 module block diagram [141]

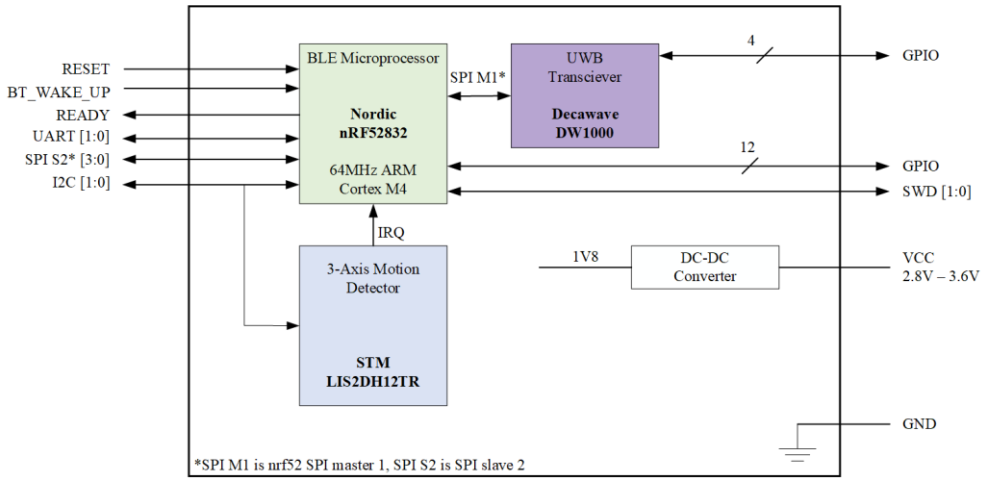

Figure 4.2 *Sleep-UWB platform*: DWM1001 module block diagram [146]

4.1 *UWB Platform*: Vital signs detection and monitoring

It has been shown that even a small displacement of a person's chest during respiration can change the magnitude or phase of the observed CIR measurements [28], [29], [68], [147]. Therefore, the feasibility of the proposed approach was experimentally tested using a developed platform based on UWB technology [68], [147], [28], [29]. In this research a custom hardware platform for acuiqring UWB CIR measurements was developed, based on the commercially available Decawave DW1000M module, as shown in Figure 4.1.

To optimize data logging a special system architecture was developed. To simplify read out of the collected logs, FatFS was implemented on the microcontroller side on SD card. Additionally, logging and communication were handled with the help of the FreeRTOS operating system. Two major operations, data gathering, and data logging were decoupled by means of circular FIFO buffers. By using FIFO circular buffers, data can be gathered continuously and held until it is ready to be logged. The platform used for data collecting was based on STM32F4 microcontroller with 64 kB of RAM which was pre-allocated and used for before mentioned buffers. Data were collected immediately after interrupt occurred, either on UWB or IMU chip. Time spent in interrupts were minimal since their only purpose was to notify corresponding data gathering tasks that new data were available. Afterward, collected data were transferred to FIFO buffers and logging task was notified. All collected data in one gathering was prepended with a timestamp generated by pre-synchronized internal RTC. To additionally increase logging speed, data were written in binary form to pre-allocated files on the SD card. In this way, execution time that may be lost because of data formatting or sector

allocations was minimized. To validate the obtained results of the IMU and CIR measurements the simultaneous measurement with the reference respiration system were conducted. The reference system was Brain Products actiCHamp which enable respiration measurement via a respiration belt [148].

4.1.1 Short-term laboratory-controlled experimental setup description

The short-term and laboratory-controlled experiments were conducted by placing UWB transmitter and receiver units in predetermined positions on the anterior and posterior thoracic walls, as shown in Figure 4.3. The transmitter generates an ultra-short UWB pulse with a minimum bandwidth of 500 MHz [28]. The information about respiration was extracted from the CIR of the UWB channel measured at the receiver side, with more detail given in Chapter 5.3). Within a UWB platform, integrated inertial measurement unit (IMU) sensors were included, as presented in Figure 4.3. The reason for including an IMU sensor in a platform was to measure the respiration rate (RR) in a non-stationary environment by coupling the UWB measurements with IMU sensors. The experimental results showed that the proposed measurement method and implemented custom platform can reliably capture different breathing patterns with an error rate within the estimated range of 10% [28]. One of the results of the estimated and reference signals is presented in Figure 4.4.

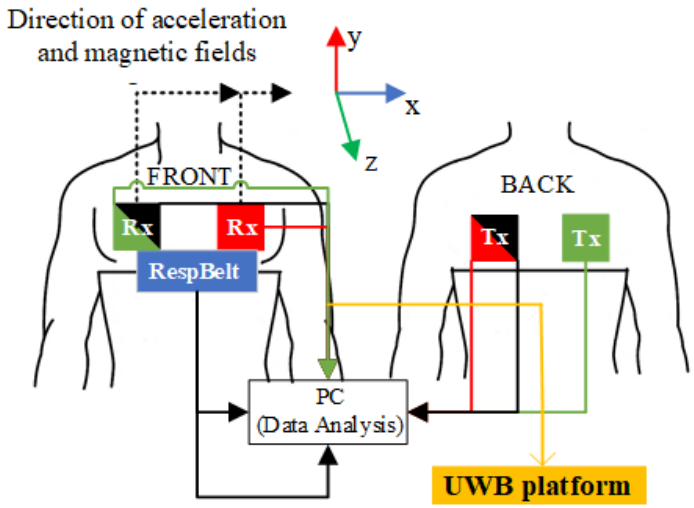

Figure 4.3 UWB platform measurement setup for the left front and back side of the thoracic wall [28]

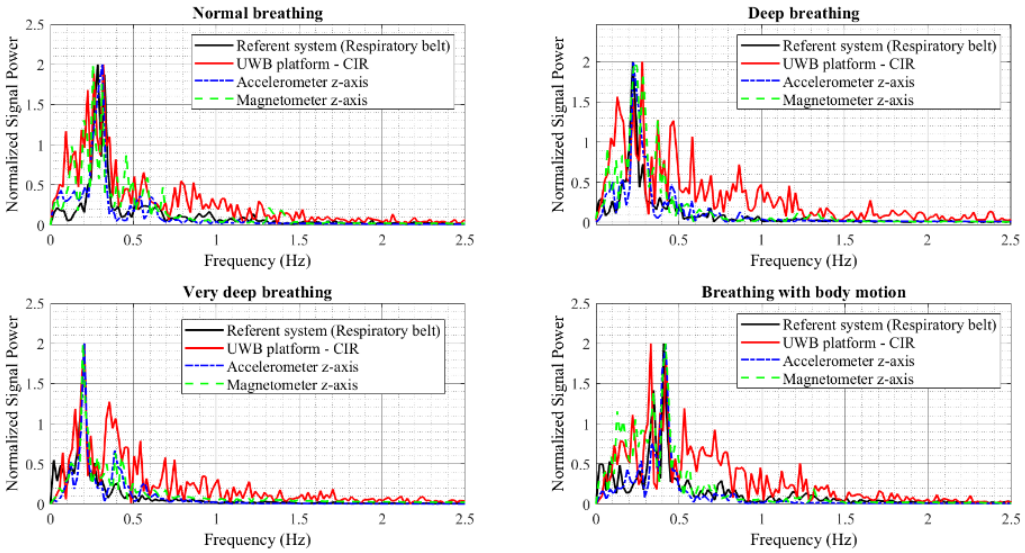

Figure 4.4 Examples of the estimated and ground truth (reference) signal in the frequency domain where the maximum value of the spectrum due to its highest energy value was detected as RR frequency for the four types of breathing (a) normal breathing, (b) deep breathing, (c) very deep breathing, (d) breathing with body motion

Additionally, a data-fusion algorithm, based on data fusion algorithms based on Extended Kalman filtering (EKF) and Naïve Bayes inference, for RR extraction was implemented [147]. The results show better estimation performance than those from individual signal sources. The obtained error rate of RR estimation by means of the proposed data fusion method was lower than 0.2 respiration per minute (rpm) compared to the reference respiration system. The duration of the measurement was 60 seconds. The reference system was Brain Products actiCHamp which enables respiration measurement via a respiration belt. The pre-processing steps and data fusion block diagram is given in Figure 4.5 and Figure 4.6.

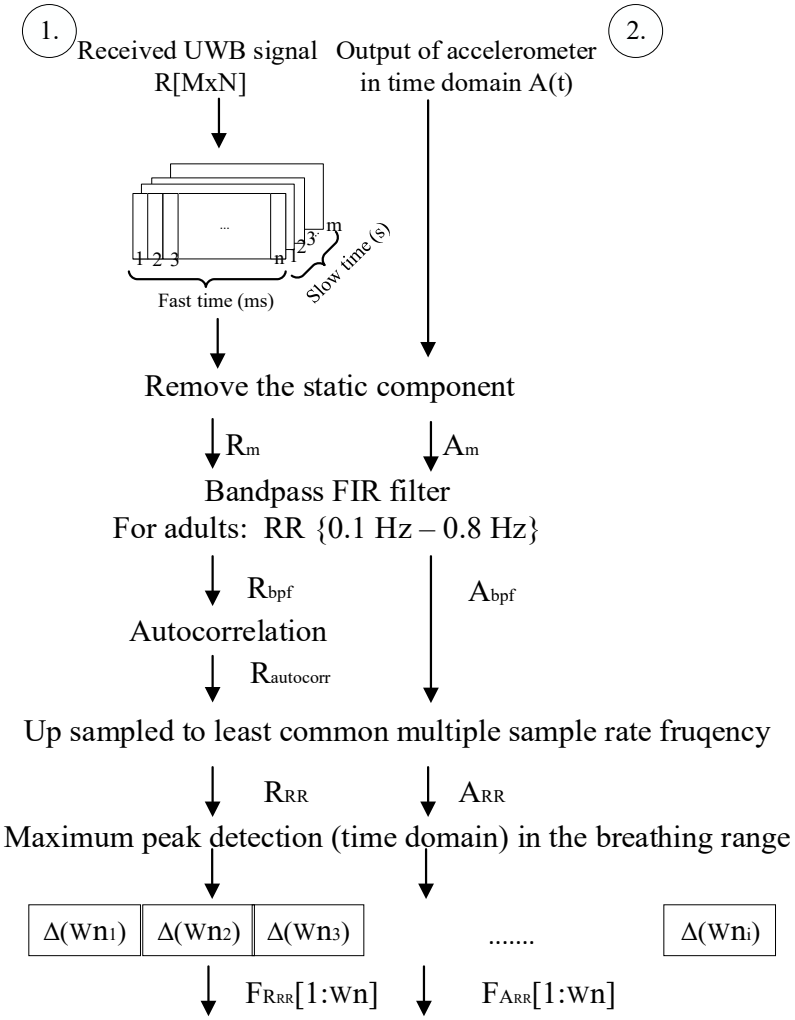

Figure 4.5 Block diagram of pre-processing steps [147]

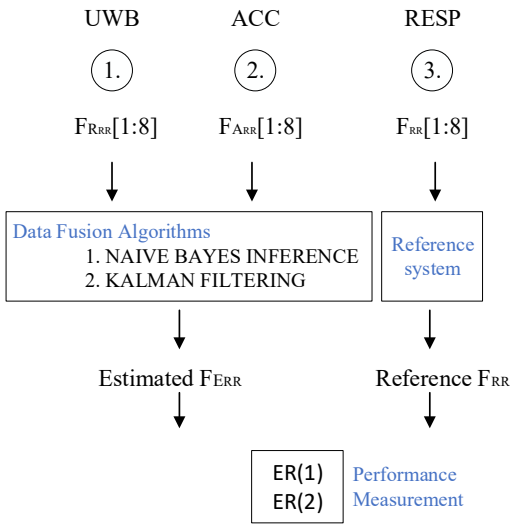

Figure 4.6 Block diagram of data fusion algorithm [147]

One of the drawbacks of the proposed system was that it was sensitive to body movement, so going further with the non-stationary experiments showed lower results as the body movements were larger. Therefore, monitoring sleep parameters, where each body movement represents a useful signal, can leverage the usage of the developed UWB platform. Moreover, one of the most common symptoms in post-acute COVID-19 patients discharged from hospitals is sleep breathing disorders. Hence, real-time monitoring and analysis of breathing and movement can be used to assess the rehabilitation process and potentially identify early signs of developing some post-COVID-19 diseases. Therefore, timely and daily available monitoring can reduce untreated breathing disorders during sleep and raise awareness of sleep among the wider population.

4.2 *Sleep-UWB Platform*: Sleep breathing patterns and postural transitions measurement

UWB transmitters (Tx_1 and Tx_2) and receivers (Rx_1 and Rx_2) were placed in predetermined positions on the left and right sides of the subject's bed. It was decided to use two pairs of nodes to leverage signals regardless of the body position of the participants. The second pair of nodes was set in a lower position than the first one and was more sensitive to body movement than the first. The transmitters generated an ultra-short UWB pulse with a minimum bandwidth of 500 MHz. From the UWB channel impulse response, information about the micro-displacement of the body caused by breathing and body movement was extracted. The proposed approach was based on the assumption that the chest movement caused by breathing and body movement continuously changes the parameter of the communication channel and thus modulates the observed signal strength on the receiver side, assuming that the transmitter signal strength and the relative position of the receiver and transmitter unit do not change their relative position over time [68], [147], [28], [29].

To capture CIR from both Node 1 (Tx_1-Rx_1) and Node 2 (Tx_2-Rx_2), the time-division multiplexing (TDM) scheme was used. In TDM, each node takes turns transmitting packets to the other node, so that the receiver can capture the CIR from both nodes. First, Tx_1 and Rx_1 were configured to communicate with each other using a single-side two-way ranging (SS-TWR) scheme [149], and start sending packets from Tx_1 to Rx_1. After a fixed period of time, 100 ms and after a short delay (5 ms) to ensure that all packets from Tx_1 have been received, it was switched on Tx_2 to transmit mode and start sending packets from Tx_2 to Rx_2. And, after

a short delay to ensure that all packets from Tx_2 have been received, it was switched back to the Tx_1 to transmit mode and repeat the cycle.

By using TDM, the platform is able to capture the CIR from both nodes. However, you should be aware that the accuracy and reliability of the CIR measurements may be affected by the switching between nodes, as well as by other factors such as multipath interference and noise in the wireless channel. Therefore, you should carefully design and test your system to ensure that it meets the desired performance requirements.

Furthermore, based on the information obtained from the diagnostics register (see Chapter 5.3.1), 40 samples of a CIR accumulator are extracted.

The structure of the received data from the DW1000 consists of the following:

- **Timestamp**
- **Diagnostics data**: *dwt_rxdiag_t* structure
  (described in detail in Chapter 5.3.1)
- **CIR data**: *dwt_readaccdata* function

, and with a sample rate of 10 Hz.

The receiver frame quality diagnostic values, stored at a *dwt_rxdiag_t* structure provided within the information in Table 4.2 [141].

Table 4.2 Receiver frame quality diagnostic structure [141]

Type	Name
*dwt_rxdiag_t**	Diagnostics

uint16 *maxNoise*;// *LDE max value of noise*
uint16 *firstPathAmp1*; // *Amplitude at floor (index FP) + 1*
uint16 *stdNoise*; // *Standard deviation of noise*
uint16 *firstPathAmp2*; // *Amplitude at floor (index FP) + 2*
uint16 *firstPathAmp3*; // *Amplitude at floor (index FP) + 3*
uint16 *maxGrowthCIR*; // *Channel Impulse Response max growth CIR*
uint16 *rxPreamCount*; // *count of preamble symbols accumulated.*
uint16 *firstPath*; // *First path index*	

The accumulator data (CIR data) was read using a function [141]:

*dwt_readaccdata (uint8*buffer, uint16 len, uint16 bufferOffest);*

Table 4.3 Description of the parameters in the function *dwt_readaccdata* [141]

Type	Name	Description
*uint8**	*buffer*	*Pointer to the buffer, which is read accumulator data, is written*
uint16	*len*	*The length of data to be written*
uint16	*bufferOffest*	*The offset at which to start reading the data*

The accumulator data consists of a 16-bit real integer and a 16-bit imaginary integer, as detailed in Chapter 5.3.1. Each tap in the fast time was sampled with the 1.016 ns sample interval. Additional *Sleep-UWB platform* technical specification are presented in Table 4.4.

Table 4.4 Technical specifications of the proposed *Sleep UWB platform*

Parameter	Value
Center frequency	3.9936 and 4.4928 GHz
The bandwidth of the pulse	500 and 900 MHz
Pulse repeat frequency	64 MHz
Data rate transmission	up to 6.8 Mbps
Peak power limit	0 dBm/50 MHz
Transmit power	- 41.3 dBm/MHz
Integrated antenna	Omnidirectional Portron dielectric antenna
Sample rate: slow time (UWB)	10 Hz
Sample rate: fast time (UWB)	1.016 ns
A sample rate PSG reference system	100 Hz
Length of the packet in the fast time	1016 samples (only 40 samples extracted)

4.2.1 Clinical study experimental setup description

The experimental measurements were conducted in the University Psychiatric Hospital Vrapče, the Department of Clinical Psychophysiology and Organically conditioned mental disorders, Center for Sleep and Wake Disorders. The experimental setup is shown in Figure 4.7. Two pairs of nodes were connected to the Raspberry Pi 3 Model B gateway device, which was then connected to the user interface on the PC via an Ethernet connection. The data were

simultaneously measured within PSG reference measurement and post-time-synchronized with it (described in detail in Chapter 5.2 and Chapter 5.3).

Some participants lie in positions that are not entirely right, supine, prone and left (classified by PSG) but are between. In our research, it was most likely that the sensor would detect the participant in the supine position, but he was more on one side. Moreover, the gold standard sensor for body position has some drawbacks for the female participants due to female anatomical construction – so there are more falsely detected positions. In postprocessing, we have used a camera sensor to overwrite the annotations. The average anterior size of the chest region, l_a, (with included shoulder) was 51.7 ± 5.97 cm, and the average lateral size of the chest region, l_l, was 34.93 ± 12.9 cm. The average anterior size was around $2 \cdot l_l$. Therefore, the position of the first node was 60 cm above the bed, and the second node was 40 cm.

An experimental setup in the clinical environment is given in Figure 4.7.

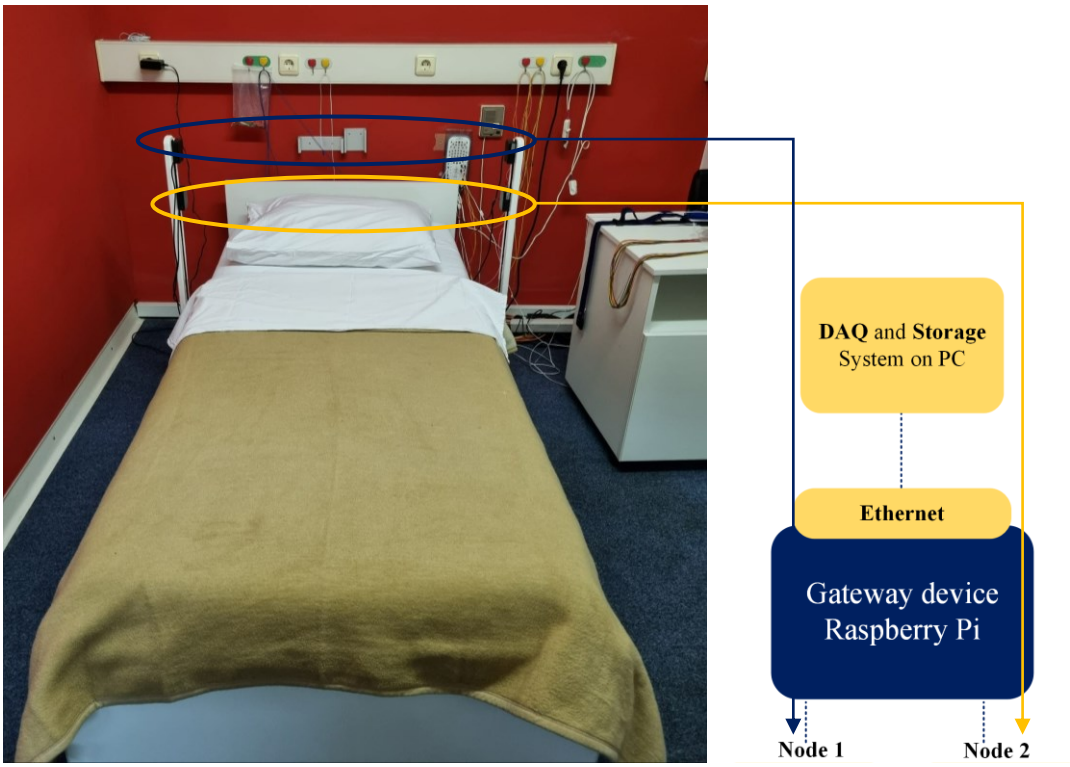

Figure 4.7 Experimental setup and relative position of the UWB nodes and the subject

Moreover, the detection accuracy depends on the body orientation regarding the position of the Tx and Rx modules. Hence, for a signal-to-noise ratio maximization, in this study, the two pairs of nodes were used to ensure that the body's postural transition and breathing patterns can be detected at least by one pair of modules. As shown in Figure 4.8, if the

participant was in a supine position, a longer part of a second node communication channel was a human body; that was not the case for the first node. Therefore, based on the participant's position, the node that covers a frontal plane was more sensitive to breathing detection, as the most noticeable changes are happening in the frontal plane, as shown with dashed lines in Figure 4.8.

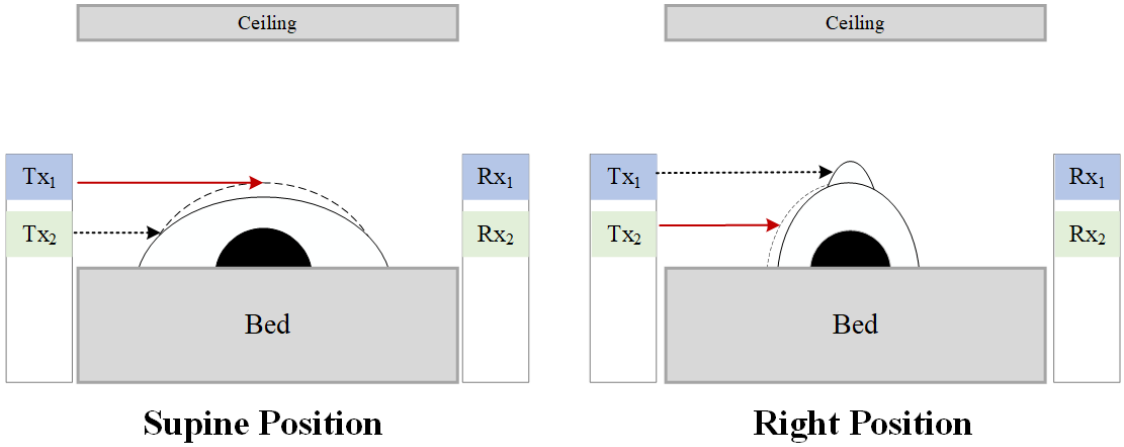

Figure 4.8 Measurement setup in different body positions

Chapter 5
Clinical study

In this chapter, the clinical study procedure will be covered. Thereafter, the gathered dataset will be described, and data signal analysis will be provided along with a detailed evaluation of the obtained results.

The clinical study was carried on within the University Psychiatric Hospital Vrapče, the Department of Clinical Psychophysiology and Organically conditioned mental disorders, **Center for Sleep and Wake Disorders**. Before the measurement, UWB devices are placed in this predetermined place (two transmitters, two receivers) on the two sides of the bed, as shown in Figure 4.7. The UWB transmitter transmits a UWB signal to the receiver and measures the change in the impulse response of the UWB communication channel. The transmitter and receiver are placed on the side of the bed at a distance of approximately 0.5 m from the patient. Ground truth measurement was obtained using a **Sleepware G3 Philips Respironics PSG (Alice 6)**, more precisely from the following sensors: ECG, EMG, EEG, EOG, microphone, video camera, nasal and oral airflow, pulse oximeter, body position, thermistor, and inductance plethysmography, with 30-second epochs analysis. The ***Sleep-UWB platform*** used for a clinical study was described in Chapter 4.

Within the clinical study, twenty (20) overnight recordings were carried out, of which three were excluded; due to incomplete data collection from the *Sleep-UWB platform* (a problem with the *Sleep-UWB platform* connection with a PC – that happened during a recording), leaving **seventeen (17) recordings** for analysis, more precisely **103.41 hours of recordings**.

In Table 5.1, the patient's information along with AHI are provided, where:

- Normal: AHI < 5: **(2F; 1M)**
- Mild sleep apnea: 5 < AHI < 14: **(2F; 4M)**
- Moderate sleep apnea: 15 < AHI < 29: **(4F; 1M)**
- Severe sleep apnea: AHI > 30: **(0F; 3M)**

Table 5.1. Patients' information

ID	Sex	AHI (events/h)	Age (year)	Height (cm)	Weight (kg)	BMI (kg/m^2)
1	Male	6.8	21	184	86.1	25.7
2	Male	66	73	184	109	32.2
3	Male	35	49	187	141	40.3
4	Female	11.1	56	164	98	36.4
5	Male	14.8	59	192	100	27.1
6	Male	4.3	70	178	85	26.8
7	Female	14.5	39	172	75	25.4
8	Female	20.9	54	166	80	29.0
9	Female	1.4	42	178	77	24.3
10	Male	6.6	22	176	75	24.2
11	Female	29.8	58	170	119	41.2
12	Female	20.3	57	162	68	25.9
13	Male	53.8	65	173	102	34.1
14	Female	4.2	61	165	75	27.5
15	Female	21.9	54	166	66	24
16	Male	17.5	78	173	94	31.4
17	Male	13.5	22	177	85	27.1

Table 5.2 Number of patients per observed input information

Male	**Female**	**Age (year) > 50**	**Age (year) < 50**
9	8	11	6
BMI (kg/m^2) < 30	**BMI (kg/m^2) > 30**	**AHI (events/h) > 15**	**AHI (events/h) < 15**
11	6	8	9

Furthermore, Table 5.3 shows the overall patients' information.

Table 5.3 Overall patients' information

		Age (year)	Height (cm)	Weight (kg)	BMI (kg/m^2)	AHI (events/h)
		($\mu \pm \sigma$)				
Males (9)	**Average**	51 ±22.16	180.4±4.85	97.45±18.3	29.84±4.84	24.25±21.07
	Range	[21-78]	[173-192]	[75-141]	[24.2-40.3]	[4.3-65.4]
Females (8)	**Average**	52.63±7.35	167.88±4.86	82.25±16.60	29.21±5.86	15.51±8.98
	Range	[39-61]	[162-178]	[66-119]	[24-41.2]	[1.4-29.8]
Overall (17)	**Average**	51.74±16.91	174.53±8.43	90.3±19.09	29.55±5.36	20.14±17.08
	Range	[21-78]	[162-192]	[66-141]	[24-41.2]	[1.4-65.4]

5.1 Data collection procedure

The patients referred by the family doctor or specialist to the Sleep Clinic for overnight polysomnography with a diagnosis of suspected sleep apnea were considered. Nevertheless, it is important to emphasize that some did not show signs of apnea after the polysomnography measurement. Still, for the case of completeness, they were included in the study results.

Within the study, twenty (20) overnight recordings were carried out, of which three were excluded; due to incomplete data collection from the Sleep-UWB platform (a problem with the Sleep-UWB platform connection with a PC – that happened during a recording), leaving seventeen (17) recordings for analysis, more precisely 103.41 hours of recordings.

The patient comes to the Sleep Clinic around 8 pm, and then the researcher goes through the research details with him, and if they agree to proceed with it, they fill out sleep questionnaires and sign the consent form. Furthermore, the measures from *Appendix B* were taken. Afterward, the sleep technician goes through the placement of the PSG sensors on the body; depending on the patient's preferences for starting to sleep, the recording begins. The study respected the privacy of the patient's data. Moreover, it was conducted by all applicable guidelines based on the Helsinki declaration and its revisions, which ensured the proper implementation of procedures and the safety of persons who participated in this research. A University Psychiatric Hospital Vrapče Ethical Board and the University of Zagreb Ethical Board approved the clinical study procedure. The researcher and sleep technician observe the recording throughout the whole night.

Written informed consent was obtained from all participants. Moreover, the Epworth Sleepiness Scale (ESS) and Pittsburgh Sleep Quality Index (PSQI) questionnaires were used. An overnight PSG (Alice 6, Respironics, Philips) was used to perform ground-truth measurements. PSG was recorded for approximately eight hours per patient, totaling 103.41 hours of recording. In postprocessing analysis, the start time of a *Sleep UWB platform* measurement was synchronized with the PSG recording.

Ground truth measurement was obtained using a Sleepware G3 Philips Respironics PSG, shown in Figure 5.1, more precisely from the following sensors: ECG, EMG, EEG, EOG, microphone, video camera, nasal and oral airflow, pulse oximeter, body position, thermistor, and inductance plethysmography, with 30-second epochs analysis.

Figure 5.1 Alice 6 LDxN Philips Respironics PSG reference device [168]

Some of the specifications of the Alice 6 LDxN reference device with the Alice 6 LDx base system (International version) used in this study are given in Table 5.5. Furthermore, the example of the one epoch (30 seconds) in Sleep G3 sleep diagnostic software is presented in Figure 5.2. Moreover, Table 5.4 shows a PSG data table description.

Table 5.4 PSG data table description

Signal Labels	Physical Dimensions	Sample Rate (Hz)	Signal Description
EOG ROC-A2	μV	200	left and right electro-oculogram (EOG) leads (left eye and right eye)
EOG LOC-A2	μV	200	
EEG F3-A2	μV	200	occipital, central, and frontal electroencephalogram (EEG) leads
EEG F4-A1	μV	200	
EEG C3-A2	μV	200	
EEG C4-A1	μV	200	
EEG O1-A2	μV	200	
EEG O2-A1	μV	200	
EMG Chin	μV	200	chin electromyogram (EMG) lead
Flow Patient	-	100	nasal pressure transducer
Effort THO	-	100	chest and abdominal walls motion effort
Effort ABD	-	100	
Snore	-	500	snore sensor (microphone)
ECG I	μV	200	electrocardiogram (ECG) I lead
SpO2	%	1	oxygen saturation by pulse oximetry by finger probe
Body	-	1	patient position (supine, left, right, prone, up)
Leg 1	μV	200	left and right tibialis anterior EMG leads
Leg 2	μV	200	
PulseRate	-	1	pulse rate
EEG A1-A2	μV	200	ground reference points for all EEG and EOG leads

Table 5.5 Alice 6 LDxN specifications [150]

Sensors	Number of channels
EEG	32
EMG	5
ECG	3 physical and 4 derived
EOG	2
Pressure transducer	1
Thermal (flow)	1
Microphone; Piezo snore sensor	1
Actimeter	2 inputs
zRIP DuraBelt Integrated RIP driver	8 inputs
Pulse oximeter	1
Video camera	1

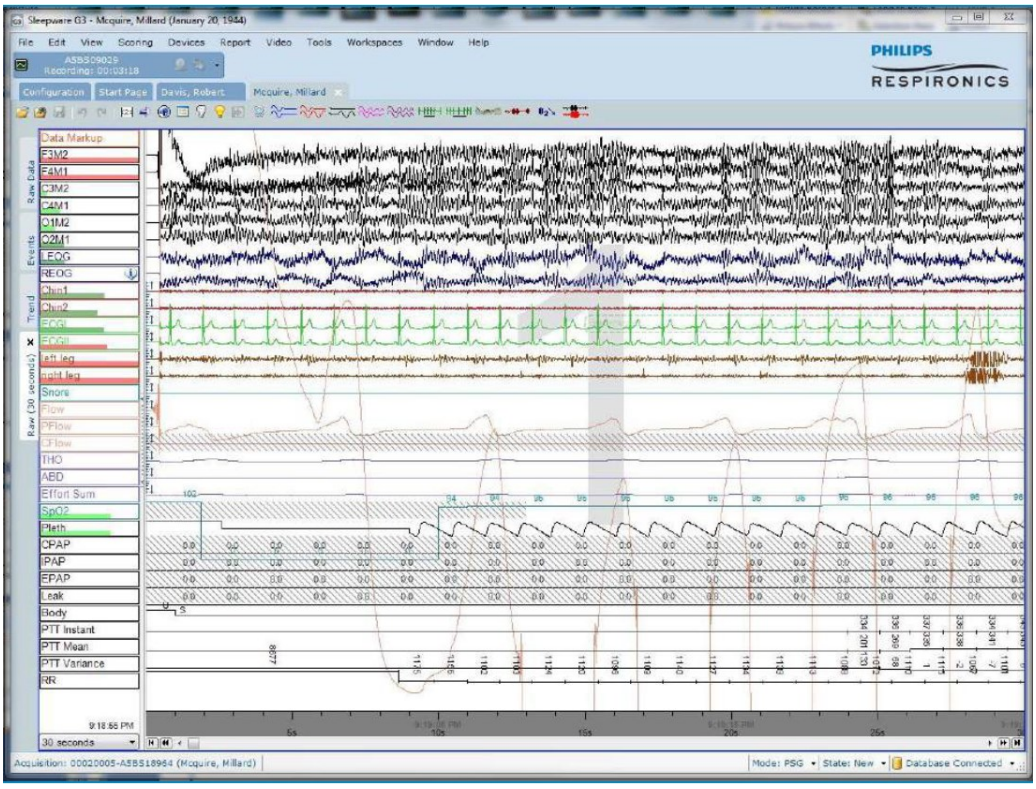

Figure 5.2 Example of the one window (first epoch) of the PSG recording with the included used sensors signals. Taken from [151]

After placing the PSG sensors, the Sleep-UWB platform was set on the predetermined position on the left and right of the bed (distance between left and right side was 113 cm), where the platform follows the surface of the chest and abdomen, around 60 cm from the bed's headboard. The position of the first node was 60 cm above the bed, and the second node

was 40 cm. Since the proposed clinical study was a proof of concept for testing the proposed method and performance of the *Sleep-UWB platform* in the clinical environment, the researcher was writing all the additional events that were happening through the recording. Afterward, events were extracted before data analysis. Mostly, events were related to the patient's micturition, cable detachment, long parasomnia episodes, or due to a sleep technician entering the room at the patient's invitation.

The sleep postural transition was calibrated directly after setting up both the system and starting recording. There, researcher asked the patient if they could perform the following steps:

1) go from supine to the right, and stay 10 seconds in that position;
2) go back to supine, and stay 10 seconds in that position;
3) go from supine to the left, and stay 10 seconds in that position;
4) go back to supine, and stay 10 seconds in that position;
5) go from supine to prone; stay 10 seconds in that position;
6) go back to supine, and stay 10 seconds in that position.

Most of them said they were unable or felt uncomfortable performing the last two steps (5 and 6). Therefore, due to the small number of the dataset, the information was taken from the whole duration of the recording.

5.2 Dataset description

Data were gathered from the patients referred for overnight polysomnography at University Psychiatric Hospital Vrapče, Department of Clinical Psychophysiology and Organically conditioned mental disorders, Center for Sleep and Wake Disorders. The polysomnography device used in the study was Sleepware G3 Philips Respironics PSG. The dataset contains over 3000 annotated events from 17 patients. In addition, regarding event annotations, they are made automatically by Sleepware G3 software. The trained sleep medical technician double-checks them for each 30-second epoch according to the strictly defined set of rules [38]. Further, it should be emphasized that various respiratory event filters can be set by the event filters window in the Sleepware G3 software, as shown in Figure 5.3. Respiratory events were set by default settings for adult patients. All the recordings had an ApnVel configuration.

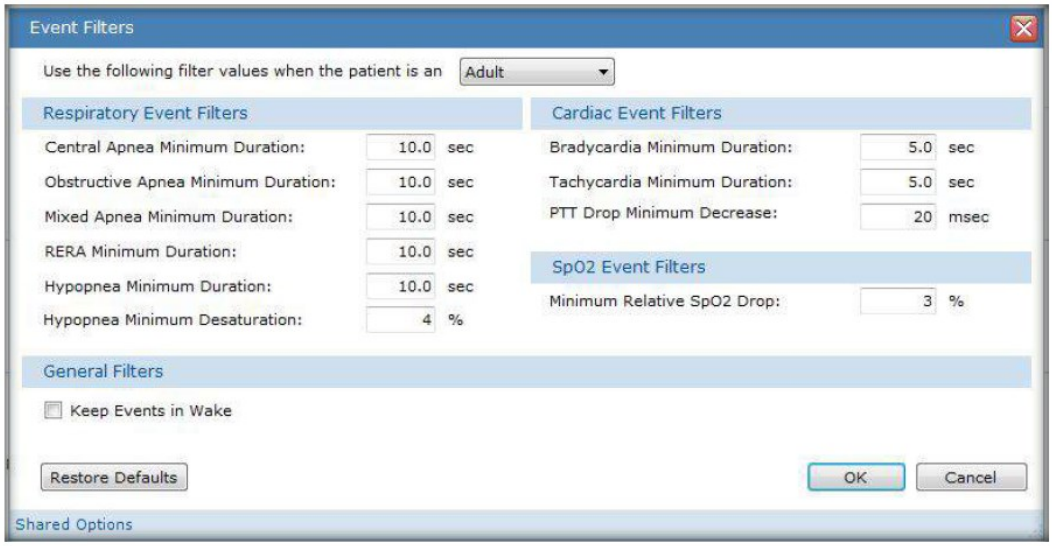

Figure 5.3 Event filters option in the Sleepware G3 software [151]

In addition, in the *Standard Analysis* option, there was a tab called *Hypopnea*, shown in Figure 5.4, where auto-analysis rules for hypopnea can be configured according to the following options:

i. Set the *Minimum Duration* (seconds) value in a range of 0.0 up to 600.00, where the default value was 10.0

ii. Set the *Maximum Duration* (seconds) value in a range of 0.0 up to 600.00, where the default value was 60.0

iii. Set the *Amplitude Ratio* (percentage) value in a range of 0.0 up to 100.0, where default value was 50.0%

iv. Set the *Hysteresis* (percentage) value in a range of 0.0 up to 100.0, where default value was 60.0%

v. If, at the same time, apnea and hypopnea auto-scored, set the rule to determine which event takes priority, where the default value was *Hypopnea*

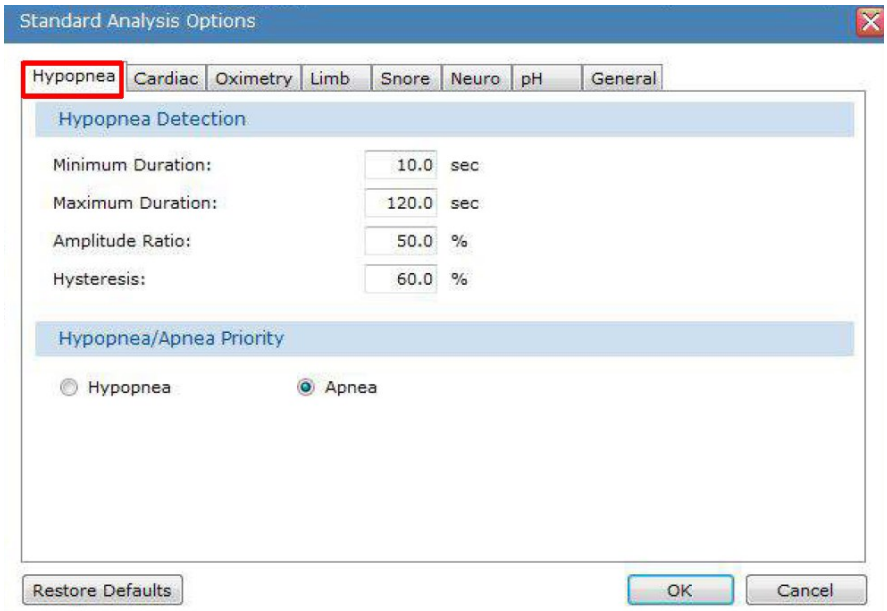

Figure 5.4 Auto-analysis option for Hypopnea event annotation – Sleepware G3 software [151]

Furthermore, from the *Channels Tab*, you can specify or modify the rules of the event you want to monitor and, moreover, see the default primary, secondary and tertiary channels used for the specific signals. As shown in Figure 5.5, the flow sensor was used for the apneas (central, obstructive, and mixed) and hypopnea. For periodic respiration, effort (chest and abdomen) sensors are used.

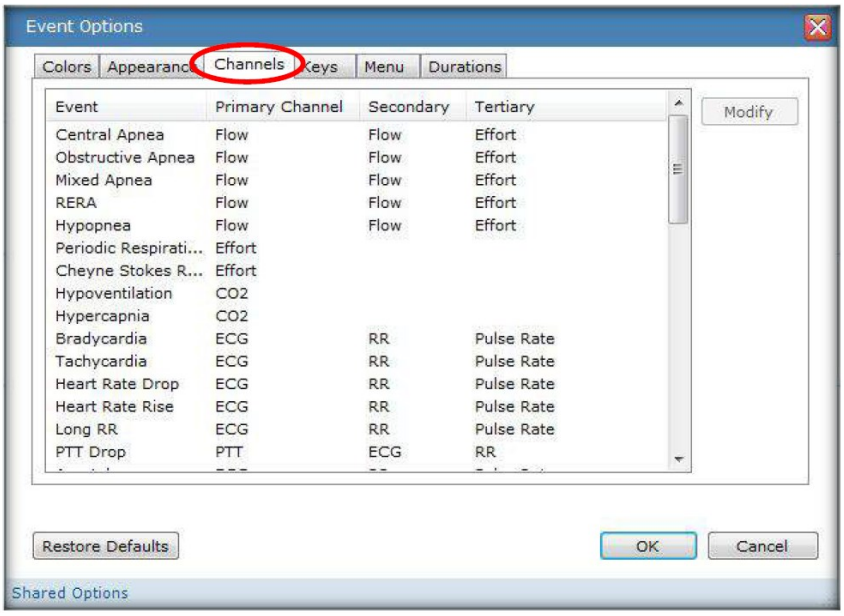

Figure 5.5 PSG event options [151]

Furthermore, sleep parameters statistics gathered from the PSG are given in Table 5.6.

Table 5.6 Sleep parameters statistics from the PSG clinic report

Dataset size: (17)	**mean ±SD**
SE (%)	76 ± 12.52
TST (min)	337.6 ± 69.4
Sleep Onset (min)	36.45 ± 29.38
WASO (min)	68.54 ± 42.32
TRT (min)	447.07 ± 44.09
Leg Movement	198.82 ± 161.26

TST: total sleep time; WASO: wake after sleep onset; TRT: total recording time

The data from the Sleep-UWB platform were collected using a Raspberry Pi 3 Model B as a gateway device. An Ethernet connection from the gateway device to the user interface on the PC was used for the data transfer. On the PC, the Phyton script aggregated data and saved it locally to the PC. The received packet is shown in Figure 5.6. The sampling rate was 10 Hz. Therefore, every 1 second the platform, was sending 14.56 Kbps per node. Approximately the measurement duration was eight hours per patient and around **419.328 MBit for one node** of data per recording.

Timestamp	**Node label: (‘A’ or ‘B’)**	**Diagnostics data**	**CIR data**
40 bits	8 bits	8 x 16 bits	40 x (2x16 bits)

Figure 5.6 Received packet per one node

5.3 Data analysis

This subchapter will describe the data analysis obtained from the *Sleep-UWB platform*. The first phase was preprocessing methods related to the channel impulse response (CIR) signal adjustment and frames selection, as presented in Figure 5.7. Furthermore, the preprocessing steps relevant to the breathing signal will be applied, such as bandpass filtering in a frequency range of breathing (8-20 breaths/minute, or 0.1 up to 0.4 Hz)[2]. In addition, the detection method for the sleep postural transition will also be covered. Afterward, the frame-based segmentation based on the weighted Short-time Fourier transform (STFT) and Hanning window will be undertaken for breathing and sleep postural transition detection. Furthermore,

[2] One breathing cycle consists of two consecutive phases: inspiration and expiration, wherein the first phase of thoracic volume increases. In the second phase, expiration, the deoxygenated air flows out of the lungs with increased pressure. In adults, breathing rate (BR), in the rest state, is around 12 to 20 breaths per minute. [33]

the influence of each patient's obesity on the detection of breathing and the analysis of sleep postural transitions are presented. Human obesity was estimated using the information on the height, weight, and circumference of specific body segments. Afterward, the influence of sleep breathing irregularity and sleep postural transitions on the success of the analysis was depicted. In addition, the accuracy of each node has been presented. More details are provided in Subchapter 5.3.1.

Moreover, an analysis of the breathing patterns (normal sleep breathing without SDB episodes, apnea, hypopnea) and sleep postural transition (supine to side (left, right) and side (left, right) to supine) was implemented, as shown in Figure 5.8 and Figure 5.9. More details are provided in Subchapter 5.3.2.

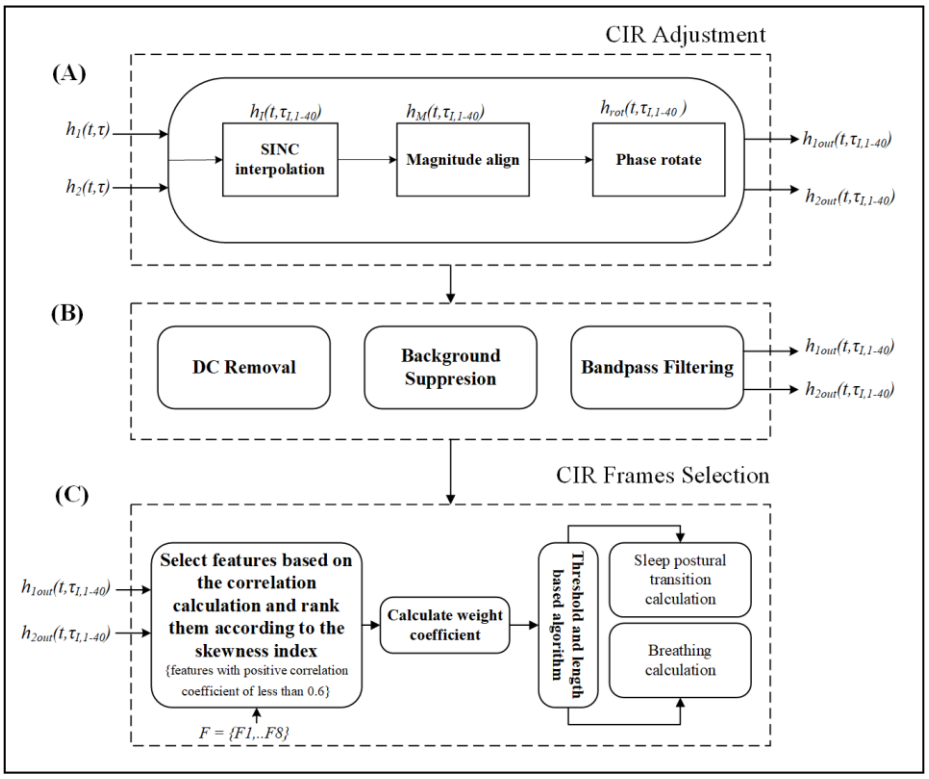

Figure 5.7 CIR preprocessing and processing steps, where (A) was CIR signal adjustment, and (B) filtering and smoothing, and (C) was a CIR frames selection

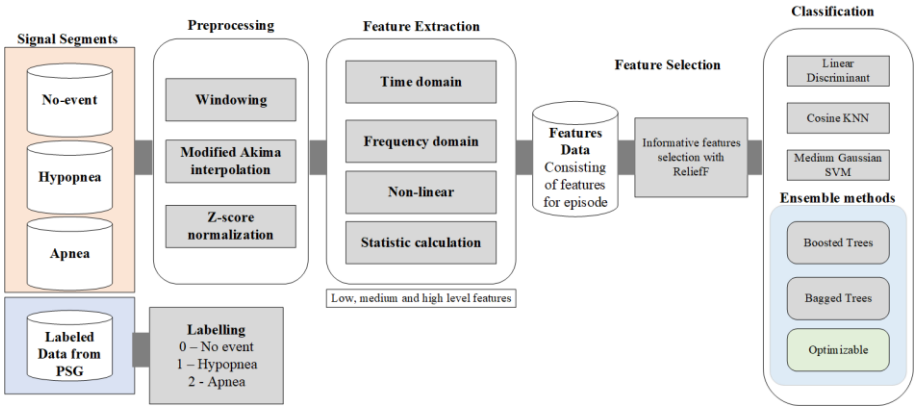

Figure 5.8 Block diagram of the breathing patterns analysis steps (normal sleep breathing without SDB episodes, apnea, hypopnea)

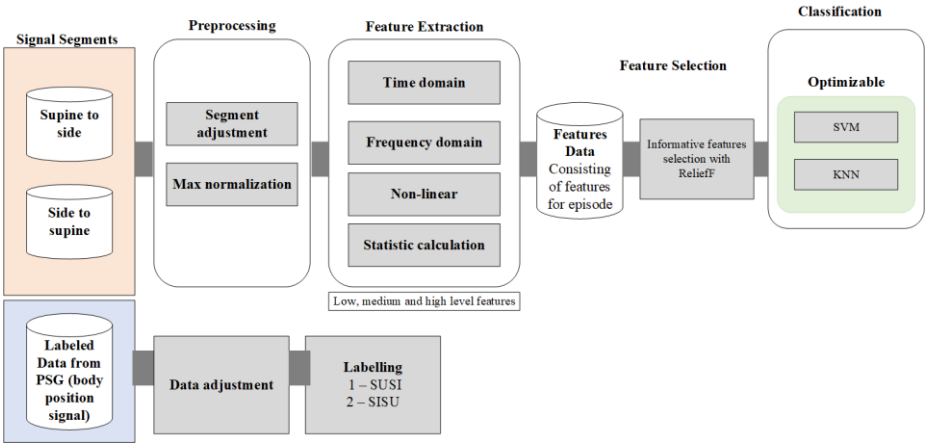

Figure 5.9 Block diagram of the sleep postural transition analysis steps (supine to side and side to supine)

5.3.1 Methods for breathing and sleep postural transition detection

In the experimental setup, the DW1000 802.15.4a UWB transceivers are adjusted to operate on channel 4 (center frequency of 3993.6 MHz and bandwidth 1331.2 MHz) and with a preamble length of 1024 and data rate of 6.8 Mb/s, and PRF 64 MHz. The DW1000 extracts accumulator data and features presented in a built-in channel diagnostics register for each measurement. The UWB transceivers, through accumulator data, provide a CIR estimation that was extracted from the preamble of a UWB packet [152]. They contain complex 16-bit real and 16-bit imaginary integer values. The diagnostics register provides the following data, which was represented as vector ***D*** [141]:

- *MaxNoise* (LDE max value of noise),
- *firstPathAmp1* (Amplitude at the floor (index FP) +1),
- *stdNoise* (Standard deviation of noise level),

- *firstPathAmp2* (Amplitude at the floor (index FP) +2),
- *firstPathAmp3* (Amplitude at the floor (index FP) +3),
- *maxGrowthCIR* (channel impulse response max growth CIR),
- *rxPreamCount* (count of preamble symbols accumulated),
- *firstPath* (first path index).

This research used both accumulator data (CIR) and diagnostic data. The output of the CIR and input to the breathing patterns and sleep postural transitions analysis are the I/Q-values of the CIR. The example of the magnitude and complex value of the CIR is presented in Figure 5.10, where *FP0* shows the first point of the multipath components (MPCs), i.e., direct link or LOS between Tx and Rx, the *FP1* and *FP2* are the following echoes of the arriving MPCs path between the transceivers. The sample rate between each tap in the fast time was T_{ft} = 1.016 ns, and for the PRF of 64 MHz, there are 1016 complex values in the fast time. Here, in a received packet, only 40 complex values in the fast time have been taken into account; according to the *FP0* index value, it was taken 20 indexes before and after [72], [153]–[155]. It was empirically conducted that all MPCs lay in the first 40 ns of each CIR.

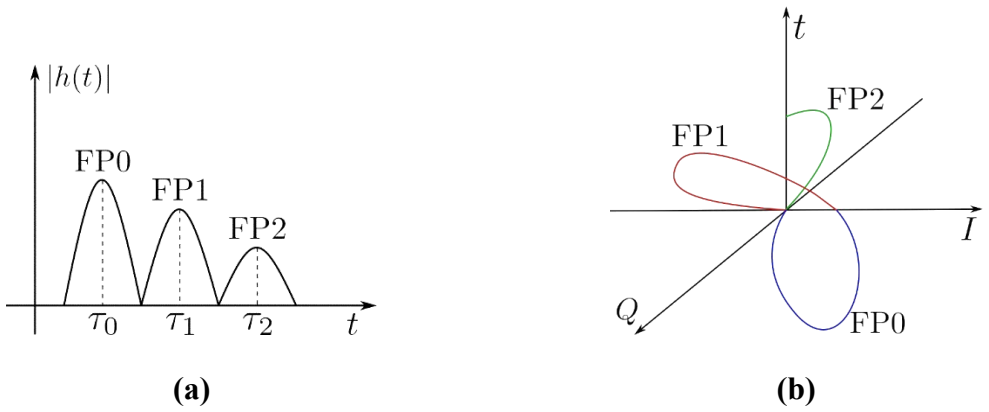

Figure 5.10 The example of the (a) magnitude and (b) complex value (I/Q) CIR measurement representation, where FP0 is the first multipath component, and FP1 and FP2 are the second and third

The overall CIR was represented by two-dimensional fast-slow time matrix, $h(t,\tau)$, where τ represents fast time, and t slow time indexes, and M number of slow time packets, N length of the channel impulse response:

$$\boldsymbol{h(t,\tau)} = \begin{pmatrix} \boldsymbol{h_{r_{1,1}} + jh_{i_{1,1}}} & \boldsymbol{h_{r_{1,2}} + jh_{i_{1,2}}} & & \boldsymbol{h_{r_{1,1}} + jh_{i_{1,1}}} \\ \vdots & \vdots & \vdots & \vdots \\ \boldsymbol{h_{r_{m,1}} + jh_{ri_{m,1}}} & \boldsymbol{h_{r_{m,2}} + jh_{i_{m,2}}} & \dots & \boldsymbol{h_{r_{m,N}} + jh_{i_{m,N}}} \\ \vdots & \vdots & & \vdots \\ \boldsymbol{h_{r_{M,1}} + jh_{i_{M,1}}} & \boldsymbol{h_{r_{M,2}} + jh_{i_{M,2}}} & \dots & \boldsymbol{h_{r_{M,N}} + jh_{i_{M,N}}} \end{pmatrix} \quad \textbf{(5.3.1.1)}$$

One example of the imaginary, real, and magnitude parts of the CIR frame is presented in Figure 5.11. Before proceeding with the preprocessing steps of sleep breathing and postural transitions signal, we need to apply two preprocessing steps regarding the CIR analysis. The first step was CIR adjustment, and the second was CIR frames selection according to the noise level and diagnostics data from vector ***D***.

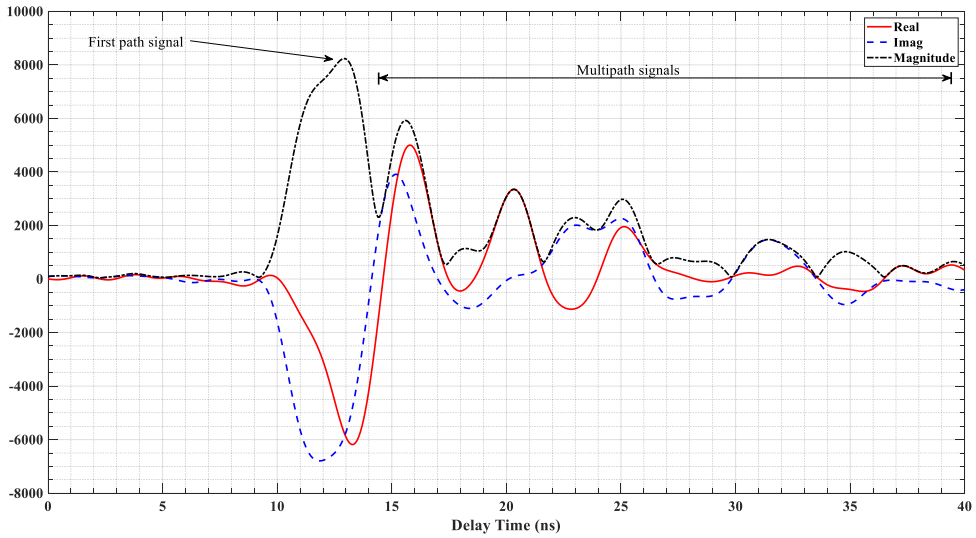

Figure 5.11 CIR frame representation with the *real*, *imag* and *magnitude* component

5.3.1.1 Channel impulse response adjustment

The CIR adjustment steps are presented in Figure 5.12, where the first step was an interpolation. Second, phase and magnitude adjustments are applied by finding the minimal delay in every CIR measurement [156]. After the minimal delay was found, phase rotation and lag correction were applied.

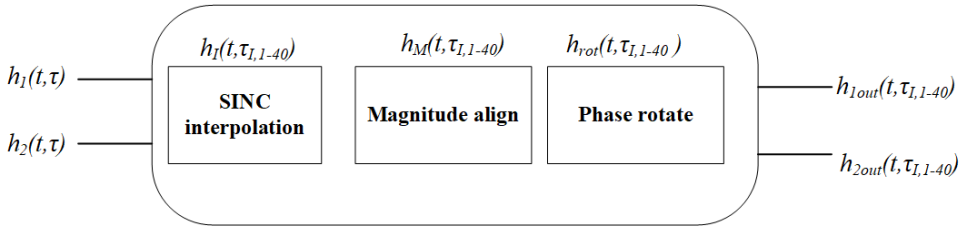

Figure 5.12 Block diagram of the CIR adjustment for Node 1 ($h_1(t,\tau)$) and Node 2 ($h_2(t,\tau)$)

Interpolation of the CIR measurement was applied to match the time resolution given by DW1000 received timestamp register (T_R = 15.8 ps). The interpolation was done by applying Whittaker-Channon interpolation, where N is the samples in the fast time [156]:

$$\boldsymbol{h_I(\tau) = \sum_{n=1}^{N} h[nT_{ft}] \cdot sinc(\tau - nT_{ft})} \quad \textbf{(5.3.1.2)}$$

Furthermore, for the correction of the magnitude, the cross-correlation was undertaken for every CIR measurement, and it was shifted to the index where the maximum correlation coefficient occurs (h_M). The cross-correlation was achieved by correlating the observed CIR measurement with the reference CIR measurement, where the reference CIR was filtered measurement in the idle condition. Additionally, phase rotating was achieved by rotating an observed CIR in small steps of φ, from 0 up to 2π, then applying the Euclidean norm between it and reference CIR measurement. Finally, the phase was shifted by the index, where the minimum phase distance was calculated [156].

$$\boldsymbol{h_{rot} = \min_{\theta} \| h_{ref} - h_M e^{j\theta} \|} \quad \textbf{(5.3.1.3)}$$

The output of the CIR adjustments was presented in the following equation, and the output I/Q CIR is presented in Figure 5.13, together with the raw and reference CIR:

$$\boldsymbol{h_{out} = |h_M| \cdot e^{\theta_{rot}}} \quad \textbf{(5.3.1.4)}$$

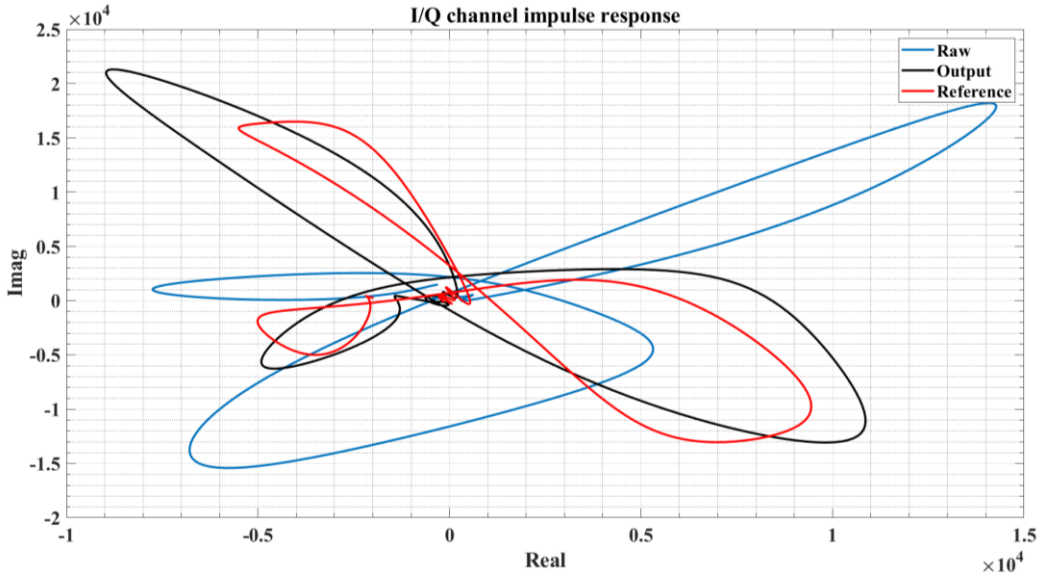

Figure 5.13 Result of the CIR's adjustment for one CIR frame; raw CIR is represented with the blue line, reference CIR with the red line, and output CIR with the black line

5.3.1.2 Filtering method

After a CIR adjustment, the following steps are applied before a frame selection and feature extraction:

- **DC suppression**: The DC noise was removed by averaging its value through all the number of slow time indexes [157]
- **Background static suppression**: the slow time indexes data are subtracted with their average along fast time [157], as presented in the following equation:

$$\boldsymbol{h_m(t,\tau) = h_{out}(t,\tau) - \frac{1}{MN}\sum_{i=1}^{M}\sum_{j=1}^{N} h_{out_{i,j}}(t,\tau)} \quad \textbf{(5.3.1.5)}$$

- **Bandpass filtering:** Butterworth 5th order was applied in a frequency range (0.1 – 0.4 Hz) where breathing was expected. Figure 5.14 shows around four minutes of the CIR signal after a bandpass filtering.

After this step, the moving clutter (body movement) and breathing signal will maintain in the CIR data.

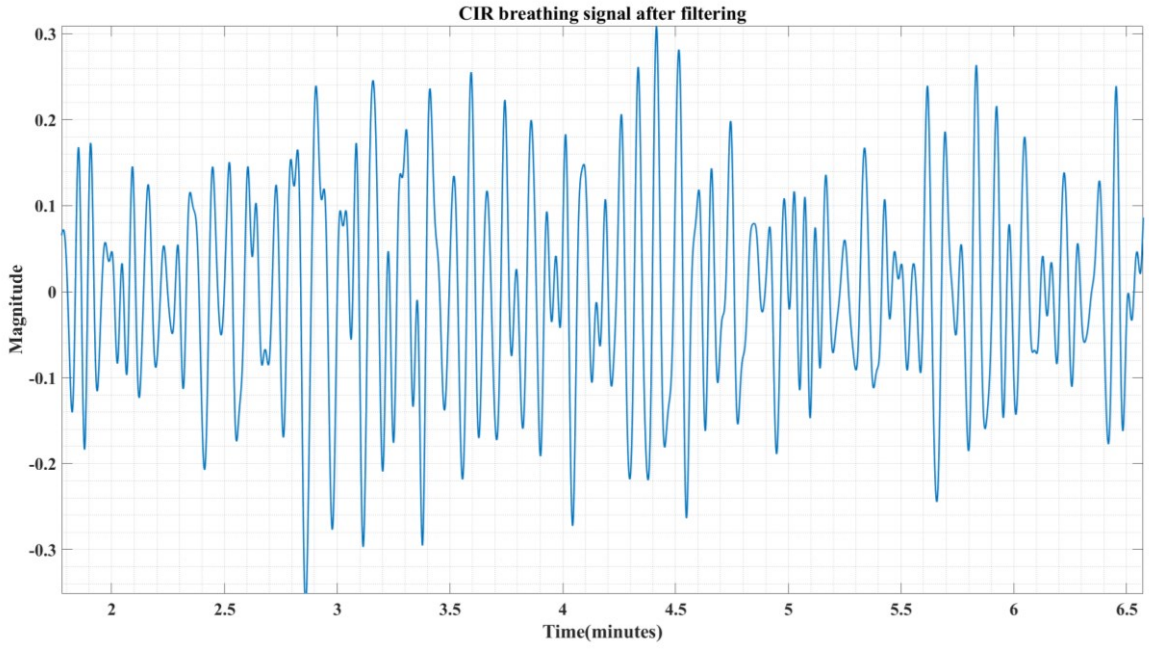

Figure 5.14 CIR signal after bandpass filtering

5.3.1.3 Channel impulse response frames selection

There was a reasonable assumption that some of the CIR frames in the measurements are more sensitive to capturing breathing than others. Therefore, a CIR frame selection was

critical step before sleep breathing analysis. Hence, from the adjusted CIR data and diagnostics data presented in vector $\boldsymbol{D}$, the following features (*Feature 1. – Feature 8.)* are calculated. Afterward, the selected features are used to calculate a CIR frames coefficient of weighting (σ_w). It is worth mentioning that the reason for using two nodes was that in a certain situation or sleep body position, one of the nodes will be more sensitive to capturing the breathing, but regarding the sleep postural transitions the second, lower node was more sensitive to capture sleep postural transition, and it will be used for a σ_w calculation.

The list of the calculated features are following:

Feature 1 (F1): Mean excess delay, or more precisely, the mean delay of the MPCs [152], [158]:

$$\boldsymbol{\tau_{MED}} = \int_{0}^{M} \boldsymbol{t} \cdot \frac{|\boldsymbol{h(t)}|^2}{\boldsymbol{E_h}} \, \boldsymbol{dt} \tag{5.3.1.6}$$

Feature 2 (F2): RMS delay spread, or more precisely, time interval through the MPCs are spread [152], [158]:

$$\boldsymbol{\tau_{RMS}^2} = \int_{0}^{L} (\boldsymbol{t} - \boldsymbol{\tau_{MED}})^2 \cdot \frac{|\boldsymbol{h(t)}|^2}{\boldsymbol{E_h}} \, \boldsymbol{dt} \tag{5.3.1.7}$$

Feature 3 (F3): Power difference between estimated received signal strength and estimated power of the first impulses [72]:

$$\boldsymbol{P_D} = \boldsymbol{10 \log_{10}} \frac{\boldsymbol{maxGrowthCIR} \times \boldsymbol{2^{17}}}{\boldsymbol{F_1^2 + F_2^2 + F_3^2}} \tag{5.3.1.8}$$

Feature 4 (F4): Ratio of power maximum noise and power in the first path (closer to the value 1, the CIR is more NLOS) [72]:

$$\boldsymbol{R_{MAXNOISE/FP}} = \frac{\boldsymbol{P_{MAXNOISE}}}{\boldsymbol{F_2}} \tag{5.3.1.9}$$

Feature 5 (F5): Kurtosis is providing information about the received MPCs [158]:

$$\boldsymbol{\kappa} = \frac{\boldsymbol{E}\left[\left(|\boldsymbol{h(t)}| - \boldsymbol{\mu_{|h(t)|}}\right)^4\right]}{\boldsymbol{E}\left[\left(|\boldsymbol{h(t)}| - \boldsymbol{\mu_{|h(t)|}}\right)^2\right]^2} \tag{5.3.1.10}$$

Furthermore, the following individual data from the diagnostics vector ***D*** will be taken into account:

Feature 6 (F6): *stdNoise* (Standard deviation of noise level)

Feature 7 (F7): *maxGrowthCIR* (channel impulse response max growth CIR)

Feature 8 (F8): *MaxNoise* (LDE max value of noise)

Figure 5.15 shows the feature correlation matrix, where a high correlation was shown between *F1* and *F2*, *F1* and *F5*, *F6* and *F8*. Features that correlate by more than 60% are removed (*F2*, *F5* and *F8*).

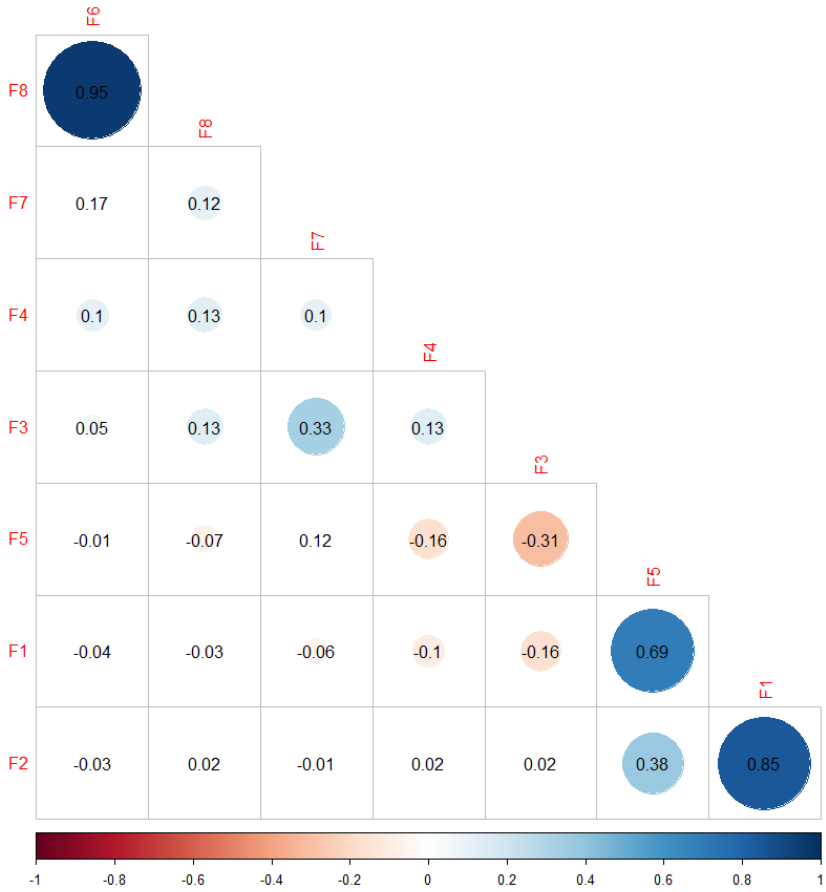

Figure 5.15 Noise features correlation matrix for Node 2

Therefore, the feature vector was represented as an $x_j \in \mathbb{R}^5$, where $j \in \{0, M\}$, and M was the number of the CIR measurements. With the weight coefficients calculation, the goal is to calculate the noise level. Therefore, it was decided to calculate the skewness coefficient for each feature vector, as it measures the tailedness of a distribution. Tailedness will show how often outliers occur, or noise in this case. Moreover, in this study, all body movements

are considered as moving clutter, and breathing can be represented as a sinusoidal function of time:

$$\boldsymbol{x(t) = a_b sin(2\pi f_b t) + e_n(t),} \quad \textbf{(5.3.1.11)}$$

where a_b and f_b are the amplitude and frequency breathing, and e_n was moving clutter (body movement).

The skewness $\tilde{\mu}_3$ coefficient was calculated for each of them, and results are given in Table 5.7, following the distribution of each feature shown in Figure 5.17. According to Table 5.7 and Figure 5.17, the σ_w was constructed, as follows:

$$\boldsymbol{\sigma_w = \sum_{i=1}^{5} F_i \beta_i,} \quad \textbf{(5.3.1.12)}$$

where regardless of the priority level the coefficient $\beta \in \{1,5\}$, was set to the negative power of ten $\{10^{-1},10^{-2},10^{-3},10^{-4}\}$ except the first priorty that was set to the 10^1. Example of the σ_w signal for one patient is presented in Figure 5.16.

Table 5.7 Skewness of the selected features

Features	F1	F3	F4	F6	F7
$\tilde{\mu}_3$	0.383	-3.101	-869.632	-0.254	-0.574
Priority level	4th	2nd	1st	5th	3rd

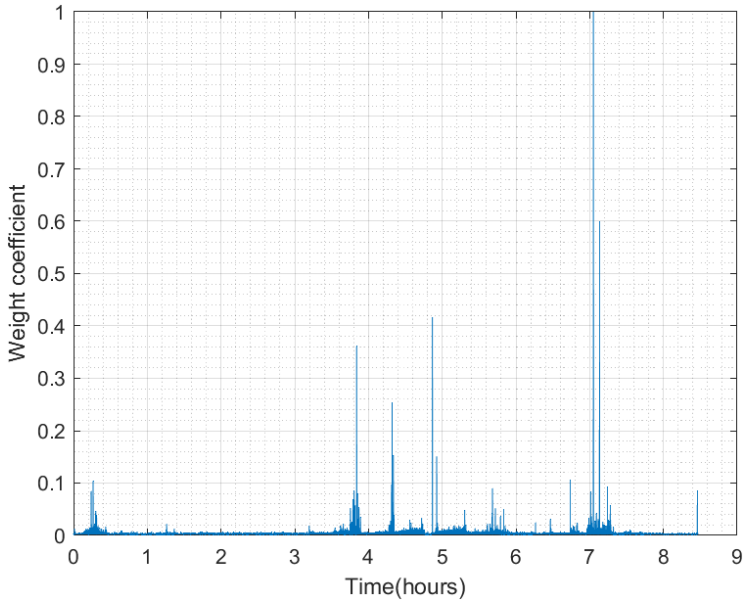

Figure 5.16 Example of the weight coefficient values for one patient

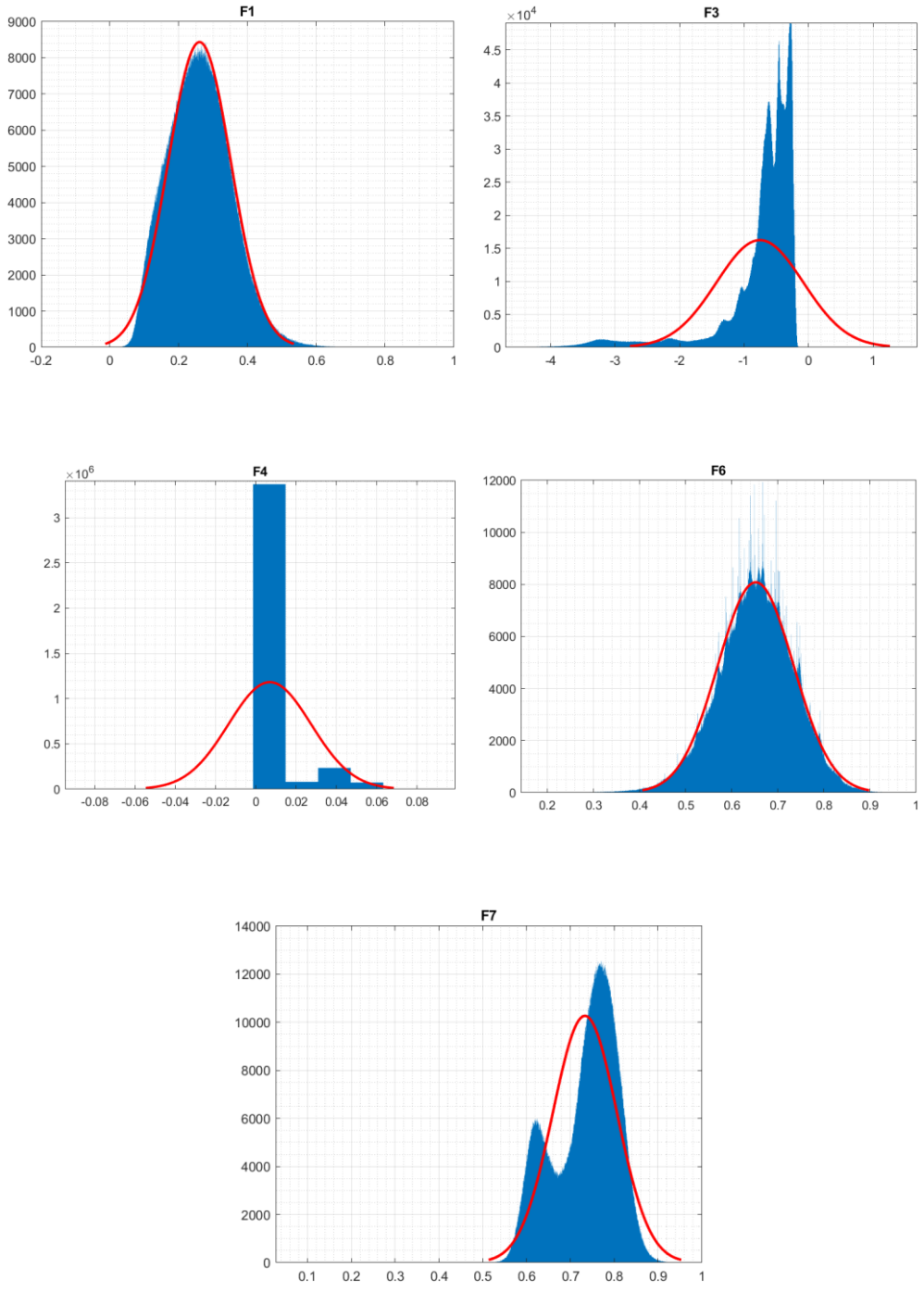

Figure 5.17 Graphical representation of distribution for selected features (*F1*, *F3*, *F4*, *F6*, *F7*)

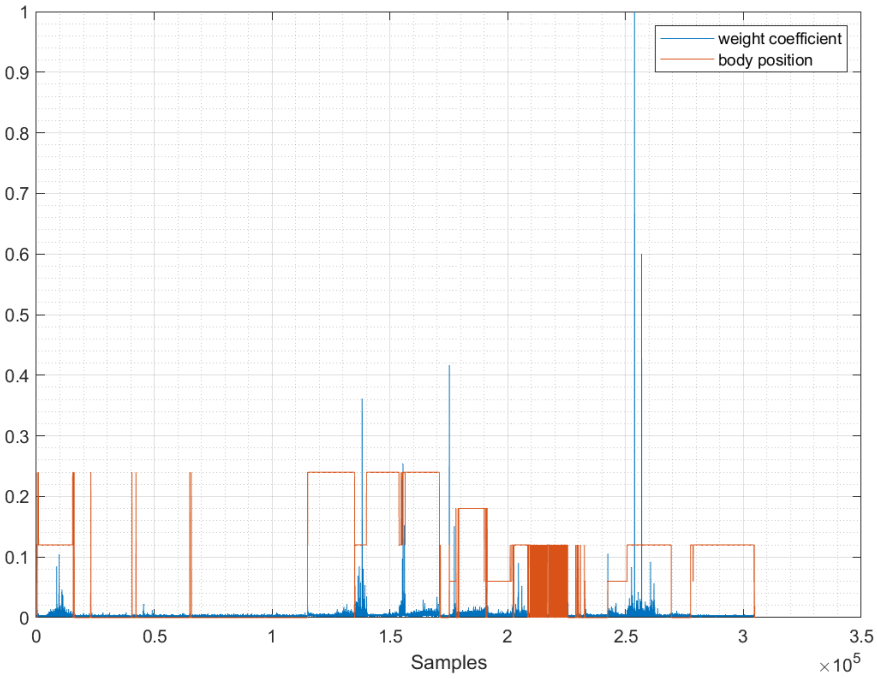

Figure 5.18 Example of the weight coefficient values for one patient with the body transition annotations

As mentioned in Chapter 4, the reason for using two nodes was that in a certain situation or sleep body position, one of the nodes will be more sensitive to capturing the breathing, but regarding the sleep postural transitions, the second, lower node was more sensitive to capture sleep postural transition, and it will be used for a σ_w calculation.

A weighted Short-Time Fourier Transform (STFT) was performed for a breathing calculation. The STFT is a method for analyzing a signal in the time-frequency domain. It was done by dividing the signal into small overlapping segments and performing a Fourier transform (FT) on each of these segments. The output of the STFT was presented as a time-frequency representation (TFR), where each bin holds its TFR – the result was represented as a three-dimensional array X_1 and X_2 [157], [159]:

$$\boldsymbol{X_1 = \sum_{l}^{N_1-1} H_{1_l} w(n-l) e^{-j2\pi lk/N_1},} \quad \textbf{(5.3.1.13)}$$

$$\boldsymbol{X_2 = \sum_{l}^{N_2-1} H_{2_l} w(n-l) e^{-j2\pi lk/N_2},} \quad \textbf{(5.3.1.14)}$$

where k is frequency domain index, $w(l)$ is a window function, shown in Figure 5.19. H_1 and H_2 are calculated as the output of the preprocessing stage for Node 1 and Node2.

The STFT within the Hanning window was applied. The window size was 5 seconds with the step size of 50% of the window size.

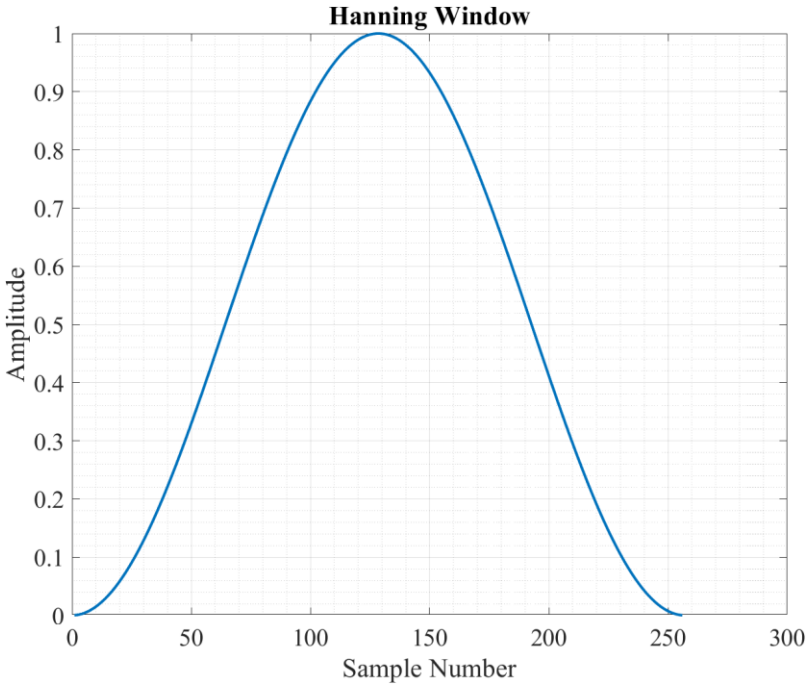

Figure 5.19 The representation of Hanning window function

Thereafter, multiplying outputs of the STFT function with labeling function Λ(·), only the part of the sleep where there was no significant body movement was considered for breathing calculation (such as during sleep postural transition). Due to physical constraints, it was impossible to accurately extract breathing if the body movement superiorly interferes with it; that was the case during sleep postural transition. The labeling function Λ(·) was computed by the following rule:

$$\boldsymbol{\Lambda(g) = \begin{cases} 1, \ if\ \sigma_w < \xi \\ 0, \ otherwise.' \end{cases}} \qquad \textbf{(5.3.1.15)}$$

where ξ was a threshold value set to the 95% of the σ_w mean value calculated each 5 minutes with an overlap of 50%, and g was the vector with the selected indexes of the "good" CIR frames.

Eventually, weighted STFT for sleep postural transition and breathing was represented as:

$$\boldsymbol{W_{br_1} = \Lambda(g) X_1} \qquad \textbf{(5.3.1.16)}$$

$$\boldsymbol{W_{br_2} = \Lambda(g) X_2} \qquad \textbf{(5.3.1.17)}$$

Furthermore, the maximum frequency in the range of 0.1 up to 0.4 Hz was detected, and it was considered as the breathing rate.

5.3.1.4 Breathing and sleep postural transition detection methods

After frame selection and frame weighting, depending on the amount of noise in a particular frame, the combined CIR was used from both nodes for further calculation. Still, the influence and results of the particular node after frame selection is shown in Table 5.8. In addition, the accuracy of each node has been presented, and it was concluded that the position of the UWB transmitter and receiver and the distance between the transmitter and receiver pairs influence the accuracy estimations of the sleep breathing and sleep postural transitions.

Table 5.8 The error statistics for the overall UWB breathing rate detection compared with the PSG measurements for Node 1 and Node 2 after stream selection

	MAE (bpm)	Min error (bpm)	Max error (bpm)	STD (bpm)	Man-Whitney U p-value
Node 1	0.544	0	4.01	0.339	$< 1x10^{-6}$
Node 2	0.521	0	2.9	0.373	$< 1x10^{-6}$

The statistical output of the error calculation before applying the CIR algorithm and after implies that the error was lower around 12 times, as shown in Table 5.9.

Table 5.9 The error statistics for the overall UWB breathing rate detection compared with the PSG measurements before and after stream selection for combined CIR

	MAE (bpm)	Min error (bpm)	Max error (bpm)	STD (bpm)	Man-Whitney U p-value
Before	4.547	0	14	3.292	$< 1x10^{-6}$
After	0.419	0	2.903	0.371	$< 1x10^{-6}$

Adding one more node increased the spatial diversity of measurements. More precisely, the node with favorable radio link or CIR measurements due to different (favorable) spatial orientations were chosen, and the other node with poor fading characteristics were ignored.

As stated in [160], the average percentage of movement during sleep for the general adult population is around 4 up to 11%. In this case, after a frame selection, for overall recording, an average of **9.15 ± 3.45%** of body movement was drop-out for a breathing analysis.

Moreover, the mean absolute error (MAE) for the overall UWB breathing rate detection when the patient was in the particular body positions (right, prone, left, and supine) compared with the PSG measurements after stream selection was enabled for combined CIR, is shown in Table 5.10. As shown in the table, the best accuracy was for the right body positions.

Table 5.10 The MAE and STD for the overall UWB breathing rate detection when the patient was in the particular body positions (right, prone, left, and supine) compared with the PSG measurements after stream selection was enabled for combined CIR

	MAE (bpm)	**STD (bpm)**	**Man-Whitney U p-value**
Right	0.118	0.077	$< 1x10^{-6}$
Prone	0.959	0.578	$< 1x10^{-6}$
Left	0.332	0.178	$< 1x10^{-6}$
Supine	0.482	0.234	$< 1x10^{-6}$

The difference in the respiratory peaks' detection in the time domain between the *Sleep UWB platform* and reference PSG device is shown through the Bland-Altman plot, Figure **5.20**.

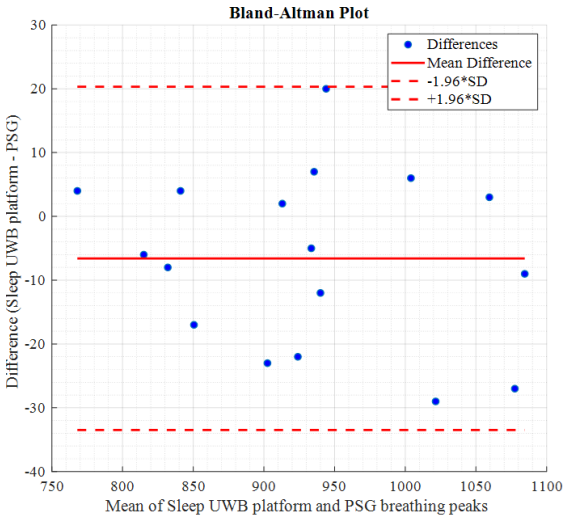

Figure 5.20 Comparison of the respiratory peak detection in time domain between *Sleep UWB platform* and PSG device

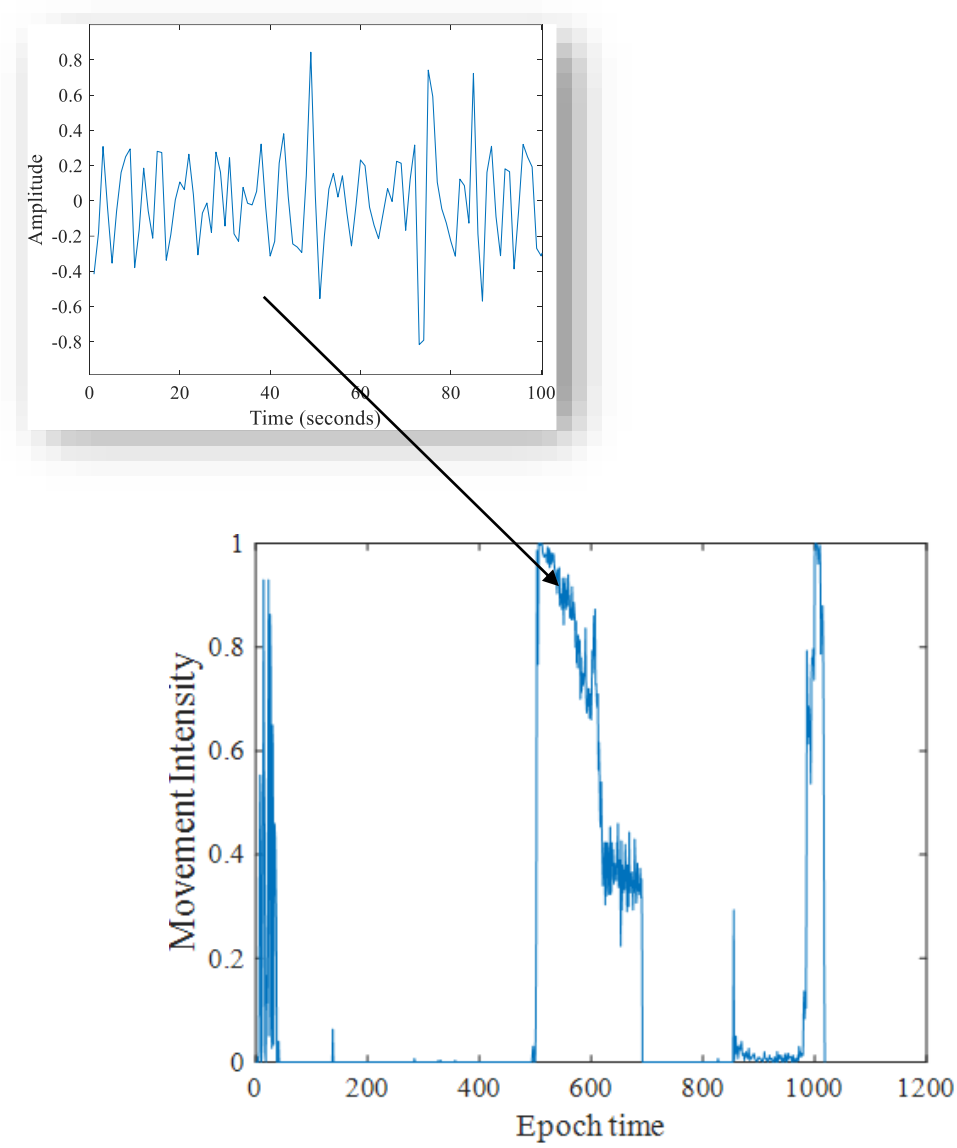

Figure 5.21 Breathing segment in the movement phase for ID03

The mean absolute error(MAE) and standard deviation (SD) compared with the reference PSG device for Node 1 and Node 2 are given in Table 5.11 and Table 5.12 for each patient. Furthermore, results after a frame selection and node selection (based on the noise level detection) are given in Table 5.13.

Table 5.11 Mean absolute error (MAE) and standard deviation (SD) for Node 1 before a stream selection

ID	MAE	STD	Man-Whitney U p-value
1	4.135	2.820	
2	4.976	3.460	
3	4.226	2.967	
4	4.106	2.896	
6	4.732	3.149	
7	3.777	2.549	
8	5.905	3.763	
9	4.579	3.113	$< 1x10^{-6}$
10	3.895	2.701	
11	7.380	4.106	
12	6.459	4.471	
13	7.805	4.283	
14	3.029	2.058	
15	3.637	2.631	
16	3.896	2.742	
17	6.563	3.194	

Table 5.12 Mean absolute error (MAE) and standard deviation (SD) for Node 2 before a stream selection

ID	MAE	STD	Man-Whitney U p-value
1	4.168	2.843	$< 1x10^{-6}$
2	4.886	3.380	
3	4.317	3.025	
4	4.197	2.911	
6	4.430	3.182	
7	3.787	2.544	
8	5.763	3.776	
9	4.671	3.166	
10	3.285	2.246	
11	6.647	4.370	
12	7.380	4.106	
13	7.134	4.532	
14	3.113	2.19	
15	3.962	2.736	
16	4.006	2.720	
17	8.289	4.136	

Table 5.13 Mean absolute error (MAE), standard deviation (SD) and percentage of the extracted minutes (%) for combined node selection after stream selection

ID	MAE	STD	Percentage of the extracted minutes (%)	Man-Whitney U p-value
1	0.429	0.378	3.641	$< 1x10^{-6}$
2	0.437	0.382	2.011	
3	0.444	0.384	12.213	
4	0.423	0.375	29.950	
6	0.504	0.408	13.910	
7	0.407	0.367	20.821	
8	0.408	0.367	8.56	
9	0.440	0.383	3.807	
10	0.368	0.345	8.708	
11	0.417	0.372	9.705	
12	0.402	0.320	14.1	
13	0.512	0.492	10.93	
14	0.298	0.208	9.983	
15	0.321	0.315	9.33	
16	0.396	0.361	7.643	
17	0.458	0.391	4.162	

The movement analysis was performed using a threshold algorithm, where from the obtained number of the movement indexes higher than the thresholds, the restlessness and duration of movements (number of movements) are calculated [118]. Restlessness was divided into small, medium, and large:

(b) **Small:** magnitude of movement smaller than 40%

(c) **Medium:** magnitude of movement from 40% up to 80%

(d) **Large:** magnitude of movement higher than 80%

Duration was divided into smaller than 1 second, between 1 and 10 seconds, and higher than 10 seconds.

The restlessness was analysed over epoch time, where one epoch represents 30 seconds of recordings. The example of body movement variability (BMV) for the patients (ID6, ID9, ID11, ID113 and ID16) are shown in Figure 5.22., Figure 5.23, Figure 5.24, Figure 5.25 and Figure 5.26, along with information on the sleep stage. As shown, the algorithm can detect large movements related to the awakening, as much as the smaller movements related to the turnovers and movements in the bed.

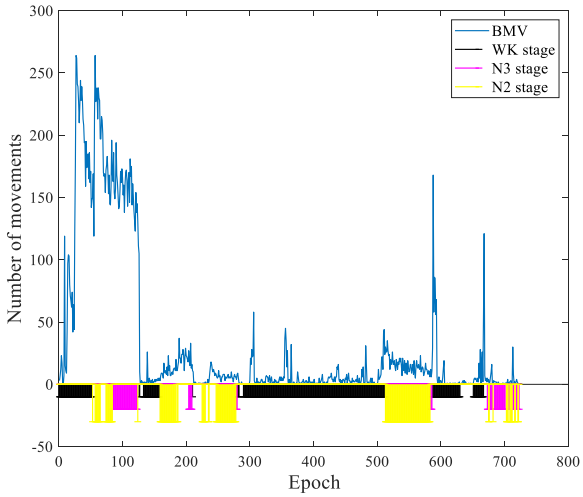

Figure 5.22 Body movement variability (BMV) through the epoch time for the patient ID6

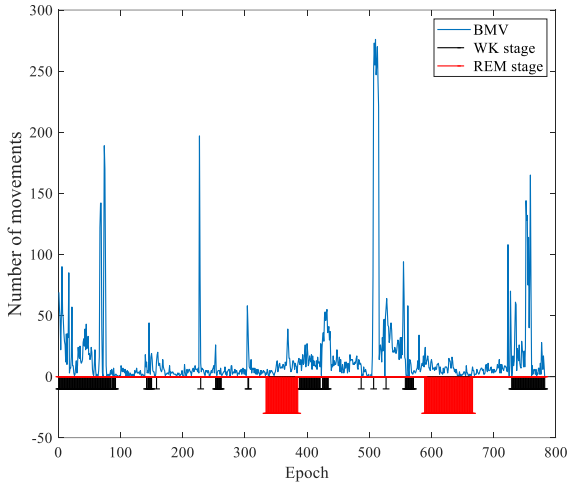

Figure 5.23 Body movement variability (BMV) through the epoch time for the patient ID9

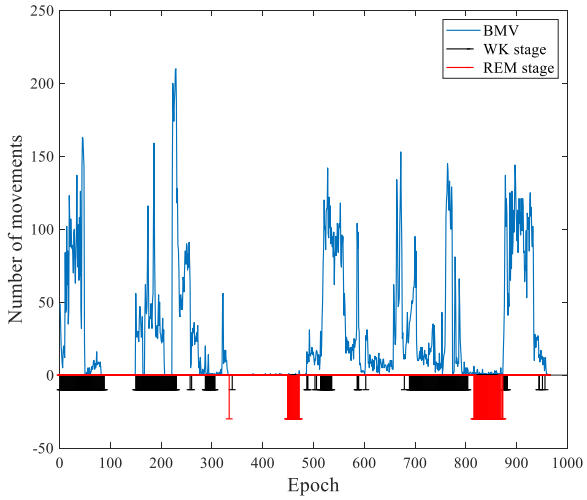

Figure 5.24 Body movement variability (BMV) through the epoch time for the patient ID11

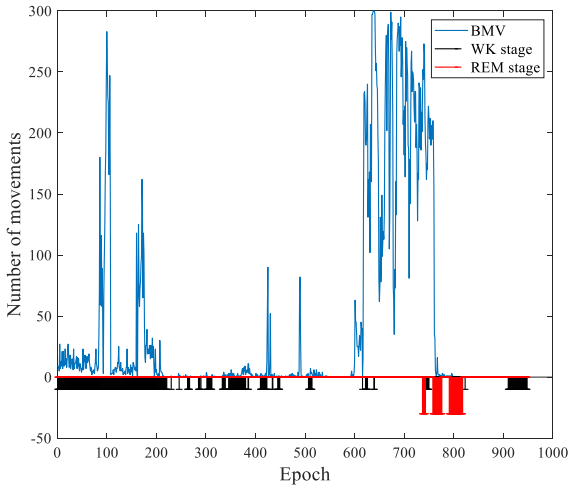

Figure 5.25 Body movement variability (BMV) through the epoch time for the patient ID16

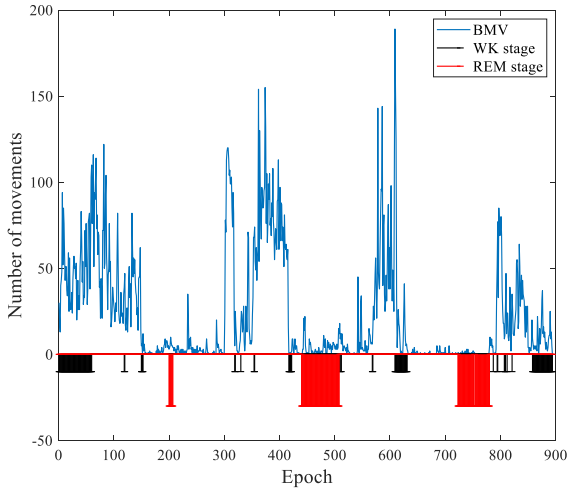

Figure 5.26 Body movement variability (BMV) through the epoch time for the patient ID13

The percentage of restlessness and number of body movements per epoch was presented in Table 5.14, along with information from the clinical report, where sleep efficiency was calculated using the following equation:

$$\boldsymbol{Sleep\ Efficiency} = \frac{\boldsymbol{Total\ sleep\ time}}{\boldsymbol{Time\ in\ bed}} \times \mathbf{100} \qquad \textbf{(5.3.1.18)}$$

Moreover, the scatter plot of the restlessness data and the sleep onset is shown in Figure 5.27.

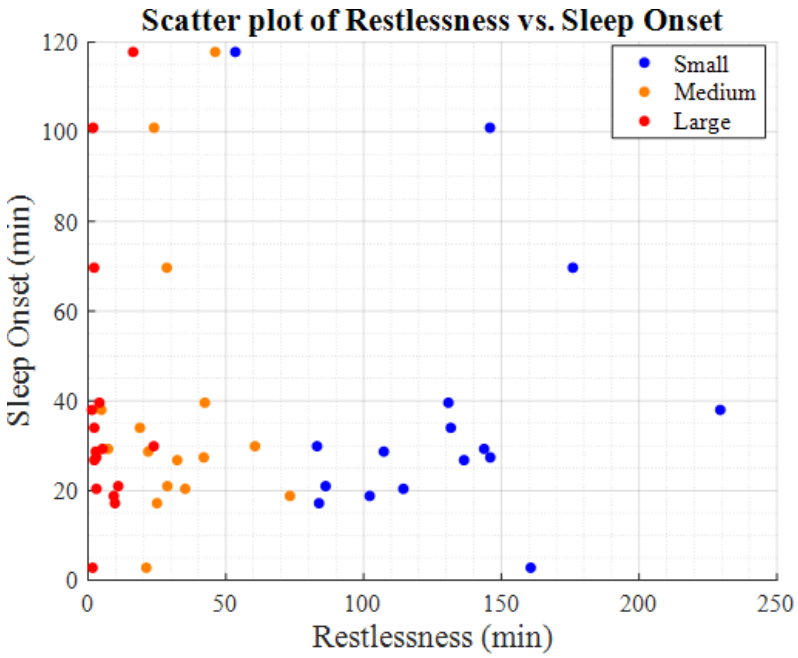

Figure 5.27 Restlessness versus Sleep Onset for small, medium, and large movement

Table 5.14 Percentage of restlessness and number of body movements per epoch along with a clinical report data

ID	Restlessness (min)			Movements per epoch			From clinical report:			
	Small	Medium	Large	< 1 sec	1 sec > & <10 sec	> 10 sec	Sleep Onset (min)	Sleep Efficiency (%)	WASO (min)	TST (min)
1	143.73	7.266	5.226	449	59	16	29.3	70	103.5	310.5
2	**229.45**	4.815	1.390	222	56	8	38	73	100.9	376
3	102.22	**73.278**	9.311	119	41	216	18.8	94.2	10.4	477
4	83.110	60.566	**23.803**	440	301	**222**	29.9	81.1	66	411.5
6	86.211	28.763	10.938	338	159	107	21	51.2	154.1	183.5
7	83.818	25.016	9.746	79	366	24	17.2	79	75.1	347
8	114.43	35.243	3.013	124	659	0	20.4	84.6	40.1	333
9	131.64	18.798	2.228	457	236	21	34	79	46.2	302.5
10	107.31	21.830	2.765	425	246	21	28.7	64.2	108.9	247
11	130.77	42.355	4.115	222	360	88	39.6	63	136.8	300
12	175.97	28.566	2.170	454	276	57	69.7	73.8	42.5	315.5
13	136.45	32.338	2.290	319	356	30	26.8	83.4	47	370.5
14	145.87	23.931	1.836	394	419	18	100.9	72.4	20.2	318
15	160.65	21.120	1.641	507	237	37	2.8	87.8	52	394
16	53.458	46.123	16.361	281	124	151	117.8	53.1	112.2	253
17	145.97	41.985	2.960	186	707	0	27.4	86	37.3	397

As shown in Table 5.14 and Figure 5.29, a maximum number of large movements was obtained for patient ID04 (Female, BMI: 36.4 kg/m^2, 56 years, AHI: 11.1 events/h) – as shown in Figure 5.28, where the noticeable movements can be seen from epoch 400 up to 1000.

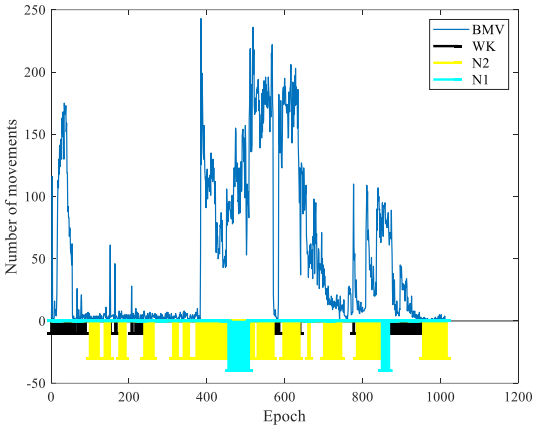

Figure 5.28 Body movement variability (BMV) through the epoch time for the patient ID4

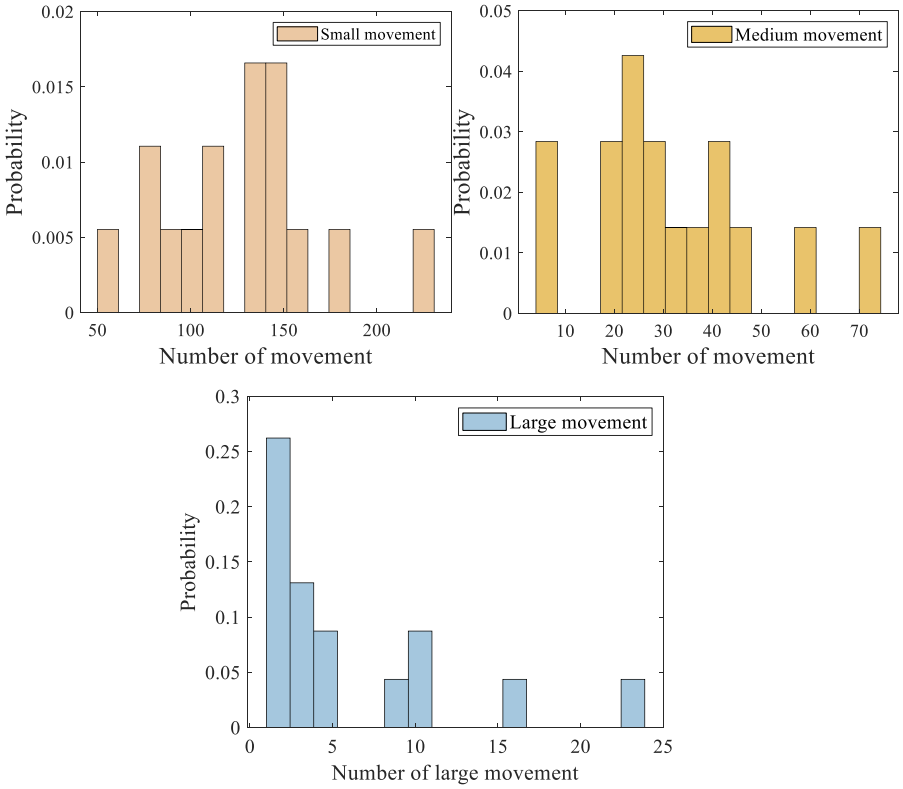

Figure 5.29 Number of small, medium, and large movements

Table 5.15 shows a comparison of turnover detection (sleep postural transitions). The turnovers from the PSG are obtained from the information on sleep position change from supine to side (right and left), supine to prone and vice versa. During measurements, it was noticed that the PSG body position sensors had their uncertainty and was showing the changing in the body position body without it actually happening. The researcher tries to update annotations in the post-recording phase using information from the camera. Still, it needs to be emphasized that the reference system has an error at the input.

Regardless, in Table 5.15 it was evident that the error in accurate sleep postural detection was higher for the higher AHI.

Table 5.15 Comparison of turnovers detection obtained from PSG and Sleep-UWB platform

ID	Sleep postural transition detection performance		OSA severity
	Accuracy (%)	F-1 score (%)	AHI (events/h)
1	83.56	91.04	6.8
2	54.7	65.57	66
3	43.75	52.3	35
4	69.3	76.07	11.1
6	93.02	95.12	4.3
7	72.09	82.19	14.5
8	70.37	82.6	20.9
9	79.31	88.46	1.4
10	94.5	93.67	6.6
11	51.33	52.08	29.8
12	81.96	89.09	20.3
13	53.87	63.78	53.8
14	97.82	98.8	4.2
15	90.65	87.71	21.9
16	73.56	80.82	17.5
17	76.19	76.47	13.5

The influence of a supine position percentage on a AHI index was presented in Figure 5.30.

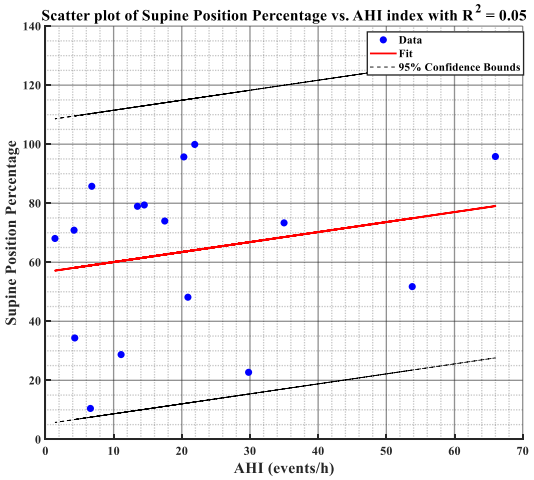

Figure 5.30 Supine sleep position percentage vs AHI index for each patient

The influences of each patient's obesity on the detection of breathing and the analysis of sleep postural transitions are presented in Figure 5.31. For breathing, there was no significant influence, but for sleep, postural transition detection with a lower BMI, the accuracy of the sleep postural transition detection was higher, as shown in (c).

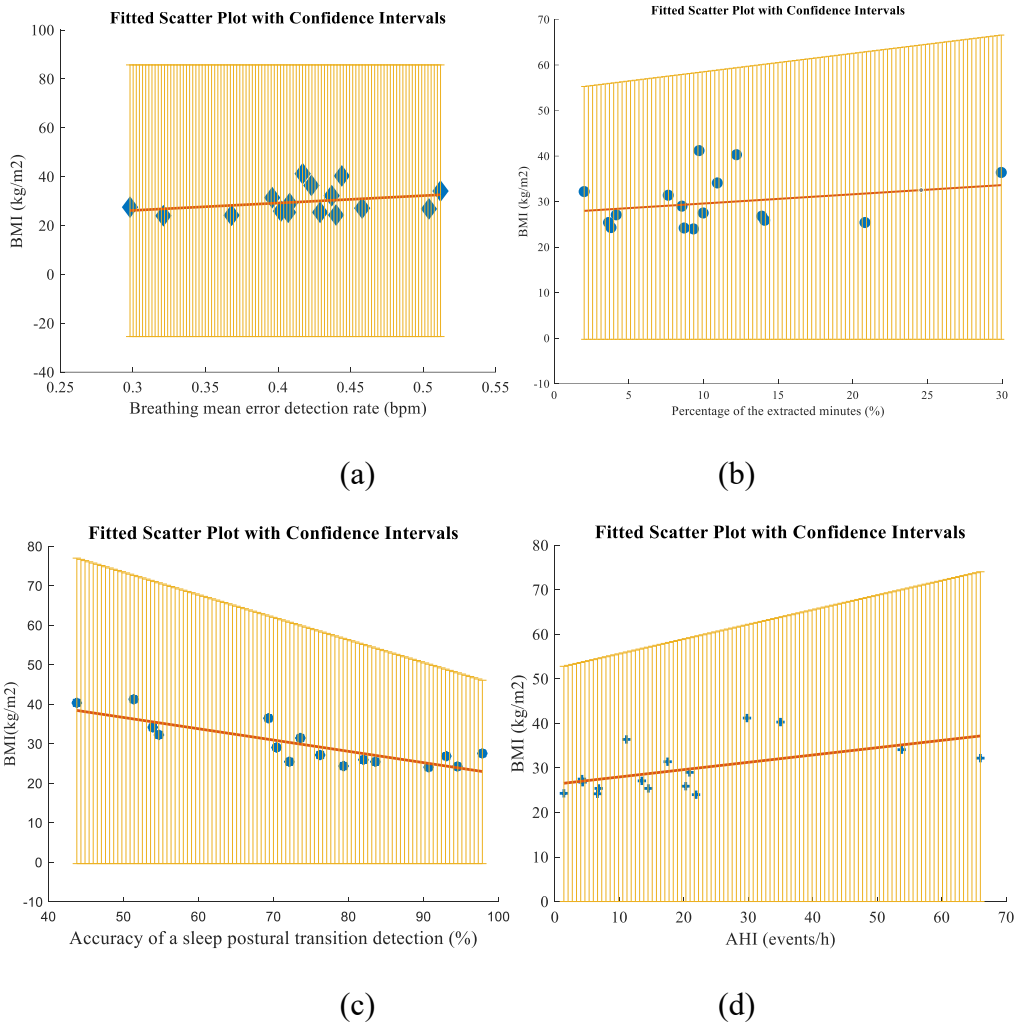

Figure 5.31 Fitted scatter plot with confidence interval for: (a) BMI vs Breathing detection error, (b) BMI vs Percentage of the extracted minutes for breathing calculation, (c) BMI vs Accuracy of sleep postural transition detection, (d) BMI vs AHI

5.3.2 Classification models

After the preprocessing and processing steps, feature engineering methods are applied to the sleep breathing and postural transition patterns to classify respiration and body position events during sleep.

The breathing patterns (*RespEvent*) are classified as follows:

- **No event** (normal sleep breathing without SDB episodes): **Class 0**
- **Apnea event** (obstructive, central, mixed): **Class 2**
- **Hypopnea event: Class 1**

The sleep postural transition events (*PosEvent*) are classified as follows:

- **Side to Supine** (right to supine and left to supine): **Class 1**
- **Supine to Side** (supine to right and supine to left): **Class 2**

In total, **3138 respiratory events** are used, around 1000 events per class (No event, Hypopnea, Apnea), as shown in Table 5.16. The length of each segment varies according to the event duration, where the maximum event was 124.5 seconds long, and the minimum was 10.5 seconds. Moreover, the +10 seconds before and after events were taken into account due to an uncertainty of the accurate labeling of the start time of each event. Afterward, the events are segmented into single segments for further feature extraction and implementation of classification methods.

For the *PosEvent*, 74 segments per class were extracted from the overnight recordings, as shown in Table 5.17.

Table 5.16 Number of *RespEvent* segments for each class

	Train	**Test**	**Σ**
No event	749	321	1070
Hypopnea	743	318	1061
Apnea	705	302	1007
Σ	2197	941	3138

Table 5.17 Number of *PosEvent* segments for each class

	Train	**Test**	**Σ**
Side to Supine	59	15	74
Supine to side	59	15	74
Σ	118	30	148

Since segments are of different duration (Figure 5.34), in order to achieve the same dimension of the input signal to the model, all segments are interpolated to a total of 160 seconds using the modified Akima piecewise cubic Hermite interpolation [161]. It is a piecewise cubic interpolation method that uses a different cubic polynomial to approximate the function in each interval between the data points. One of the main advantages of the Akima interpolation method is that it creates a smooth and continuous function that passes through the data points and maintains the continuity of the first and second derivatives at the data points. The integrated Matlab (version: R2022b) function *makima* was used. In comparison with the original interpolation equation, the integrated Matlab function uses modified weights coefficients:

$$\boldsymbol{w_1 = |\delta_{i+1} - \delta_i| + \frac{|\delta_{i+1} - \delta_i|}{2}}, \tag{5.3.1.19}$$

$$\boldsymbol{w_2 = |\delta_{i-1} - \delta_{i-2}| + \frac{|\delta_{i-1} - \delta_{i-2}|}{2}}, \tag{5.3.1.20}$$

$$\boldsymbol{\delta_i = \frac{v_{i+1} - v_i}{x_{i+1} - x_i}}, \tag{5.3.1.21}$$

where δ_i is slope in the interval from $[\, x_i, x_{i+1} \,]$, and w_1 and w_2 are weights values. Furthermore, after an interpolation method was applied, the variability of the new sampling rate for calculating the features was taken into account after interpolation. Figure 5.32 and Figure 5.33 shows the power spectrum of each observed sleep-breathing pattern before and after interpolation was applied.

Furthermore, before starting with the calculation of the features and classification, the normalization of each segment was done using a z-score normalization:

$$\boldsymbol{z = \frac{x - \mu}{\sigma}}, \tag{5.3.1.22}$$

where x, μ and σ denote sample, mean and standard deviation, respectively.

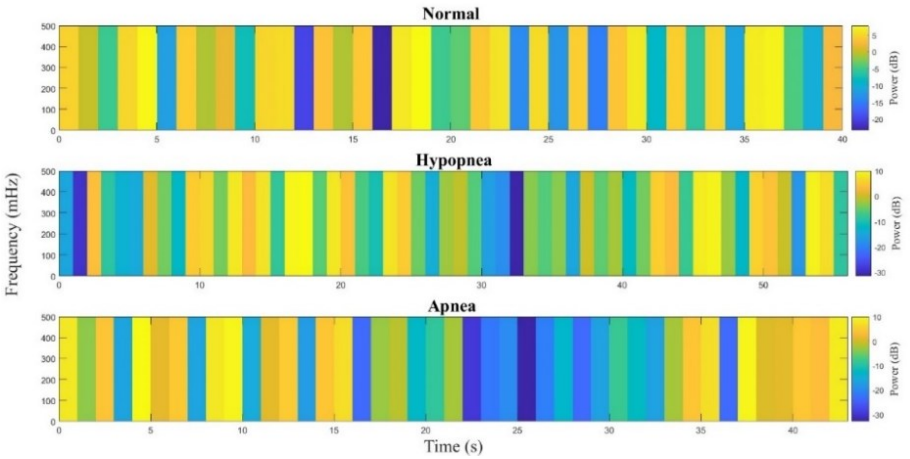

Figure 5.32 Power spectrogram of each breathing pattern:
Normal breathing without SDB episodes; Hypopnea; Apnea (OSA)

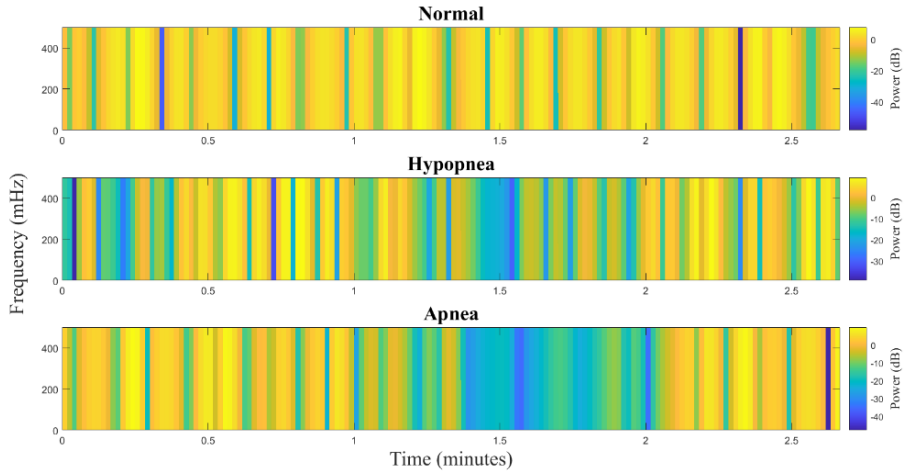

Figure 5.33 Power spectrogram of each breathing pattern after modified Akima piecewise cubic Hermite interpolation: Normal breathing without SDB episodes; Hypopnea; Apnea (OSA)

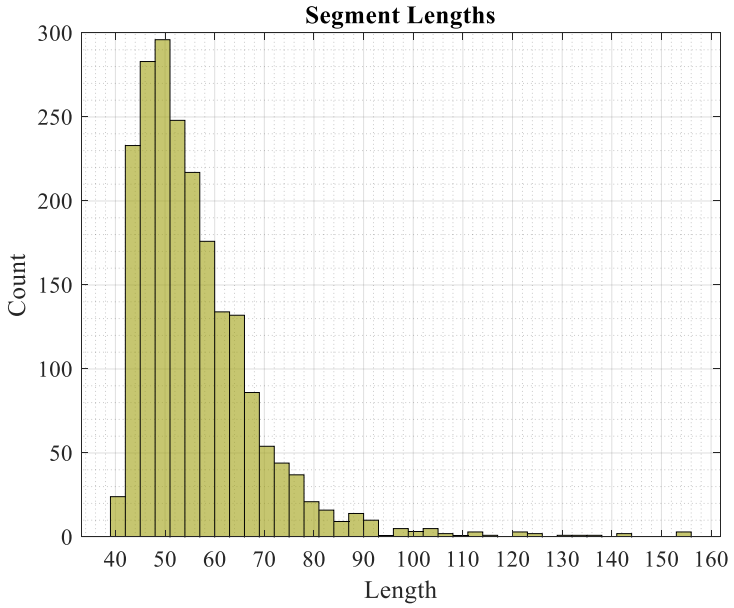

Figure 5.34 Apnea and hypopnea signal lengths

Regarding a evaluation performance, *F-1* measure, accuracy (train and test), and sensitivity were calculated. Moreover, the ROC curve was shown for each of the used machine learning models.

The *F-1* score, defines as a harmonic mean of the precision and recall indicators is used for measure of performance, and it was defined as:

$$\boldsymbol{F-1=\frac{2\times TP}{2\times TP+FP+FN}} \quad \textbf{(5.3.1.23)}$$

Moreover, the accuracy and sensitivity are represented by following equations:

$$\boldsymbol{Accuracy=\frac{TP+TN}{TP+TN+FP+FN}} \quad \textbf{(5.3.1.24)}$$

$$\boldsymbol{Sensitivity=\frac{TP}{TP+FN}} \quad \textbf{(5.3.1.25)}$$

5.3.2.1 Features extraction methods for sleep breathing and postural transitions patterns

5.3.2.1.1 Features extraction methods for sleep breathing

For a breathing patterns classification, the following group of features was used:

- statistical features,
- frequency domain features,
- time-domain features,
- time-frequency domain features.

Statistical features [10]**:**

1. Mean value
2. Min value
3. Median value
4. Interquartile range
5. Mean/median absolute deviation
6. Standard deviation
7. Kurtosis value[162]:

$$\boldsymbol{K=\frac{\sum_{i=1}^{N}(x_i-AM)^4}{(N-1)SD^4}} \quad \textbf{(5.3.1.26)}$$

8. Skewness value [162]:

$$S = \frac{\sum_{i=1}^{N}(x_i - AM)^3}{(N-1)SD^3} \quad \textbf{(5.3.1.27)}$$

Time domain features [6], [14], [162], [163]**:**

9. Envelope signal
10. Length of time between breaths (min, max, mean, std)
11. Amplitude variation
12. Respiratory rate
13. Maximum autocorrelation
14. Short-time energy
15. **Respiratory peaks:** Mean of heights, standard deviation of heights, skewness of heights, number of peaks, mean inter-peak distance, standard deviation of peak-distance skewness of inter-peak distance, sum of peak heights

The amplitude variation of the signal during apnea and hypopnea can be used to distinguish between them because apnea typically has a lower amplitude variation than hypopnea. Moreover, the respiratory rate during apnea typically results in a lower respiratory rate compared to hypopnea.

Frequency domain features [162] [57]**:**

16. Power spectral density (PSD)
17. Ratio of low-frequency to high-frequency power
18. Dominant frequency
19. Spectral entropy [164]:

$$Spectral\ entropy = -\sum_{i=1}^{N} f_t(i) log\, f_t(i), \quad \textbf{(5.3.1.28)}$$

f_t is the normalized magnitude of the *ith* frequency bin in the spectrum of the frame f_t.

Non-linear features [6], [14], [119], [161], [162]**:**

20. Sample entropy

    The sample entropy was used for quantifying a regularity of signal.

21. Approximate entropy

Time-frequency domain features [6], [14], [162], [163]**:**

22. Spectrogram based on the STFT calculation
    a. Spectral power
    b. Spectral edge frequency
    c. Harmonic to noise ratio (HNR)

There are **32 features** overall.

5.3.2.1.2 Features extraction methods for sleep postural transitions patterns

Regarding a *PosEvent*, an amount of movement within 1 second or fast movement, and the amount of movement quantity for a time window of 20 seconds, or slow movement within the average, area, variance and entropies of the motion signals were computed was computed [139], as well with following features:

Time domain features [118], [119], [162], [165], [166]**:**

- Acceleration: the difference between consecutive samples of the signal
- Jerk (second derivative)
- Movement latency
- RMS value
- Peak value
- Variance

Non-linear features [118], [119], [162], [165], [166]**::**

- Spectral entropy
- Approximate entropy

Frequency domain features [167], [168]**:**

- Crest factor
- the Wavelet Daubechies (db4) was calculated, with a decomposition level of 8. And for each level, it was calculated: mean absolute values, standard deviation, skewness, kurtosis, an average power of the signal coefficients in every subband and the ratio of the absolute mean values of signal coefficients of adjacent subbands.

There are **227 features** overall.

5.3.2.2 Features selection methods

Feature selection can be made by determining the relevance of the individual features [169]. They are ranked by some metrics, and if they do not satisfy the threshold, they are removed from the feature set. The second way of feature selection is by relevance and redundancy determination on the features' subset, where their significance is calculated by some information metrics or by classification algorithms; and redundant features detection is implemented implicitly in the procedure [169].

Filters methods for individual features are carried out by using information metrics (correlation coefficient, information gain or symmetrical uncertainty), chi-square, χ^2 (for categorical variables), Fisher's score and Relief family, etc. [169]. Here, the **ReliefF method** was used.

First, new feature values are compared between each class to see whether they are statistically different. This was done to test and understand the feasibility of detecting and classifying the specific class. For *RespEvent*, the Kruskal-Wallis test was applied to examine the significance of the difference, and all the hypothesis tests were rejected with a **p-value < 0.01.**

A whole set of 32 features was used for the breathing patterns classification. The ReliefF feature ranking is shown in Figure 5.35. The violin plot for four of the most significant features was shown in Figure 5.36. Moreover, to see the correlation between each of the input features for each class, a correlation plot is presented in Figure 5.37, Figure 5.38, and Figure 5.39. Despite some highly correlated features, the entire set of features was considered.

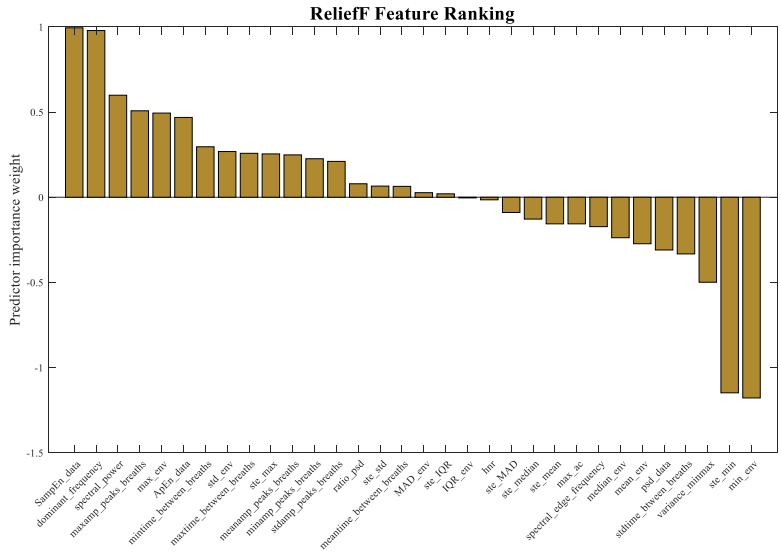

Figure 5.35 *RespEvent*: ReliefF rank ratio

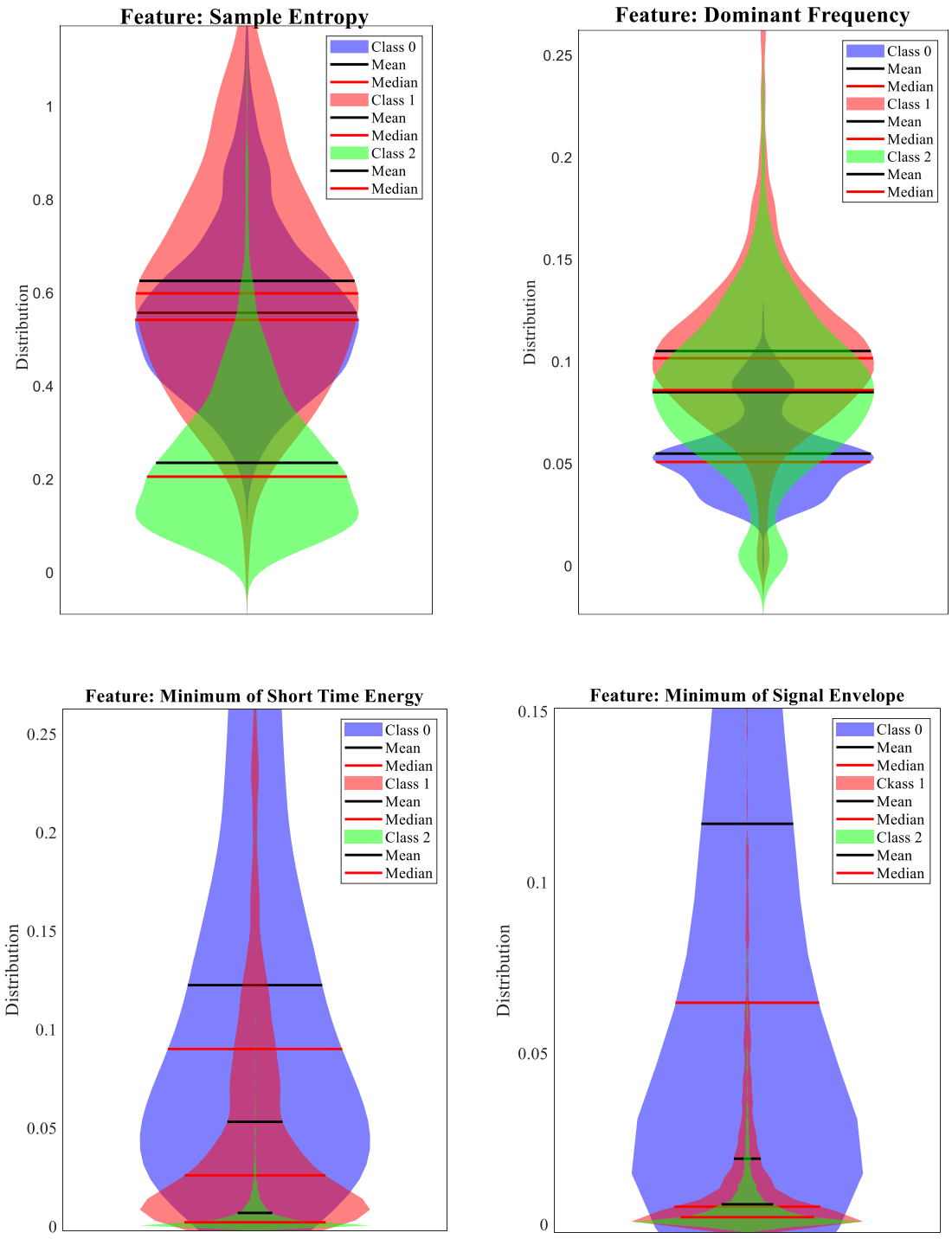

Figure 5.36 Violin plot of the distribution for each class of the four features: Sample Entropy, Dominant Frequency, Minimum of Short Time Energy, and Minimum of Signal Envelope.
Class 0: No event, **Class 1**: Hypopnea event, **Class 2**: Apnea event

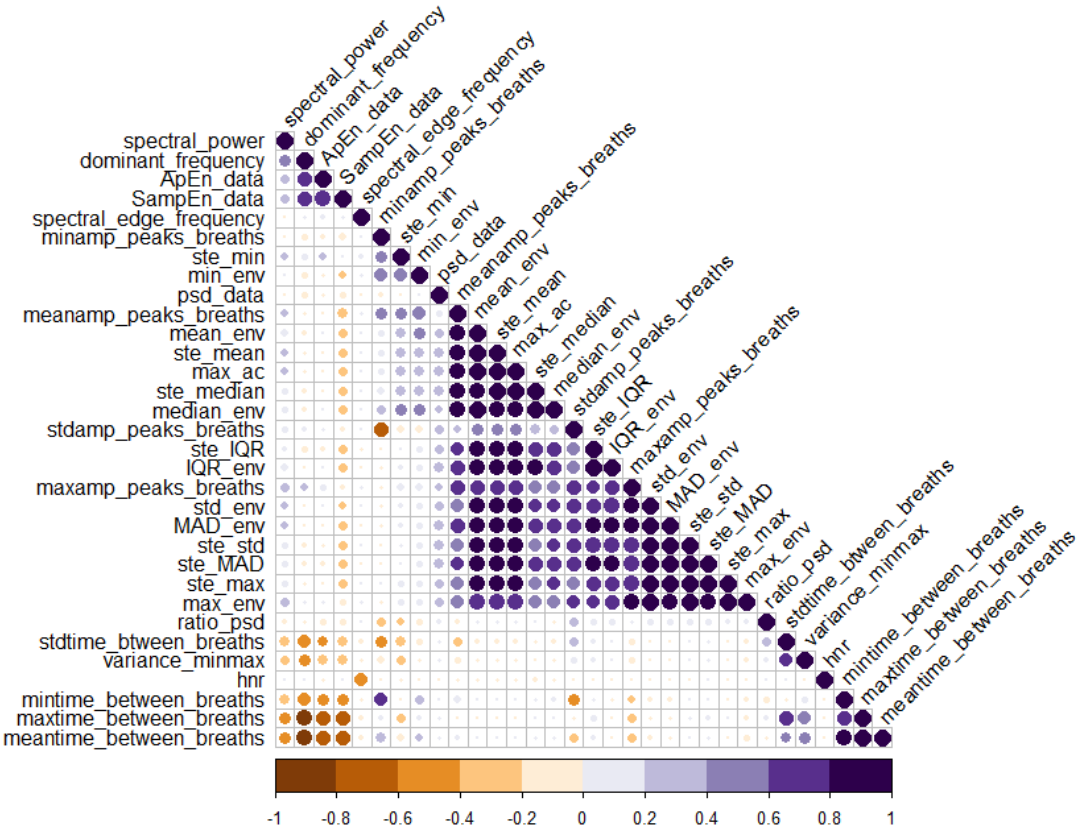

Figure 5.37 Class 0: No event. Correlation plot

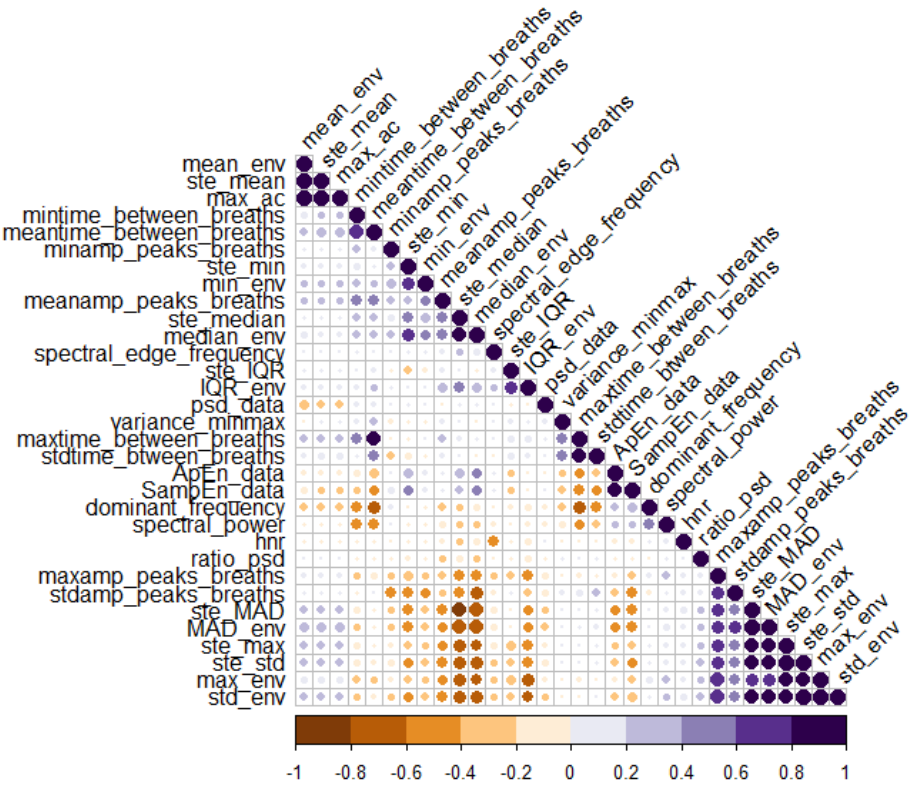

Figure 5.38 Class 1: Hypopnea. Correlation plot

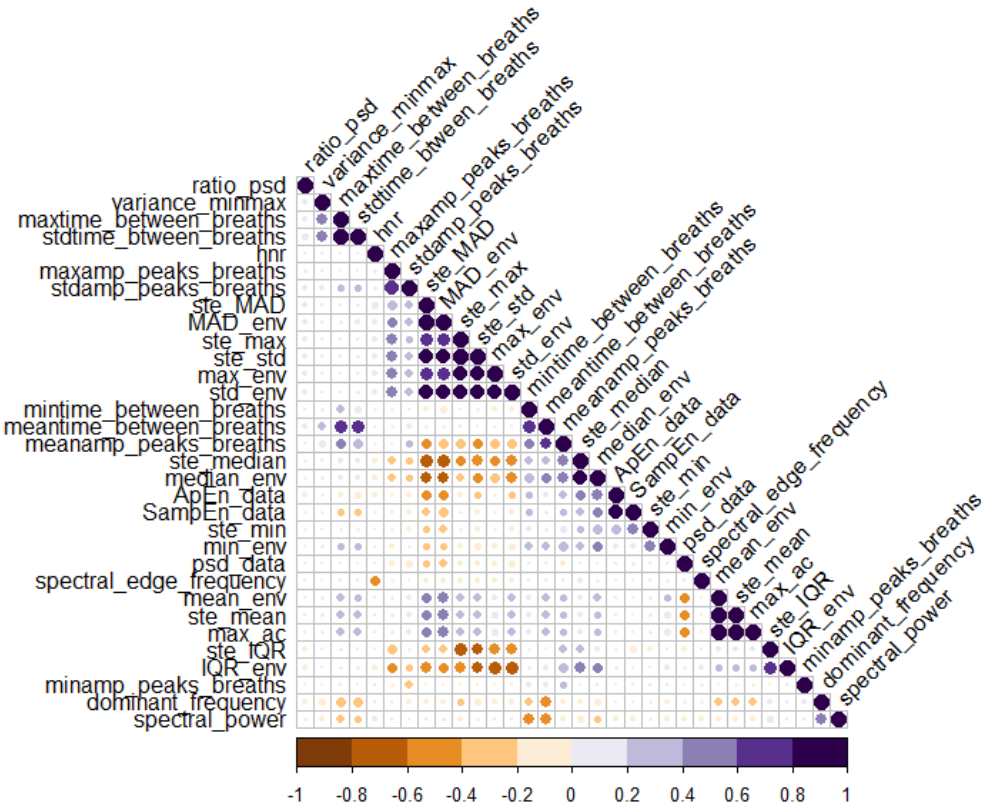

Figure 5.39 Class 2: Apnea. Correlation plot

For the sleep postural transition classification (*PosEvent*), it was decided to use the first ten best features. This was because the input feature set includes 53 features from the Wavelet Daubechies (db4), 23 features from the spectral entropy, and 65 PSD features, among others. So, ten features were shown to be relevant after an iterative procedure. The ReliefF feature ranking is shown in Figure 5.40. In addition, a violin plot for the two features was shown in Figure 5.41.

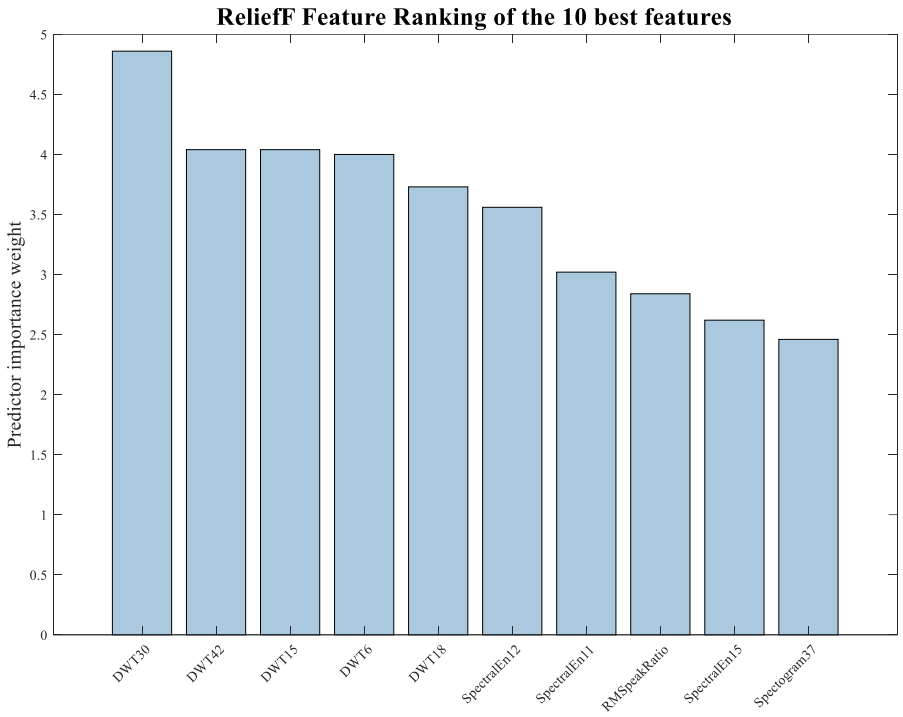

Figure 5.40 ***PosEvent***: ReliefF rank ratio of selected 10 best features

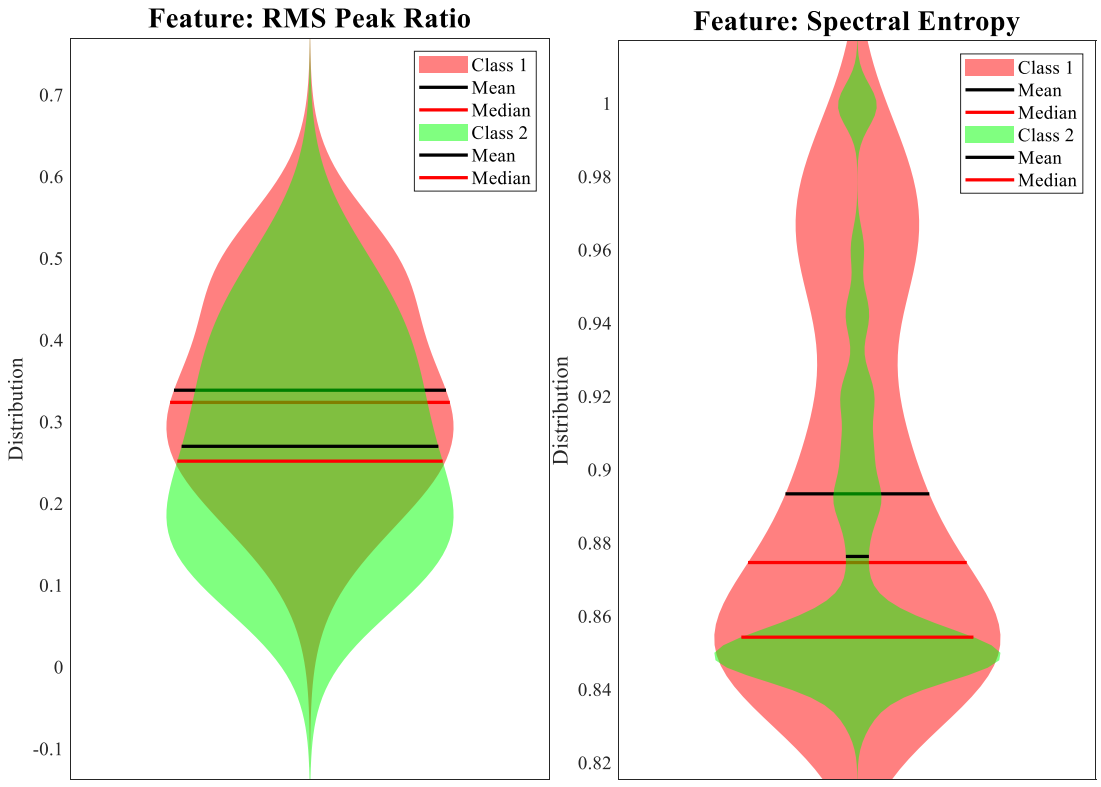

Figure 5.41 Violin plot of the distribution for each class of the two features: RMS Peak ratio, Spectral Entropy. **Class 1**: Side to supine, **Class 2**: Supine to side

5.3.2.3 Respiratory events classification

For the respiratory events (*RespEvent*) classification, the following machine models were used:

- Linear Discriminant Analysis
- Cosine KNN
- Medium Gaussian SVM
- Ensemble methods (Bagged Trees, Boosted Trees, and Optimizable)

Linear Discriminant Analysis: Linear Discriminant Analysis (LDA) is a dimensionality reduction technique. LDA projects features into a lower dimensional space such that the classes are separable in the new space.

Cosine KNN: Cosine KNN is a variant of the KNN (K-Nearest Neighbors) algorithm that uses cosine similarity between data points to determine the nearest neighbors instead of Euclidean distance.

Medium Gaussian SVM: Gaussian SVM is a type of SVM that uses a Gaussian kernel to transform the input data into a higher dimensional space, allowing it to capture non-linear relationships. Medium Gaussian SVM is an SVM model that uses a medium-sized Gaussian kernel.

Ensemble methods: Ensemble methods are machine learning algorithms that combine the predictions of multiple base models to achieve better performance. **Bagged Trees** is an ensemble method that uses bootstrapped samples of the training data to train multiple decision tree models and average their predictions. **Boosted Trees** is another type of ensemble method that trains a sequence of decision tree models, where each model attempts to correct the mistakes of the previous model. For the optimization variant, a Bayesian optimizer was used.

The used parameters for each of the models are given in Table 5.18. Additionally, 5-fold cross-validation has been used.

The performance evaluation is given in Table 5.19. The best accuracy was obtained for the ensemble models. Regardless, all models show suitable accuracy when comparing the accuracy of the classification of normal breathing and apnea or hypopnea class. The apnea and hypopnea classifications are slightly worse since the signal can be similar in some cases.

But the apnea to hypopnea classification does not have clinical significance compared to the apnea/hypopnea to normal breathing classification. The accuracy of each model for

classification normal to apnea/hypopnea was larger than 90%, and for the optimizable ensemble, models were 97.22% which was comparable with the state-of-the-art paper given in Chapter 3.3.1.

Table 5.18 Parameters setup for used classifiers models

Model	Parameters
Linear Discriminant Analysis	Covariance structure: Full
Cosine KNN	Number of neighbors: 10 Distance metric: Cosine Distance weight: Equal
Medium Gaussian SVM	Kernel function: Gaussian Kernel scale: 5.7 Box constraint level: 1 Multiclass method: One-vs-All
Boosted Trees	Ensemble method: AdaBoost Learner type: Decision tree Learning rate: 0.1 Maximum number of splits: 20 Number of learners: 30
Bagged Trees	Ensemble method: Bag Learner type: Decision tree Maximum number of splits: 20 Number of learners: 30 Number of predictors to sample: Select All
Optimizable Ensemble	Learner type: Decision tree Iterations: 30 Optimizer: Bayesian optimization Acquisition function: Expected improvement per second plus

Table 5.19 Performance evaluation for multiclassification (32 features) One-vs-All.
Class 0: No Event; Class 1 – Hypopnea, Class 2 – Apnea

Model	Validation Accuracy (%)	Test Accuracy (%)	F1-score (%)			Sensitivity (%)		
			Class 0	Class 1	Class 2	Class 0	Class 1	Class 2
Linear Discriminant Analysis	85.39	86.5	92.02	79.54	84.59	93.2	79.5	83.5
Cosine KNN	86.57	87.4	93.79	80.11	85.11	90.9	84.8	83.5
Medium Gaussian SVM	87.94	89.8	94.42	83.01	86.03	92.9	84.5	86
Ensemble methods								
Boosted Trees	88.6	91	96.41	84.45	91.39	95.9	82.7	87.1
Bagged Trees	88.9	90.8	97.09	84.45	84.72	96.1	84.1	86.1
Optimizable	89.4	90.9	97.22	85.21	85.46	96.1	85.1	86.7

The ROC curves within an AUC value for each class and each model are presented in Figure 5.42.

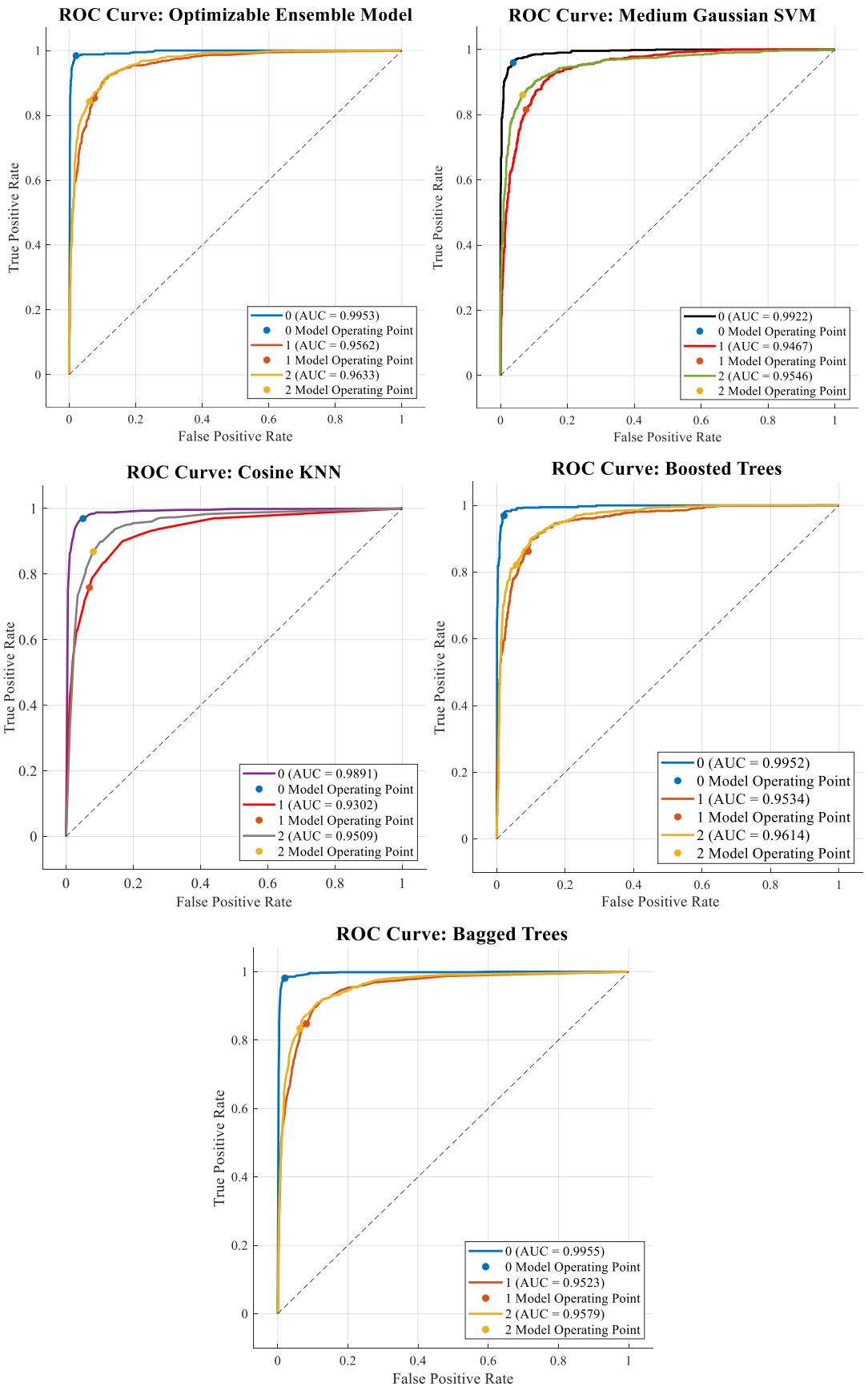

Figure 5.42 Performance evaluation of *RespEvent* classification models presented by ROC curve (TP vs. FP); where 0: No Event; 1 – Hypopnea, 2 – Apnea

5.3.2.4 Sleep postural transition classification

The position "Up" was not taken into account, along with a "Prone" position, as the percentage of each class was not comparable with the rest of the sleep positions, as shown in Table 5.20 and Table 5.22. Therefore, the following sleep postural transitions were observed:

1) supine to left,
2) supine to right,
3) left to supine,
4) right to supine

, where the first two are joined in one class called *Supine to Side*, and the last two are joined in class *Side to Supine*; therefore, there are:

1) supine to side (Class 1),
2) side to supine (Class 2).

According to the state-of-the-art literature, the best results were achieved by authors [157], but they performed on the controlled group of volunteer subjects, and the overall accuracy for the best case was 73.7 ±0.8%. They used a deep learning algorithm with data augmentation techniques and had a sequence of 10 seconds for each subject and in the control environment. The controlled experiments include short recordings in an awake state where the researchers guide the participants to turn on one or other sleep positions. Here, the sleep postural transitions were taken from whole recordings, which makes the classification more complex since each transition was not with the same intensity or 100% in the supine position, than something in between, as shown in Figure 2.6.

Table 5.20 Overall mean + SD value percentage of body position

Sleep position	**($\mu \pm \sigma$) (%)**
Supine	63.621 ± 27.788
Right	21.735 ±24.249
Left	7.373 ± 12.324
Prone	2.174 ± 5.083

Table 5.21 The percentage of the dominant sleep position with information on AHI and handedness for each patient

ID	Dominant sleep position (%)		Handedness	AHI (events/h)
1	Supine	85.736	Right	6.8
2	Supine	96.822	Right	66
3	Supine	73.345	Right	35
4	Supine	28.713	Right	11.1
6	Supine	34.351	Right	26.8
7	Supine	79.405	Right	25.4
8	Right	51.667	Left	29.0
9	Supine	68.060	Right	24.3
10	Right	74.783	Right	24.2
11	Right	65.515	Right	41.2
12	Supine	95.692	Right	25.9
13	Supine	51.750	Right	34.1
14	Supine	70.865	Right	27.5
15	Supine	99.914	Right	24
16	Supine	73.974	Right	31.4
17	Supine	78.956	Right	27.1

The rank sum test was applied, and the null hypothesis was rejected with a p-value smaller than 10^{-6}, as shown in Figure 5.43.

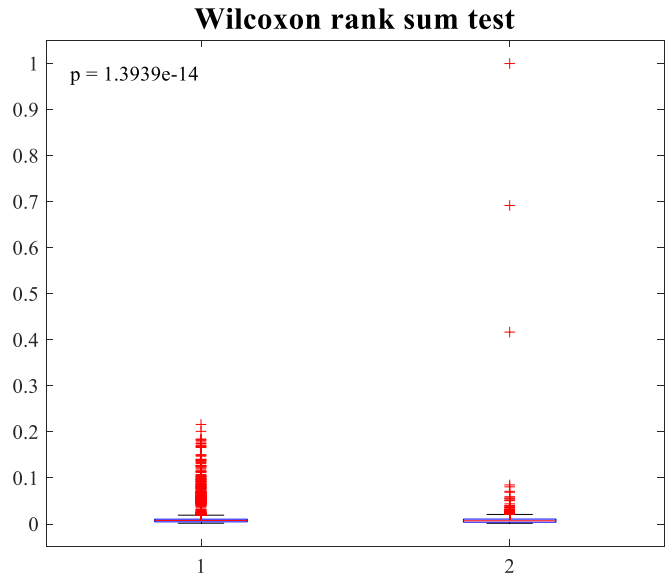

Figure 5.43 Wilcoxon rank sum test for Class 1 (Side to Supine) and Class 2 (supine to side) with a p-value < 10^{-6}

Table 5.22 The percentage of sleep position for each patient (sleep position "Up" was not considered)

ID	Sleep position percentage (%)			
	Right	**Left**	**Supine**	**Prone**
1	9.561	4.683	85.736	0
2	0	2.834	95.822	0.013
3	26.154	0	73.345	0
4	7.165	16.4	28.722	3.910
6	29.686	26.647	34.351	0.709
7	0.656	19.876	79.405	0
8	51.667	0.079	48.158	0
9	31.845	0.008	68.060	0
10	74.783	0.822	10.476	13.631
11	65.515	0.014	22.715	0.239
12	4.016	0.219	95.692	0.012
13	0	41.510	51.750	0.019
14	20.654	0.011	70.865	0.075
15	0	0.022	99.914	0
16	25.671	0.354	73.974	0
17	0.385	4.485	78.956	16.173

The parameters setup for different classifiers is presented in Table 5.23. Besides the Bayesian optimization described earlier, a grid search was used in a KNN classifier. It involves exhaustively searching for the best hyperparameters by training a model for every combination of hyperparameters in a predefined grid. The best hyperparameters are determined by evaluating the performance of each model on a validation set.

Table 5.23 Parameters setup for different classifiers models for *PosEvent* classification

Models	Parameters
Optimizable KNN	Number of neighbours: 5 Distance metric: Mahalanobis Distance weight: Inverse Optimizer: Grid search Number of grid divisions: 10
Optimizable SVM	Kernel function: Linear Kernel scale: 1 Box constraint level: 1.0291 Multiclass method: One-vs-One Optimizer: Bayesian optimization

The validation accuracy for the optimizable KNN was 69.8%, where the *F-1* score for Class 1 (side to supine) was 73.87% and for Class 2 (supine to side) was 64.1%. Although accuracy seems unsuitable, it needs to be taken into account that the sleep postural transition was taken during the whole recording, so the intensity of the turnovers can be different from case to case and, with that, make the classification more complex and inaccurate. Regardless, the obtained accuracy was similar when comparing state-of-the-art results [157] and the proposed approach. The ROC curves within the AUC value for both models are given in Figure 5.44.

Table 5.24 Performance evaluation for *PosEvent* classification

Model	Validation Accuracy (%)	Test Accuracy (%)	F1-score (%)		Sensitivity (%)	
			Class 1	Class 2	Class 1	Class 2
Optimizable SVM	63.5	61.5	63.9	63.16	63.3	63.8
Optimizable KNN	69.8	67.7	73.87	64.1	65.1	78.8

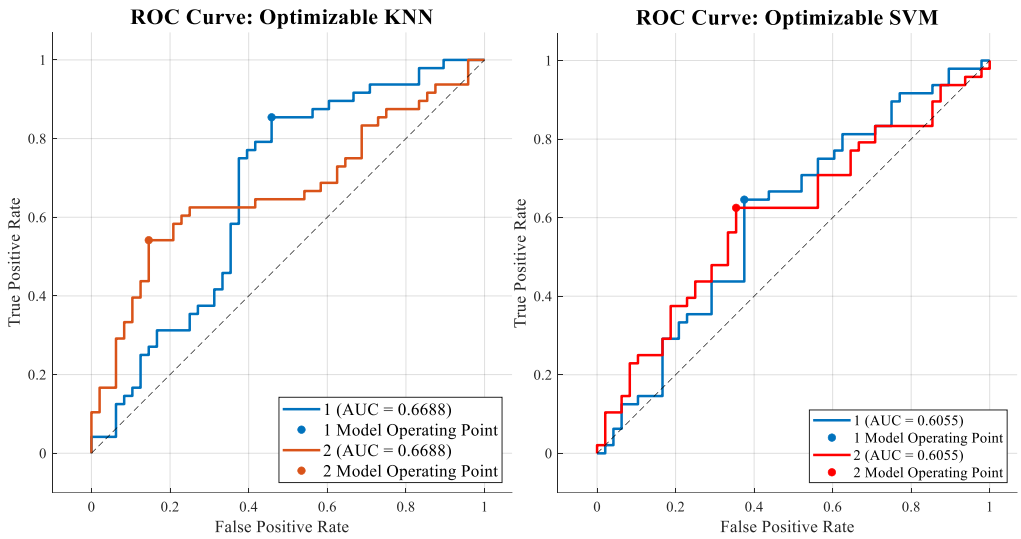

Figure 5.44 Performance evaluation of *PosEvent* classification for proposed models presented by ROC curve (TP vs. FP); where 1 – Side to supine, 2 – Supine to side

Chapter 6
Method for sleep parameters analysis

In a narrow sense, the quality of sleep is defined by the events that disturb sleep, such as spontaneous awakening and apneic events. More broadly, besides sleep duration and latency, sleep quality includes quantitative aspects, such as the subjective sleep perspective. Therefore, within the objective parameters of this study, subjective questionnaires are included, such as the Epworth Sleepiness Scale (ESS) and STOP-BANG questionnaire, along with sleep questionnaires used before and after sleep, including the Stanford Sleepiness Scale.

Some results from the ESS questionnaire are presented in Table 6.1, where EQ1 up to EQ8 are defined as following questions:

- **EQ1:** Sitting and reading
- **EQ2:** Watching TV
- **EQ3:** Sitting inactive in a public place (e.g., a theater or a meeting)
- **EQ4:** As a passenger in a car for an hour without a break
- **EQ5:** Lying down to rest in the afternoon when circumstances permit
- **EQ6:** Sitting and talking to someone
- **EQ7:** Sitting quietly after lunch without alcohol
- **EQ8:** In a car, while stopped for a few minutes in traffic

Table 6.1 The Epworth Sleepiness Scale results

ID	EQ1	EQ2	EQ3	EQ4	EQ5	EQ6	EQ7	EQ8	Total
1	0	1	0	0	1	0	1	0	3
2	1	0	0	0	0	0	0	0	1
3	0	0	0	1	2	0	1	0	4
4	1	2	0	3	2	0	0	1	9
5	2	2	2	1	2	1	2	1	13
6	1	1	0	0	0	0	0	0	2
7	3	2	1	2	2	1	1	1	13
8	0	1	0	0	1	0	0	0	2
9	3	0	0	0	1	0	2	0	6
10	1	0	1	1	0	0	1	0	4
11	2	2	1	0	1	0	1	0	7
12	1	1	1	1	1	1	1	1	8
13	3	3	0	0	0	0	0	0	6
14	0	0	0	0	0	0	0	0	0
15	1	2	3	2	2	1	3	0	14
16	0	2	1	0	1	0	2	1	7
17	2	2	1	0	2	0	1	1	9
Mean	1.29	1.23	0.65	0.65	1.05	0.23	0.94	0.35	8

ID – patient identification number
No chance of dozing =0
Slight chance of dozing =1
Moderate chance of dozing =2
High chance of dozing =3

Analysis of sleep parameters can be performed from many points of view and based on that, bring some conclusion of quality of sleep [41], [44], [62], [170]–[174], where it needs to be emphasized that quality of sleep is a broad term. Based on some parameters, the individual can have a higher quality of sleep and, on the other side, worsening quality. Consequently, quality of sleep is not generalized, and **it needs to be emphasized which parameters were included in the model** to determine the sleep quality. One example of a sleep quality assessment was presented by Dafna et al. [62] based on full-night audio recordings of sleep apnea patients. The 145 patients with obstructive sleep apnea were recorded in a clinical setting, with an 82.1% accuracy in detecting sleep/wake stage, 3.9% error in detecting sleep

latency, 11.4% error in estimating total sleep time, and 11.4% error in estimating sleep efficiency. In the paper [62], the typical sleep quality parameters included in the sleep quality analysis are:

- Total sleep time (TST),
- Sleep latency (ST),
- Sleep efficiency (SE),
- Wake-time after sleep onset (WASO),
- Awakening index (AI) – average awakening per hour.

Furthermore, in the paper [62], the sleep quality-related features are presented, more precisely **rhythmic features** (*Breathing rhythmic period* and *Breathing rhythmic intensity*). Where the movement or posture transition leads to the temporal lower sleep quality, the more periodic the respiration is, the better sleep quality is.

However, in most papers, the variability of certain sleep parameters through sleep time was not considered. In a clinical report, taking the scalar value as a sleep quality parameter without considering the variability of specific parameters throughout one night of measurement could lead to output data with a **degree of uncertainty**. For example, using an average of respiratory events through the total sleep time may not accurately reflect an individual's overall sleep patterns, as sleep quality can vary throughout the night due to factors such as sleep stage, sleep architecture, and physiological changes. Therefore, to accurately assess quality of sleep, it is important to consider the scalar value and variability of certain parameters throughout one measurement night [173].

Sleep-disordered breathing (SDB) conditions, such as OSA, come with plentiful comorbidities [1], [39]. As stated in [31], we spend about one-third of our life either sleeping or aiming to sleep. Therefore, timely and daily accessible monitoring of it can decrease untreated SBD and increase awareness among the wider population. Commonly, the parameter showing the severity of sleep apnea is the AHI index, which is an average respiratory event related to apneas and hypopneas over a TST. Following the AHI index results, the clinicians can distinguish if the patient needs to include the treatment, such as using a CPAP device.

Furthermore, suppose the AHI index is above the predefined value for giving a CPAP device. In that case, the patient is diagnosed with sleep apnea and is eligible for treatment

with a CPAP device, which can be reimbursed by health insurance. If the AHI falls below the threshold, the patient will not be reimbursed for treatment.

The distribution of respiratory events over time is a complex stochastic process. As stated before, it can be affected by various factors such as sleep architecture, body position, sleep state, sleep stage, and time of night effects. These factors have different impacts on each patient. However, AHI is still the standard for diagnosing patients, determining treatment eligibility, and evaluating new devices and treatments.

Moreover, one of the disadvantages is that the AHI index does not cover the relative dependency of the body position, sleep stage, and anthropometric data versus the respiratory events [173]. Consequently, the model was developed, which includes information about the body movement variability, body position, sleep stage, snoring and anthropometric measures, as well as the subjective questionaries and behavioral characteristics of the patients on the day of the measurements, covering the lack of information given by the scalar metric, the AHI index.

For instance, the drawback of taking the overall AHI index is represented in Figure 6.1. Treatment and established diagnosis are probably the same for both individual patients. Still, they have different patterns, and the adjacent information and results do not coincide. Therefore, taking into account additional information and making new metrics, more information can be leveraged from the sleep recording. Moreover, in some patients, the apneic events are related to the body positions, so-called **positional OSA** [175], [176]. Still, on another side, for some, the apneic events are distributed during all sleep states and positions. Besides positional OSA, there is often a **"REM-related" OSA**, as during a REM stage, there is a decreased tone of the genioglossus muscle in the tongue [177].

The clinical report gives some helpful information about the sleep architecture regarding a respiratory event occurrence, and one example is shown in Table 6.2. Still, the report does not cover the variability of the specific index during a time and the relative dependency with some additional beneficial information.

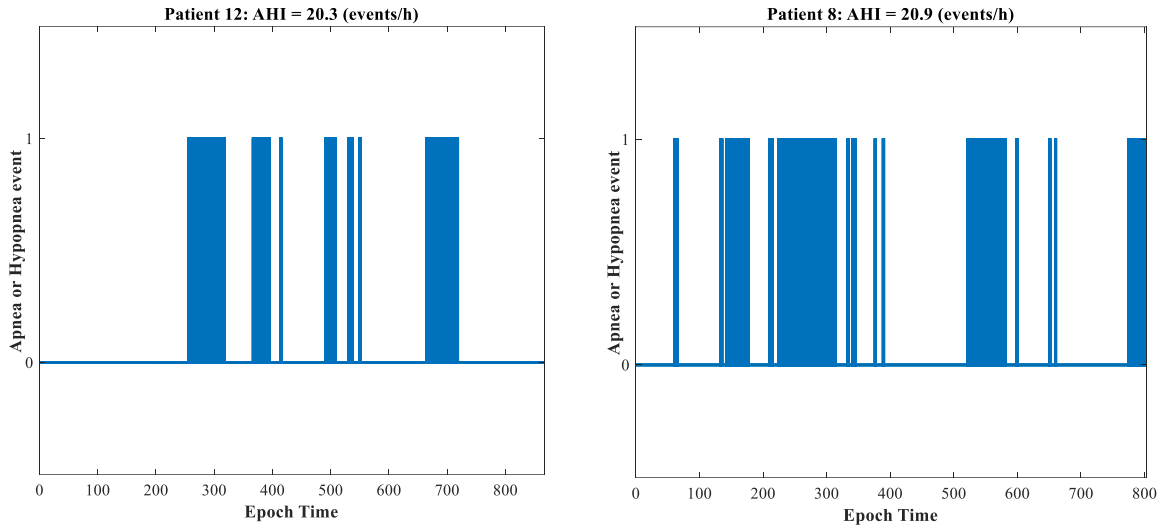

Figure 6.1 AHI index over time for two patients, where on the x-axis was the epoch (30 seconds) time

Table 6.2 Example of the clinical report for one patient regarding respiratory events

	CA	OA	MA	Apnea	Hypop*	A+H	RERA	Total
Number:	3	1	1	5	29	34	0	34
Mean Dur (sec):	15.2	11.5	10.5	16.0	25.4	23.7	0.0	23.7
Max Dur (sec):	16.0	11.5	10.5	16.0	45.5	45.5	0.0	45.5
Total Dur (min):	0.8	0.2	0.2	1.1	12.3	13.4	0.0	13.4
% of TST:	0.2	0.1	0.1	0.4	4.0	4.3	0.0	4.3
Index (#/h TST):	0.6	0.2	0.2	1.0	5.6	6.6	0.0	6.6
REM Count:	2	0	0	2	3	5	0	5
NREM Count:	1	1	0	2	26	28	0	28
REM Index:	2.4	0.0	0.0	2.4	3.6	5.9	0.0	5.9
NREM Index:	0.2	0.2	0.0	0.5	6.0	6.5	0.0	6.5

*Above Index Values Based on Total Sleep Time ■ Hypopneas were scored per AASM definition VIII4.B (3% desaturation).

6.1 Statistical model for sleep parameters analysis

The statistical model that uses a self-exciting point process approach and a linear regression model to study the effects of various factors on the point-to-point rate of respiratory events in sleep apnea was developed. A similar approach has been made by Chen et al. [173]. They have developed dynamic models of obstructive sleep apnea for predicting respiratory events based on the generalized point process and generalized linear regression model. Moreover, they have done research on the 936 participants from the MESA (Multi-Ethnic Study of Atherosclerosis) dataset [178]. Here, the emphasis will be on the influence of the different data sources and types of attributes, where the primary division was based on statical and dynamical input variables, as shown:

$$I = \underbrace{I_{SleepStage} + I_{position} + I_{snoring} + I_{body\ movement\ variability}}_{\textbf{Dynamic}} + \underbrace{I_{SQ} + I_{A}}_{\textbf{Static}}, \qquad \textbf{(6.1.1)}$$

where I_A are anthropometric measures and I_{SQ} is the data from the sleep questionnaires.

The data from the overnight sleep study can be divided into three categories:

1) sleep data information obtained from PSG and *Sleep UWB platform*,
2) sleep questionnaires,
3) clinical summary report.

An example of clinical report data is given in Table 6.2.

To provide a more insightful temporal AHI analysis, the data from all the categories will be considered in certain points. Attributes values are given in Table 6.3.

Table 6.3 Attribute value description

Attribute	Data type	Class
Body position	categorical	0:Non supine (right, back, up, prone) 1: Supine
Body movement variability	categorical	Intensity of the body movement through the time (obtained from Sleep UWB platform): the medium and large movements were taken into account. If there is large or medium movement, it is 1; otherwise, 0.
Sleep stages	categorical	00001: Wake; 00010: REM; 00100: N1; 01000: N2; 10000: N3
Snoring	categorical	0: No Snoring; 1: Snoring
BMI	numerical	Body Mass Index
WHR	numerical	Waist-to-hip ratio
NCR	numerical	Neck circumference-to-height ratio
EES index	numerical	No chance of dozing = 0 Slight chance of dozing = 1 Moderate chance of dozing = 2 High chance of dozing = 3
Stop Bang index	numerical	Low risk: 0-2 Yes answers Medium risk: 3-4 Yes answers High risk: 5-8 Yes answers or 2 answers Yes + male 2 answers Yes + BMI > 35 kg/m^2 2 answers Yes + neck circumference for males higher than 42 cm, and for females higher than 40 cm

When dealing with binary variables, a **Poisson regression model** is commonly used to model count data and is appropriate for modeling the relationship between a binary independent variable and a Poisson-distributed dependent variable represented as a scalar AHI value. Moreover, for the point-to-point capturing of the influence on the AHI changes, a **Hawkes point process** was used to model the timing of events where one event can trigger another event [179]. In a Hawkes point process, the events are not independent, and the occurrence of one event can increase the probability of another event occurring. The Hawkes point process is a self-exciting process characterized by its **conditional intensity function**, $\lambda(t|H_t)$. The equation of the conditional intensity function for a Hawkes point process is given as follows:

$$\boldsymbol{\lambda(t|H_t) = \lambda(t) * f(H_t),} \qquad \textbf{(6.1.2)}$$

where $f(H_t)$ is the history function, which describes the effect of past events on the current event rate. H_t is the history of past events up to time *t*. The history function is a mathematical function that describes how the occurrence of past events affects the current event rate. It is typically specified as a product of influence functions, one for each past event. History function is typically a complex function which is difficult to compute. Therefore, the history function is approximated by using a small interval of time *w*, assuming that the number of events in interval follows a Poisson distribution with a rate parameter given by the Hawkes process.

Once the model parameters are estimated, we can use the likelihood function to test hypotheses about the data and make predictions about future events. The likelihood function for a Hawkes process with a small interval of time, s, and assuming that the number of events in that interval follows a Poisson distribution with a rate parameter given by the Hawkes process can be expressed as follows:

$$\boldsymbol{L(\theta) = \prod_{i=1}^{n}(\lambda(t_i|H_{t_i}) \cdot w)^{k_i} \cdot e^{-\{\lambda(t_i|H_{t_i}) \cdot w\}},} \qquad \textbf{(6.1.3)}$$

where $L(\theta)$ is the likelihood function, θ is the set of parameters of the Hawkes process, *w* is the duration of the small interval of time, *k* is the number of events observed in the interval *w*, and *n* is the total number of events.

The likelihood function is a product of Poisson probability mass functions, where each term corresponds to the probability of observing *k* events in the interval *w*, given the rate parameter $\lambda(t|Ht)$ at time *t*.

Furthermore, a Poisson regression model in combination with a Hawkes point process was applied. The Poisson regression model would be expressed as follows:

$$\log\left(\lambda(t|H_t)\right) = \beta_0 + \beta_1 x_1 + .. + \beta_n x_n \quad \textbf{(6.1.4)}$$

Several trials are investigated based on the input attribute values, as given in Table 6.4.

Trial 1 includes body position (BP), sleep stage (SS), snoring (S), body movement variability (BMV) data. Moreover, a history data on respiratory events were included based on the idea given in [173], and the model is represented as:

$$\log\left(\lambda(t|H_t)\right) = \beta_{BP} x_{BP}(t) + \beta_{SS} x_{SS}(t) + \beta_S x_S(t) + \beta_{BMV} x_{BMV}(t) + \beta_H \lambda_l(t|H_t), \quad \textbf{(6.1.5)}$$

where x_{SS} sleep stage data that are encoded with a one-hot encoding as presented in Table 6.3, x_{BP} is a body position data, x_S is a snoring data, and x_{BMV} is body movement variability data obtained from *Sleep-UWB platform*, labeled as provided in Table 6.3. Furthermore, the Poisson regression model includes 300 seconds of history data as an independent variable, using the conditional intensity function, *λ(t|Ht)*, on the observed interval [173]. To smooth the influence of the history data on the model, the *3-order* Lagrange interpolation was used. The 10 points in the 300 seconds interval have been used to interpolate, and Lagrange values have been calculated in the position where the maximum rate of the respiration position occurs in each interval and the k-neighbors from both sides of the maximum. Lagrange coefficients are calculated using the following equation:

$$l_i(x) = \prod_{\substack{j=1 \\ j \neq i}}^{n+1} \frac{x - x_j}{x_i - x_j}, \quad \textbf{(6.1.6)}$$

and the function is given as follows:

$$y(x) = \sum_{i=1}^{n+1} y_i l_i(x) \quad \textbf{(6.1.7)}$$

Trial 2 includes sleep stage, body position data within a body movement variability data, and the model is represented as:

$$\log\left(\lambda(t|H_t)\right) = \beta_{SS} x_{SS}(t) + \beta_{BP} x_{BP}(t) + \beta_{BMV} x_{BMV}(t) \quad \textbf{(6.1.8)}$$

Afterward, for the last trial (**Trial 3**), the output of the Trial 2 is multiple with static input variables obtained from the sleep questionnaires or anthropometric data taken before or after the recording, where I_{static} is defined as:

$$\boldsymbol{Istatic = ESS + SBI + AM,} \tag{6.1.9}$$

where *AM* is:

$$\boldsymbol{AM = \frac{BMIn + WHR \times 2^{-1} + NHR \times 2^{-2}}{BMIn + WHR + NHR}} \tag{6.1.10}$$

Table 6.4 Input attributes value for each trial

Trial	Attribute values	Description
1	Body position, sleep stage, snoring, body movement variability, and history data of respiratory events	Some of these features are directly related to sleep and breathing patterns and are likely to be the most important for predicting AHI.
2	Sleep stage, body position, body movement intensity	Influence of the body movement intensity along with a sleep stage and body position on the respiratory events occurrence
3	Trial 2 multiple with the static variables	The influence of subjective metrics within anthropometric measures

6.2 Performance evaluation

A goodness-of-fit analysis was performed using a nonparametric Kolmogorov-Smirnov (KS) test, with a 5% significance level, where the Trial 1 and Trail 2 KS results are compared with the setup used in [173]. It is worth mentioning that in [173] they used the influence of historical data, and did research on broad population, and did not include patients with an AHI lower than 10 events/h. Here, for completeness, the normal up to severe AHI was considered (ID04, ID05, ID12, ID15, ID16, ID17 were not taken into account). Therefore, the set is formed where there are:

- Normal: AHI < 5: **(2F; 1M)**
- Mild sleep apnea: 5 < AHI < 14: **(1F; 2M)**
- Moderate sleep apnea: 15 < AHI < 29: **(2F)**
- Severe sleep apnea: AHI > 30: **(0F; 3M)**

The influence of each input variable on the AHI value, more precisely AHI rate during each input variable and a 95% confidence interval, for Trial 1 and Trial 2 are given in Table 6.5 and Table 6.6. Furthermore, Table 6.7 shows the AHI value in each sleep state and an arousal index value from the clinical report.

Table 6.5 Influence of each input variable on AHI value for Trial 1

ID	Supine Position	N1 stage	N2 stage	N3 stage	REM stage	Snore	Movement
	Rate 95% Confidence Interval						
1	3.95 [0.53, 29.42]	3.89 [0.50,30.31]	1 [0.14, 7.40]	0.38 [0.02, 6.26]	1.5 [0.18, 12.58]	0	1 [1.00, 1.00]
2	1.55 [0.85, 2.83]	24.48 [12.84,46.6]	17.52 [9.21,33.3]	15.56 [7.27,33.3]	0	0 [0.60, 4.38]	1.19 [0.91, 1.55]
3	2.26 [1.36, 3.77]	7.18 [4.05, 12.72]	5.67 [3.52, 9.12]	6.88 [3.58,13.2]	7.41 [4.49,12.2]	0 [0.13, 7.27]	2.07 [1.19, 3.61]
6	57.34 [5.95,552.0]	0.67 [0.07, 6.05]	0.26 [0.03, 2.42]	0.05 [0.00, 0.90]	0	0 [0.00, 0.28]	5.06 [0.00,Inf]
7	1.1 [0.63, 1.93]	15.56 [7.98, 30.35]	9.88 [5.59,17.4]	10.04 [3.65,27.6]	3.33 [1.28, 8.67]	0 [0.07, 3.83]	2.74 [1.04, 7.25]
8	2.56 [1.49, 4.39]	39.42 [15.87,97.9]	5.22 [3.17, 8.58]	3.75 [1.86, 7.54]	9.21 [4.84, 17.53]	0 [0.12, 6.59]	1.7 [0.94, 3.10]
9	0.48 [0.10, 2.40]	0	0.55 [0.07, 4.47]	0	9.14 [3.17, 26.38]	0 [0.06, 8.92]	22.57 [0.00, Inf]
10	0	5.27 [2.09, 13.32]	4.55 [2.30, 8.99]	0	0	0 [1.03, 5.38]	3.08 [0.00, Inf]
11	1.13 [0.74, 1.74]	15.45 [9.90, 24.12]	14.33 [9.65,21.2]	7.75 [4.27,14.0]	18.12 [11.31,29.0]	0 [0.82, 4.16]	1 [1.00, 1.00]
13	2.46 [1.78, 3.41]	24.44 [16.59,36.0]	23.77 [16.81,33.6]	4.9 [2.13,11.2]	29.68 [20.72,42.5]	0 [0.17,2.85]	1.15 [0.84, 1.58]
14	0.81 [0.30, 2.18]	0	3.71 [1.58, 8.69]	0	19.15 [5.37, 68.24]	0	0.77 [0.15, 3.92]

Table 6.6 Influence of each input variable on AHI value for Trial 2

ID	Supine Position	N1 stage	N2 stage	N3 stage	REM stage	Movement
	Rate 95% Confidence Interval					
1	4.83 [0.66, 35.39]	5.56 [0.75, 41.34]	1.01 [0.14, 7.45]	0.31 [0.02, 5.02]	1.44 [0.17, 12.10]	0.1 [0.01, 1.55]
2	1.59 [0.87, 2.89]	45.07 [24.64,82.4]	33.8 [18.59,61.4]	24.2 [11.72,49.95]	0	2.02 [0.75, 5.46]
3	5.39 [3.41, 8.49]	13.55 [7.88, 23.32]	6.07 [3.81, 9.66]	5.17 [2.73, 9.82]	16.99 [10.83,26.6]	0.52 [0.07, 3.93]
6	63.4 [7.94, 506.27]	0.57 [0.07, 4.80]	0.29 [0.04, 2.41]	0.05 [0.00, 0.86]	0	0.02 [0.00, 0.24]
7	1.17 [0.68, 2.03]	20.21 [10.99,37.1]	13.77 [8.11, 23.37]	16.29 [6.54, 40.56]	3.56 [1.38, 9.18]	0.52 [0.07, 3.96]
8	3.74 [2.33, 5.99]	39.14 [15.83,96.7]	7.43 [4.76, 11.58]	3.71 [1.86, 7.40]	20.43 [11.69,35.7]	0.77 [0.11, 5.62]
9	0.72 [0.14, 3.75]	0	0.43 [0.05, 3.81]	0	4.76 [1.69, 13.39]	0.49 [0.04, 6.51]
10	0	7.62 [3.41, 17.06]	5.72 [3.07, 10.65]	0	0	2.79 [1.31, 5.94]
11	1.28 [0.84, 1.94]	32.5 [23.14,45.6]	24.5 [17.92,33.5]	9.21 [5.10, 16.64]	46.27 [32.54,65.7]	1.93 [0.86, 4.36]
13	2.4 [1.82, 3.17]	33.17 [24.21,45.4]	30.88 [23.89,39.9]	6.04 [2.69, 13.57]	42.2 [32.07,55.5]	0.86 [0.21, 3.51]
14	0.98 [0.37, 2.57]	0	3.28 [1.39, 7.75]	0	25.42 [9.07, 71.26]	0

Table 6.7 AHI value in each sleep state, along with an arousal index value from the clinical report

ID	AHI (events/h)	REM index	NREM index	Supine index	Nonsupine index	Snore index	Arousal index
1	6.8	5.9	6.5	8	4 (left)	0	17
2	66	0	62.7	75.7	30 (left)	0.6	36.9
3	35	59.3	29.5	44.2	9.8 (right)	0.1	12.7
6	4.3	0	3.9	19.6	2.4 (right)	0	20.6
7	14.5	4.4	16.3	15.7	10.4 (left)	0	25.8
8	20.9	63.3	17.1	32.6	8.5 (right)	0	8.5
9	1.4	4.7	0.5	1	2 (right)	0	17.7
10	6.6	0	6.3	0	8 (right)	0	28.7
11	29.8	45.6	24.9	43.5	25.9 (right)	0	16.2
13	53.8	47.8	54.3	77.3	32.8 (left)	1.3	39.4
14	4.2	16.2	3.4	3.9	4.6 (right)	0	7.2

Based on the data given in the clinical report and the data obtained as an output of the model, with included 95% confidential intervals, it was shown that for most of the patients, the dominant position was supine, and REM was the dominant sleep stage.

Moreover, the influence of the movement gathered with a *Sleep UWB platform* can be compared with the arousal index (from the clinical report). As shown in Figure 6.4 for patient ID10, the arousal index was 28.7, and the rate of AHI during the movement was 2.79 with 95% confidential intervals [1.31, 5.94].

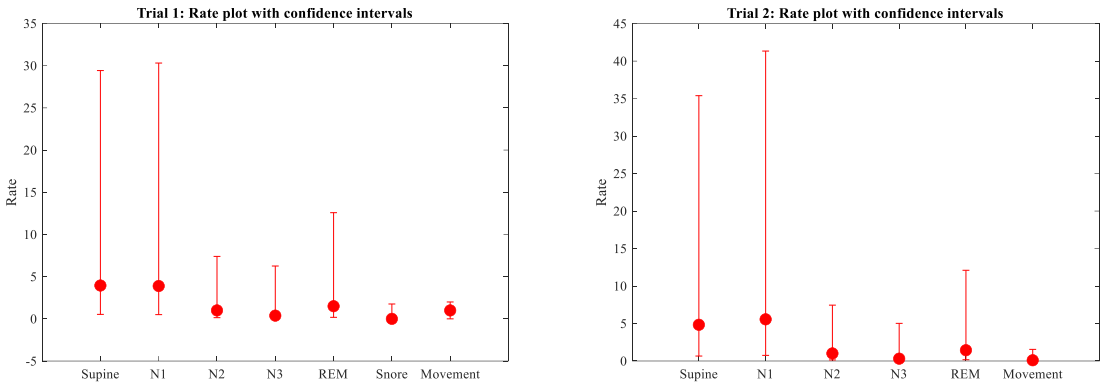

Figure 6.2 ID01: Rate plot with confidence intervals for Trial 1 and Trial 2 (AHI: 6.8, REM index: 5.9, NREM index: 6.5, Supine index: 8, Nonsupine index: 4 (left), Snore index: 0, Arousal index: 17)

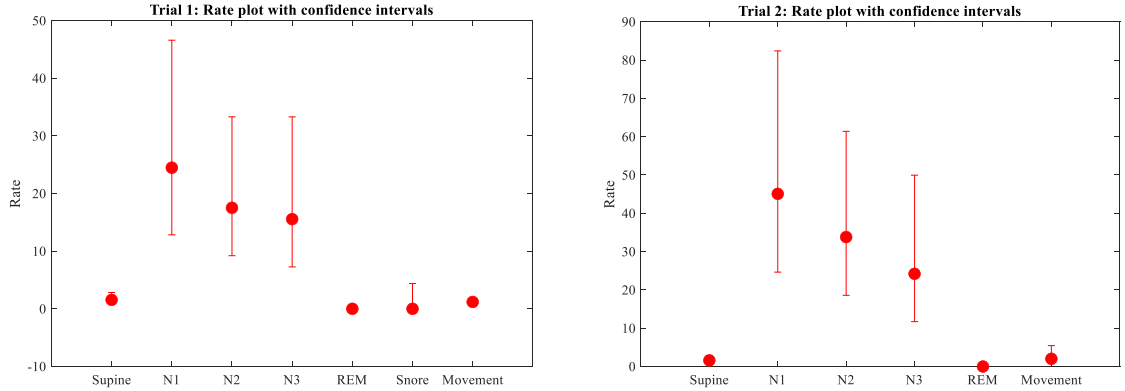

Figure 6.3 ID02: Rate plot with confidence intervals for Trial 1 and Trial 2 (AHI: 66, REM index: 0, NREM index: 62.7, Supine index: 75.7, Nonsupine index: 30 (left), Snore index: 0.6, Arousal index: 36.9)

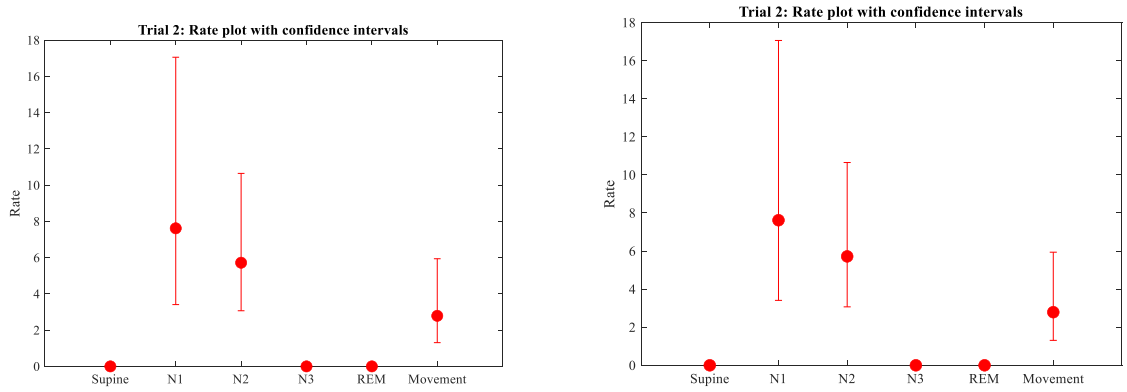

Figure 6.4 ID10: Rate plot with confidence intervals for Trial 1 and Trial 2 (AHI: 6.6, REM index: 0, NREM index: 6.3, Supine index: 0, Nonsupine index: 8 (right), Snore index: 0, Arousal index: 28.7)

Regarding Trial 3, it was shown that the static data didn't influence the AHI value. This can be due to an insufficient number of patients. Figure 6.5 shows that the variability of the I_{static} value is similar for each of the patients. Therefore, for Trail 3, it was concluded that it needs to carry on more extensive studies.

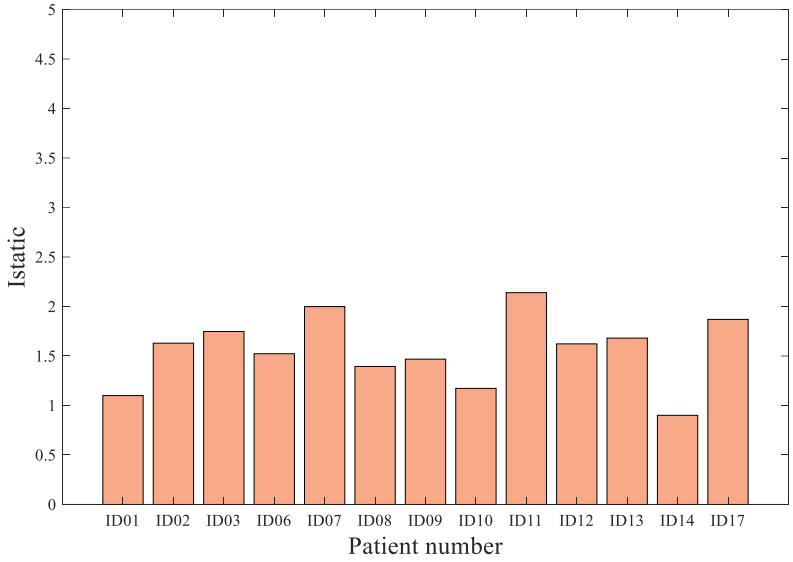

Figure 6.5 I_{static} values for each patient

As a consequence of taking AHI smaller than 14 events/hour, the goodness-of-fit results are slightly worse. Still, the results show the influence of each input attribute on the AHI severity.

The goodness of fit analysis is presented in Figure 6.6 for Trial 2, the *Chen model* (model shown in [173]) and Trial 1. The Trial 1 and *Chen* [173] models include AHI's historical information that significantly improves the output of the models. Still, Trial 2 only consists of body position, sleep stage, and body movement variability information. With that in mind, it can be concluded that for the patients mentioned above, the medium and large body movements correlate to apnea and hypopnea.

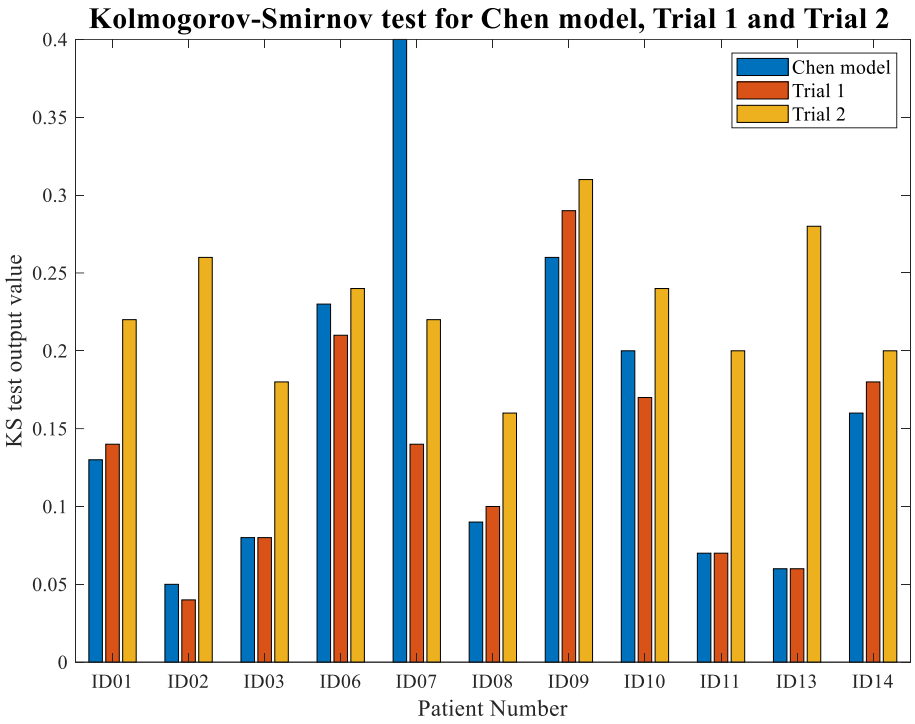

Figure 6.6 Kolmogorov-Smirnov test output for Trial 1, Trial 2, and Chen model presented in [173]

Moreover, based on the history modulation [173], the 300 seconds prediction output for ID03 and ID08 for Trial 1 is given in Figure 6.7, where it can be seen that for ID03 the positional OSA potentially happened on the other side and for the ID08 the AHI was distributed through the whole night.

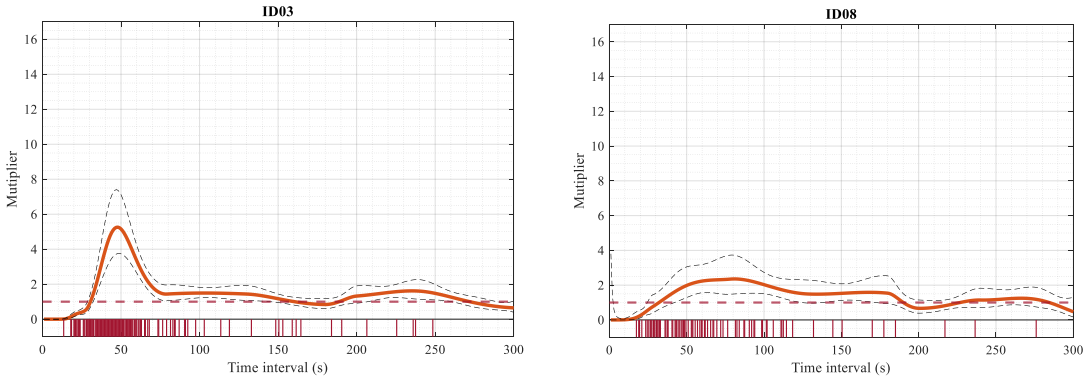

Figure 6.7 300 seconds of the history modulation for ID03 and ID08.
ID03 (Male, 49 years, BMI: 40.3 kg/m^2, AHI = 35 events/h)
ID08 (Female, 54 years, BMI: 29 kg/m^2, AHI = 20.9 events/h)

Chapter 7
Conclusions

7.1 Main findings

This research brings an innovative solution for sleep parameters monitoring and analysis based on the transmittive approach (UWB CIR measurement) that uses the UWB technology to enable the application of low-cost commerical off-the-shelf transceivers, as an alternative to more complex UWB radar solutions presented in the state-of-the-art papers. This method offers numerous benefits over the radar-based approach, encompassing reduced complexity, diminished power consumption, and enhanced data rates.

Moreover, UWB CIR measurements exhibit robustness to multipath fading and maintain functionality in settings where traditional radar systems might experience challenges. It was shown that the *Sleep UWB platform* could detect breathing and classify breathing patterns with an accuracy comparable with state-of-the-art solutions for sleep assessment, such as cameras, on-body, or on-bed sensors. Moreover, the body movement analysis within a promisingly accurate sleep postural transition classification makes the proposed *Sleep UWB platform* a complete unit. Further investigation of the SDB prediction calculation and sleep postural transition classification needs to be investigated.

The method was based on the assumption that the signal propagation channel was continuously changing due to the breathing and movement of the person which causes the small variations of propagation channel properties and thus the measureable modulation of the received signal.

Most of the existing similar solutions employing the UWB technology are based on the radar approach where a reflected signal from the person's chest is monitored and the change in the received distance or time of arrival is calculated to extract other parameters of interest (such as body movement or breathing). Unlike previously investigated in literature UWB radar approach, this research presents a non-radar transmissive solution, where movements and breathing are extracted from the CIR based on the fact that human body was part of the signal propagation path.

A custom-designed *Sleep-UWB platform* based on low complexity and low-cost UWB transceivers was developed. The experiment consisted of placing a UWB transmitters (Tx) and a receivers (Rx) in predetermined positions on the left and right sides of the subject's bed, where the transmitter generated an ultra-short UWB pulse with a minimum bandwidth of 500 MHz, as described in Chapter 4. Information on the chest movement caused by breathing was extracted from the CIR, as shown in Chapter 5.3.

The DW1000 chip uses various signal processing techniques to improve CIR estimation accuracy and reduce the impact of noise and interference. These techniques include adaptive thresholding, background subtraction, and various algorithms for peak detection and filtering. The CIR estimation performance of the DW1000 chip has been shown to be comparable to that of more expensive UWB transceivers and is sufficient for many healthcare applications, including sleep sensing and analysis.

The proposed method involves the extraction of features from sleep breathing patterns and postural transitions by utilizing CIR measurements within UWB communication. The developed *Sleep-UWB platform* exhibits the capability to detect and classify breathing patterns (normal breathing, apnea, hypopnea) with a level of accuracy comparable to existing state-of-the-art sleep assessment methodologies.

Furthermore, the system demonstrates a promising degree of precision in the analysis of body movements, particularly in the classification of sleep postural transitions (side to supine, supine to side).

In addition, a statistical model based on the output data of the PSG and *Sleep UWB platform* and subjective information gathered from the sleep questionaries and anthropometric data were taken before and after sleeping. The primary diagnostic metric for sleep apnea severity is an apnea-hypopnea index. Still, there are some drawbacks to it. Therefore, there

was a question of finding some more descriptive predictions, that are still concise and straightforward. This doctoral thesis covered a new, upgraded version of the AHI index.

The dataset for sleep analysis measurement based on the proposed system was gathered in collaboration with the University Psychiatric Hospital Vrapče, Department of Clinical Psychophysiology and Organically conditioned mental disorders, Center for Sleep and Wake Disorders. Participants received all necessary information about the research before the recording and signed a consent to participate in the research. The study respected the privacy of the participant's data. It was conducted by all applicable guidelines based on the Helsinki declaration and its revisions, which ensured the proper implementation of procedures and the safety of persons who participated in this research.

7.2 Limitations and future work

There are several drawbacks that I have noticed while concluding this research work, and I will address them in my near research future. The limitations can be grouped based on the field from which you observed the proposed doctoral research.

From the clinical and data science point of view, the more extensive data set would show more variability through various subjects, such as AHI, age, BMI, sleep position, etc.

Furthermore, from the technical point of view, it would be interesting to prove the assumption stated in this research study that the method would work in various environments.

The limitation that goes by the physical constraints of the wireless systems are body movements. Due to extensive body movements, body movements interferes with the breathing signal, and therefore during that time period, the platform cannot measure breathing rate or other vital signs.

Nonetheless, the research brought a new measurement method tested in the clinical environment, with new features extracted from the channel impulse response for breathing and movement detection and classification.

7.3 Final thoughts

Untreated sleep breathing disorders can manifest through all aspects of life and influence job performance, quality of life, and relationships. Moreover, patients with SDB have a high risk of vehicle accidents due to functional impairment, such as sleepiness, commonly occurring

during inactive situations such as driving on the highways. Therefore, research in this field is crucial and promising.

"**You can't go back and change the beginning,**
but you can start where you are now and change the ending."
(C.S. Lewis)

Bibliography

[1] C. Pollak, M. J. Thorpy, J. Yager, and M. J. Thorpy, *The encyclopedia of sleep and sleep disorders*, 3rd ed. New York, NY: Facts on File, 2010.

[2] M. H. Kryger, T. Roth, and W. C. Dement, Eds., *Principles and practice of sleep medicine*, Sixth edition. Philadelphia, PA: Elsevier, 2017.

[3] S. Ahmadzadeh, J. Luo, and R. Wiffen, "Review on Biomedical Sensors, Technologies and Algorithms for Diagnosis of Sleep Disordered Breathing: Comprehensive Survey," *IEEE Rev. Biomed. Eng.*, vol. 15, pp. 4–22, 2022, doi: 10.1109/RBME.2020.3033930.

[4] R. Gupta, S. R. Pandi-Perumal, and A. BaHammam, *Clinical atlas of polysomnography*. Oakville, ON, Canada ; Waretown, NJ, USA: Apple Academic Press, 2018.

[5] N. Ben-Israel, A. Tarasiuk, and Y. Zigel, "Obstructive Apnea Hypopnea Index Estimation by Analysis of Nocturnal Snoring Signals in Adults," *Sleep*, vol. 35, no. 9, pp. 1299–1305, Sep. 2012, doi: 10.5665/sleep.2092.

[6] J.-W. Kim *et al.*, "Prediction of Obstructive Sleep Apnea Based on Respiratory Sounds Recorded Between Sleep Onset and Sleep Offset," *Clin. Exp. Otorhinolaryngol.*, vol. 12, no. 1, pp. 72–78, Feb. 2019, doi: 10.21053/ceo.2018.00388.

[7] C. B. Pereira, X. Yu, M. Czaplik, R. Rossaint, V. Blazek, and S. Leonhardt, "Remote monitoring of breathing dynamics using infrared thermography," *Biomed. Opt. Express*, vol. 6, no. 11, p. 4378, Nov. 2015, doi: 10.1364/BOE.6.004378.

[8] E. Dafna, A. Tarasiuk, and Y. Zigel, "Automatic Detection of Whole Night Snoring Events Using Non-Contact Microphone," *PLoS ONE*, vol. 8, no. 12, p. e84139, Dec. 2013, doi: 10.1371/journal.pone.0084139.

[9] Z. T. Beattie, T. L. Hayes, C. Guilleminault, and C. C. Hagen, “Accurate scoring of the apnea-hypopnea index using a simple non-contact breathing sensor,” *J. Sleep Res.*, vol. 22, no. 3, pp. 356–362, Jun. 2013, doi: 10.1111/jsr.12023.

[10] E. Dafna, A. Tarasiuk, and Y. Zigel, “OSA severity assessment based on sleep breathing analysis using ambient microphone,” in *2013 35th Annual International Conference of the IEEE Engineering in Medicine and Biology Society (EMBC)*, Osaka, Jul. 2013, pp. 2044–2047. doi: 10.1109/EMBC.2013.6609933.

[11] E. Schires, P. Georgiou, and T. S. Lande, “Vital Sign Monitoring Through the Back Using an UWB Impulse Radar With Body Coupled Antennas,” *IEEE Trans. Biomed. Circuits Syst.*, vol. 12, no. 2, pp. 292–302, Apr. 2018, doi: 10.1109/TBCAS.2018.2799322.

[12] S.-H. Kim, Z. W. Geem, and G.-T. Han, “A Novel Human Respiration Pattern Recognition Using Signals of Ultra-Wideband Radar Sensor,” *Sensors*, vol. 19, no. 15, p. 3340, Jul. 2019, doi: 10.3390/s19153340.

[13] S. Kang *et al.*, “Non-contact diagnosis of obstructive sleep apnea using impulse-radio ultra-wideband radar,” *Sci. Rep.*, vol. 10, no. 1, p. 5261, Dec. 2020, doi: 10.1038/s41598-020-62061-4.

[14] A. Q. Javaid, C. M. Noble, R. Rosenberg, and M. A. Weitnauer, “Towards Sleep Apnea Screening with an Under-the-Mattress IR-UWB Radar Using Machine Learning,” in *2015 IEEE 14th International Conference on Machine Learning and Applications (ICMLA)*, Miami, FL, USA, Dec. 2015, pp. 837–842. doi: 10.1109/ICMLA.2015.79.

[15] “Basic Properties of UWB Signals and Systems,” in *Ultra Wideband Signals and Systems in Communication Engineering*, John Wiley & Sons, Ltd, 2007, pp. 9–24. doi: 10.1002/9780470060490.ch1.

[16] A. Q. Javaid, C. M. Noble, R. Rosenberg, and M. A. Weitnauer, “Towards detection of sleep apnea events by combining different non-contact measurement modalities,” in *2016 38th Annual International Conference of the IEEE Engineering in Medicine and Biology Society (EMBC)*, Orlando, FL, USA, Aug. 2016, pp. 5307–5310. doi: 10.1109/EMBC.2016.7591925.

[17] S. Pallesen *et al.*, “A Pilot Study of Impulse Radio Ultra Wideband Radar Technology as a New Tool for Sleep Assessment,” *J. Clin. Sleep Med.*, vol. 14, no. 07, pp. 1249–1254, Jul. 2018, doi: 10.5664/jcsm.7236.

[18] C. Li, J. Lin, and Y. Xiao, "Robust Overnight Monitoring of Human Vital Signs by a Non-contact Respiration and Heartbeat Detector," in *2006 International Conference of the IEEE Engineering in Medicine and Biology Society*, New York, NY, Aug. 2006, pp. 2235–2238. doi: 10.1109/IEMBS.2006.260148.

[19] S.-H. Kim and G.-T. Han, "1D CNN Based Human Respiration Pattern Recognition using Ultra Wideband Radar," in *2019 International Conference on Artificial Intelligence in Information and Communication (ICAIIC)*, Okinawa, Japan, Feb. 2019, pp. 411–414. doi: 10.1109/ICAIIC.2019.8669000.

[20] F. Lin *et al.*, "SleepSense: A Noncontact and Cost-Effective Sleep Monitoring System," *IEEE Trans. Biomed. Circuits Syst.*, vol. 11, no. 1, pp. 189–202, Feb. 2017, doi: 10.1109/TBCAS.2016.2541680.

[21] A. Tataraidze, L. Korostovtseva, L. Anishchenko, M. Bochkarev, Y. Sviryaev, and S. Ivashov, "Bioradiolocation-based sleep stage classification," in *2016 38th Annual International Conference of the IEEE Engineering in Medicine and Biology Society (EMBC)*, Orlando, FL, USA, Aug. 2016, pp. 2839–2842. doi: 10.1109/EMBC.2016.7591321.

[22] R. D. Cartwright, F. Diaz, and S. Lloyd, "The Effects of Sleep Posture and Sleep Stage on Apnea Frequency," *Sleep*, vol. 14, no. 4, pp. 351–353, Jul. 1991, doi: 10.1093/sleep/14.4.351.

[23] P. Hillyard *et al.*, "Comparing Respiratory Monitoring Performance of Commercial Wireless Devices," *ArXiv180706767 Phys.*, Jul. 2018, Accessed: Dec. 14, 2020. [Online]. Available: http://arxiv.org/abs/1807.06767

[24]Y. Cao *et al.*, "Contactless Body Movement Recognition During Sleep via WiFi Signals," *IEEE Internet Things J.*, vol. 7, no. 3, pp. 2028–2037, Mar. 2020, doi: 10.1109/JIOT.2019.2960823.

[25] C. Wu, Z. Yang, Z. Zhou, X. Liu, Y. Liu, and J. Cao, "Non-Invasive Detection of Moving and Stationary Human With WiFi," *IEEE J. Sel. Areas Commun.*, vol. 33, no. 11, pp. 2329–2342, Nov. 2015, doi: 10.1109/JSAC.2015.2430294.

[26] X. Liu, J. Cao, S. Tang, and J. Wen, "Wi-Sleep: Contactless Sleep Monitoring via WiFi Signals," in *2014 IEEE Real-Time Systems Symposium*, Rome, Dec. 2014, pp. 346–355. doi: 10.1109/RTSS.2014.30.

[27] M. J. Bocus, J. Paulavicius, R. McConville, R. Santos-Rodriguez, and R. Piechocki, "Low Cost Localisation in Residential Environments using High Resolution CIR

Information," in *GLOBECOM 2020 - 2020 IEEE Global Communications Conference*, Taipei, Taiwan, Dec. 2020, pp. 1–6. doi: 10.1109/GLOBECOM42002.2020.9322453.

[28] I. Čuljak, H. Mihaldinec, Ž. L. Vasić, K. Friganovic, H. Džapo, and M. Cifrek, "A Contactless Human Respiration Rate Measurement Using UWB Transversal Propagation Method," in *2019 International Symposium on Antennas and Propagation (ISAP)*, Oct. 2019, pp. 1–3.

[29] I. Čuljak, H. Mihaldinec, Z. Kovačić, M. Cifrek, and H. Džapo, "UWB Platform for Vital Signs Detection and Monitoring," in *World Congress on Medical Physics and Biomedical Engineering 2018*, Singapore, 2019, pp. 33–37. doi: 10.1007/978-981-10-9023-3_7.

[30] J. A. Dempsey, S. C. Veasey, B. J. Morgan, and C. P. O'Donnell, "Pathophysiology of sleep apnea," *Physiol. Rev.*, vol. 90, no. 1, pp. 47–112, Jan. 2010, doi: 10.1152/physrev.00043.2008.

[31] M. J. Aminoff, F. Boller, and D. F. Swaab, "We spend about one-third of our life either sleeping or attempting to do so," *Handb. Clin. Neurol.*, vol. 98, p. vii, 2011, doi: 10.1016/B978-0-444-52006-7.00047-2.

[32] R. Ravichandran, S.-W. Sien, S. N. Patel, J. A. Kientz, and L. R. Pina, "Making Sense of Sleep Sensors: How Sleep Sensing Technologies Support and Undermine Sleep Health," in *Proceedings of the 2017 CHI Conference on Human Factors in Computing Systems*, Denver Colorado USA, May 2017, pp. 6864–6875. doi: 10.1145/3025453.3025557.

[33] "Berry RB, Brooks R, Gamaldo CE, Harding SM, Marcus CL, Vaughn BV and Tangredi MM for the American Academy of Sleep Medicine. The AASM Manual for the Scoring of Sleep and Associated Events: Rules, Terminology and Technical Specifications, Version 2.0. www.aasmnet.org, Darien, Illinois: American Academy of Sleep Medicine, 2012.".

[34] "Philips, Alice NightOne, available on https://www.usa.philips.com/healthcare/ (November 2022)."

[35] "Philips, Alice 6, available on: https://www.usa.philips.com/healthcare/ (November, 2022)."

[36] American Academy of Sleep Medicine, Ed., *International classification of sleep disorders*, 3. ed. Darien, Ill: American Acad. of Sleep Medicine, 2014.

[37] M. Borsky, M. Serwatko, E. S. Arnardottir, and J. Mallet, “Towards Sleep Study Automation: Detection Evaluation of Respiratory-Related Events,” *IEEE J. Biomed. Health Inform.*, vol. PP, Mar. 2022, doi: 10.1109/JBHI.2022.3159727.

[38] R. B. Berry *et al.*, “Rules for Scoring Respiratory Events in Sleep: Update of the 2007 AASM Manual for the Scoring of Sleep and Associated Events,” *J. Clin. Sleep Med. JCSM Off. Publ. Am. Acad. Sleep Med.*, vol. 8, no. 5, pp. 597–619, Oct. 2012, doi: 10.5664/jcsm.2172.

[39] V. Tsara, A. Amfilochiou, M. J. Papagrigorakis, D. Georgopoulos, and E. Liolios, “Guidelines for diagnosis and treatment of sleep-related breathing disorders in adults and children. Definition and classification of sleep related breathing disorders in adults: different types and indications for sleep studies (Part 1),” *Hippokratia*, vol. 13, no. 3, pp. 187–191, Jul. 2009.

[40] A. S. Jordan, D. G. McSharry, and A. Malhotra, “Adult obstructive sleep apnoea,” *Lancet Lond. Engl.*, vol. 383, no. 9918, pp. 736–747, Feb. 2014, doi: 10.1016/S0140-6736(13)60734-5.

[41] I. Perez-Pozuelo *et al.*, “The future of sleep health: a data-driven revolution in sleep science and medicine,” *Npj Digit. Med.*, vol. 3, no. 1, Art. no. 1, Mar. 2020, doi: 10.1038/s41746-020-0244-4.

[42] “Sleep-related breathing disorders in adults: recommendations for syndrome definition and measurement techniques in clinical research. The Report of an American Academy of Sleep Medicine Task Force,” *Sleep*, vol. 22, no. 5, pp. 667–689, Aug. 1999.

[43] P. Wang *et al.*, “Research Progress in Millimeter Wave Radar-Based non-contact Sleep Monitoring - A Review,” in *2021 13th International Symposium on Antennas, Propagation and EM Theory (ISAPE)*, Dec. 2021, vol. Volume1, pp. 1–3. doi: 10.1109/ISAPE54070.2021.9753424.

[44] A. Malhotra *et al.*, “Metrics of sleep apnea severity: beyond the apnea-hypopnea index,” *Sleep*, vol. 44, no. 7, p. zsab030, Mar. 2021, doi: 10.1093/sleep/zsab030.

[45] R. J. Schwab *et al.*, “Identification of Upper Airway Anatomic Risk Factors for Obstructive Sleep Apnea with Volumetric Magnetic Resonance Imaging,” *Am. J. Respir. Crit. Care Med.*, vol. 168, no. 5, pp. 522–530, Sep. 2003, doi: 10.1164/rccm.200208-866OC.

[46] K. Qian *et al.*, “Can Machine Learning Assist Locating the Excitation of Snore Sound? A Review,” *IEEE J. Biomed. Health Inform.*, vol. 25, no. 4, pp. 1233–1246, Apr. 2021, doi: 10.1109/JBHI.2020.3012666.

[47] D. Pevernagie, R. M. Aarts, and M. De Meyer, “The acoustics of snoring,” *Sleep Med. Rev.*, vol. 14, no. 2, pp. 131–144, Apr. 2010, doi: 10.1016/j.smrv.2009.06.002.

[48] L. Huang, S. James Quinn, P. D. M. Ellis, and J. E. Ffowcs Williams, “Biomechanics of snoring,” *Endeavour*, vol. 19, no. 3, pp. 96–100, Jan. 1995, doi: 10.1016/0160-9327(95)97493-R.

[49] F. Dalmasso and R. Prota, “Snoring: analysis, measurement, clinical implications and applications,” *Eur. Respir. J.*, vol. 9, no. 1, pp. 146–159, Jan. 1996, doi: 10.1183/09031936.96.09010146.

[50] S. J. Quinn, L. Huang, P. D. M. Ellis, and J. E. F. Williams, “The differentiation of snoring mechanisms using sound analysis,” *Clin. Otolaryngol. Allied Sci.*, vol. 21, no. 2, pp. 119–123, 1996, doi: 10.1111/j.1365-2273.1996.tb01313.x.

[51] J. A. Fiz *et al.*, “Acoustic analysis of snoring sound in patients with simple snoring and obstructive sleep apnoea,” *Eur. Respir. J.*, vol. 9, no. 11, pp. 2365–2370, Nov. 1996.

[52] S. Agrawal, P. Stone, K. McGuinness, J. Morris, and A. E. Camilleri, “Sound frequency analysis and the site of snoring in natural and induced sleep,” *Clin. Otolaryngol. Allied Sci.*, vol. 27, no. 3, pp. 162–166, Jun. 2002, doi: 10.1046/j.1365-2273.2002.00554.x.

[53] J. Sun, X. Hu, C. Chen, S. Peng, and Y. Ma, “Amplitude spectrum trend-based feature for excitation location classification from snore sounds,” *Physiol. Meas.*, vol. 41, no. 8, p. 085006, Sep. 2020, doi: 10.1088/1361-6579/abaa34.

[54] F. Vesperini, A. Galli, L. Gabrielli, E. Principi, and S. Squartini, “Snore Sounds Excitation Localization by Using Scattering Transform and Deep Neural Networks,” *2018 Int. Jt. Conf. Neural Netw. IJCNN*, pp. 1–8, 2018, doi: 10.1109/IJCNN.2018.8489576.

[55] C. Janott *et al.*, “VOTE versus ACLTE: Vergleich zweier Schnarchgeräuschklassifikationen mit Methoden des maschinellen Lernens,” *HNO*, pp. 1–9, 2019, doi: 10.1007/s00106-019-0696-5.

[56] C. Janott *et al.*, “Snoring classified: The Munich-Passau Snore Sound Corpus,” *Comput. Biol. Med.*, vol. 94, pp. 106–118, Mar. 2018, doi: 10.1016/j.compbiomed.2018.01.007.

[57] Z. Huang *et al.*, "Prediction of the obstruction sites in the upper airway in sleep-disordered breathing based on snoring sound parameters: a systematic review," *Sleep Med.*, vol. 88, pp. 116–133, Dec. 2021, doi: 10.1016/j.sleep.2021.10.015.

[58] J. Xie *et al.*, "Audio-based snore detection using deep neural networks," *Comput. Methods Programs Biomed.*, vol. 200, p. 105917, Mar. 2021, doi: 10.1016/j.cmpb.2020.105917.

[59] B. Gürpınar, Z. Saltürk, T. L. Kumral, S. Civelek, O. Izel, and Y. Uyar, "Analysis of snoring to determine the site of obstruction in obstructive sleep apnea syndrome," *Sleep Breath.*, Nov. 2020, doi: 10.1007/s11325-020-02252-5.

[60] A. Sebastian, P. A. Cistulli, G. Cohen, and P. de Chazal, "Association of Snoring Characteristics with Predominant Site of Collapse of Upper Airway in Obstructive Sleep Apnoea Patients," *Sleep*, no. zsab176, Jul. 2021, doi: 10.1093/sleep/zsab176.

[61] A. Sebastian, P. A. Cistulli, G. Cohen, and P. de Chazal, "Unsupervised Approach for the Identification of the Predominant Site of Upper Airway Collapse in Obstructive Sleep Apnoea Patients Using Snore Signals," *Annu. Int. Conf. IEEE Eng. Med. Biol. Soc. IEEE Eng. Med. Biol. Soc. Annu. Int. Conf.*, vol. 2021, pp. 160–163, Nov. 2021, doi: 10.1109/EMBC46164.2021.9630095.

[62] E. Dafna, A. Tarasiuk, and Y. Zigel, "Sleep-quality assessment from full night audio recordings of sleep apnea patients," in *2012 Annual International Conference of the IEEE Engineering in Medicine and Biology Society*, San Diego, CA, Aug. 2012, pp. 3660–3663. doi: 10.1109/EMBC.2012.6346760.

[63] K.-F. Chung, C.-T. Lee, W.-F. Yeung, M.-S. Chan, E. W.-Y. Chung, and W.-L. Lin, "Sleep hygiene education as a treatment of insomnia: a systematic review and meta-analysis," *Fam. Pract.*, vol. 35, no. 4, pp. 365–375, Jul. 2018, doi: 10.1093/fampra/cmx122.

[64] S. K. Koul and R. Bharadwaj, *Wearable Antennas and Body Centric Communication: Present and Future*, vol. 787. Singapore: Springer, 2021. doi: 10.1007/978-981-16-3973-9.

[65] B. Zhou *et al.*, "Electrical Impedance Myography for Evaluating Muscle Fatigue Induced by Neuromuscular Electrical Stimulation," *IEEE J. Electromagn. RF Microw. Med. Biol.*, vol. 6, no. 1, pp. 94–102, Mar. 2022, doi: 10.1109/JERM.2021.3092883.

[66] M. Žilak, Ž. Car, and I. Čuljak, "A Systematic Literature Review of Handheld Augmented Reality Solutions for People with Disabilities," *Sensors*, vol. 22, no. 20, Art. no. 20, Jan. 2022, doi: 10.3390/s22207719.

[67] X. Zhang *et al.*, "Dynamics Combined with Hill Model for Functional Electrical Stimulation Ankle Angle Prediction," *IEEE J. Biomed. Health Inform.*, pp. 1–1, 2022, doi: 10.1109/JBHI.2022.3158426.

[68] I. Čuljak, Ž. Lučev Vasić, H. Mihaldinec, and H. Džapo, "Wireless Body Sensor Communication Systems Based on UWB and IBC Technologies: State-of-the-Art and Open Challenges," *Sensors*, vol. 20, no. 12, Art. no. 12, Jan. 2020, doi: 10.3390/s20123587.

[69] Y. Hao, A. Alomainy, P. S. Hall, Y. I. Nechayev, C. G. Parini, and C. C. Constantinou, "Antennas and propagation for body centric wireless communications," in *IEEE/ACES International Conference on Wireless Communications and Applied Computational Electromagnetics, 2005.*, Apr. 2005, pp. 586–589. doi: 10.1109/WCACEM.2005.1469656.

[70] R. Bharadwaj and S. K. Koul, "Experimental Analysis of Ultra-Wideband Body-to-Body Communication Channel Characterization in an Indoor Environment," *IEEE Trans. Antennas Propag.*, vol. 67, no. 3, pp. 1779–1789, Mar. 2019, doi: 10.1109/TAP.2018.2883634.

[71] A. F. Molisch, "Ultra-Wide-Band Propagation Channels," *Proc. IEEE*, vol. 97, no. 2, pp. 353–371, Feb. 2009, doi: 10.1109/JPROC.2008.2008836.

[72] A. G. Ferreira, D. Fernandes, S. Branco, A. P. Catarino, and J. L. Monteiro, "Feature Selection for Real-Time NLOS Identification and Mitigation for Body-Mounted UWB Transceivers," *IEEE Trans. Instrum. Meas.*, vol. 70, pp. 1–10, 2021, doi: 10.1109/TIM.2021.3070619.

[73] H. Zhuo, Q. Zhong, and X. Zhuo, "Contactless Respiration Monitoring During Sleep with a pair of Wi-Fi devices," in *2022 IEEE MTT-S International Microwave Biomedical Conference (IMBioC)*, May 2022, pp. 66–68. doi: 10.1109/IMBioC52515.2022.9790212.

[74] A. A. M. Saleh and R. Valenzuela, "A Statistical Model for Indoor Multipath Propagation," *IEEE J. Sel. Areas Commun.*, vol. 5, no. 2, pp. 128–137, Feb. 1987, doi: 10.1109/JSAC.1987.1146527.

[75] J. Wang, K. Yu, J. Bu, Y. Lin, and S. Han, "Multi-Classification of UWB Signal Propagation Channels Based on One-Dimensional Wavelet Packet Analysis and CNN," *IEEE Trans. Veh. Technol.*, pp. 1–1, 2022, doi: 10.1109/TVT.2022.3172863.

[76] R. Bharadwaj and S. K. Koul, "Monitoring of Limb Movement Activities during Physical Exercises using UWB Channel Parameters," in *2019 IEEE MTT-S International Microwave Biomedical Conference (IMBioC)*, May 2019, vol. 1, pp. 1–3. doi: 10.1109/IMBIOC.2019.8777814.

[77] R. Chávez-Santiago, I. Balasingham, and J. Bergsland, "Ultrawideband Technology in Medicine: A Survey," *J. Electr. Comput. Eng.*, vol. 2012, p. e716973, Apr. 2012, doi: 10.1155/2012/716973.

[78] I. Hilger *et al.*, *ultraMEDIS – Ultra-Wideband Sensing in Medicine*. IntechOpen, 2013. doi: 10.5772/55081.

[79] "'Biodigital,' Biodigital. A Better Way to Understand Health and the Human Body. https://human.biodigital.com/index.html. [Online; Accessed on: 19- May-2018]. 2018. ."

[80] A. Lazaro, D. Girbau, and R. Villarino, "Techniques for clutter suppression in the presence of body movements during the detection of respiratory activity through UWB radars," *Sensors*, vol. 14, no. 2, pp. 2595–2618, Feb. 2014, doi: 10.3390/s140202595.

[81] V. Nguyen and M. A. Weitnauer, "UWB impulse radar for vital signs sensing — A modeling framework for arbitrary periodic heart and lung motion," in *2015 IEEE Biomedical Circuits and Systems Conference (BioCAS)*, Oct. 2015, pp. 1–4. doi: 10.1109/BioCAS.2015.7348371.

[82] X. Hu and T. Jin, "Short-Range Vital Signs Sensing Based on EEMD and CWT Using IR-UWB Radar," *Sensors*, vol. 16, no. 12, Art. no. 12, Dec. 2016, doi: 10.3390/s16122025.

[83] C. Ding, J. Yan, L. Zhang, H. Zhao, H. Hong, and X. Zhu, "Noncontact multiple targets vital sign detection based on VMD algorithm," in *2017 IEEE Radar Conference (RadarConf)*, May 2017, pp. 0727–0730. doi: 10.1109/RADAR.2017.7944298.

[84] H. Shen *et al.*, "Respiration and Heartbeat Rates Measurement Based on Autocorrelation Using IR-UWB Radar," *IEEE Trans. Circuits Syst. II Express Briefs*, vol. 65, no. 10, pp. 1470–1474, Oct. 2018, doi: 10.1109/TCSII.2018.2860015.

[85] Y. Lee *et al.*, "A Novel Non-contact Heart Rate Monitor Using Impulse-Radio Ultra-Wideband (IR-UWB) Radar Technology," *Sci. Rep.*, vol. 8, no. 1, Art. no. 1, Aug. 2018, doi: 10.1038/s41598-018-31411-8.

[86] K.-K. Shyu, L.-J. Chiu, P.-L. Lee, T.-H. Tung, and S.-H. Yang, "Detection of Breathing and Heart Rates in UWB Radar Sensor Data Using FVPIEF-Based Two-Layer EEMD," *IEEE Sens. J.*, vol. 19, no. 2, pp. 774–784, Jan. 2019, doi: 10.1109/JSEN.2018.2878607.

[87] S. Wu *et al.*, "Person-Specific Heart Rate Estimation With Ultra-Wideband Radar Using Convolutional Neural Networks," *IEEE Access*, vol. 7, pp. 168484–168494, 2019, doi: 10.1109/ACCESS.2019.2954294.

[88] S. Venkatesh, C. R. Anderson, N. V. Rivera, and R. M. Buehrer, "Implementation and analysis of respiration-rate estimation using impulse-based UWB," in *MILCOM 2005 - 2005 IEEE Military Communications Conference*, Oct. 2005, pp. 3314-3320 Vol. 5. doi: 10.1109/MILCOM.2005.1606167.

[89] E. M. Staderini, "UWB radars in medicine," *IEEE Aerosp. Electron. Syst. Mag.*, vol. 17, no. 1, pp. 13–18, Jan. 2002, doi: 10.1109/62.978359.

[90] A. Fallatah, M. Bolic, M. MacPherson, and D. J. La Russa, "Monitoring Respiratory Motion during VMAT Treatment Delivery Using Ultra-Wideband Radar," *Sensors*, vol. 22, no. 6, Art. no. 6, Jan. 2022, doi: 10.3390/s22062287.

[91] T. Lauteslager, M. Tommer, K. G. Kjelgård, T. S. Lande, and T. G. Constandinou, "Intracranial heart rate detection using UWB radar," in *2016 IEEE Biomedical Circuits and Systems Conference (BioCAS)*, Oct. 2016, pp. 119–122. doi: 10.1109/BioCAS.2016.7833739.

[92] Q. Zhai, X. Han, Y. Han, J. Yi, S. Wang, and T. Liu, "A Contactless On-Bed Radar System for Human Respiration Monitoring," *IEEE Trans. Instrum. Meas.*, vol. 71, pp. 1–10, 2022, doi: 10.1109/TIM.2022.3164145.

[93] C. P. Lai, R. M. Narayanan, Q. Ruan, and A. Davydov, "Hilbert-Huang transform analysis of human activities using through-wall noise and noise-like radar," *Sonar Navig. IET Radar*, vol. 2, no. 4, pp. 244–255, Aug. 2008, doi: 10.1049/iet-rsn:20070140.

[94] M. Leib, W. Menzel, B. Schleicher, and H. Schumacher, "Vital signs monitoring with a UWB radar based on a correlation receiver," in *Proceedings of the Fourth European Conference on Antennas and Propagation*, Apr. 2010, pp. 1–5.

[95] M. Baboli, O. Boric-Lubecke, and V. Lubecke, "A new algorithm for detection of heart and respiration rate with UWB signals," in *2012 Annual International Conference of the IEEE Engineering in Medicine and Biology Society*, Aug. 2012, pp. 3947–3950. doi: 10.1109/EMBC.2012.6346830.

[96] V. Nguyen, A. Q. Javaid, and M. A. Weitnauer, “Spectrum-averaged Harmonic Path (SHAPA) algorithm for non-contact vital sign monitoring with ultra-wideband (UWB) radar,” in *2014 36th Annual International Conference of the IEEE Engineering in Medicine and Biology Society*, Aug. 2014, pp. 2241–2244. doi: 10.1109/EMBC.2014.6944065.

[97] A. Lazaro, D. Girbau, and R. Villarino, “Techniques for Clutter Suppression in the Presence of Body Movements during the Detection of Respiratory Activity through UWB Radars,” *Sensors*, vol. 14, no. 2, Art. no. 2, Feb. 2014, doi: 10.3390/s140202595.

[98] B. S, B. T, P. Y, A. Ø, L. Ts, and H. Se, “Time-lapse imaging of human heart motion with switched array UWB radar.,” *IEEE Trans. Biomed. Circuits Syst.*, vol. 8, no. 5, pp. 704–715, Oct. 2014, doi: 10.1109/tbcas.2014.2359995.

[99] H.-S. Cho, H.-K. Lyu, and Y.-J. Park, “Noninvasive heartbeat extraction from IR UWB radar signals,” in *2015 International Conference on Information and Communication Technology Convergence (ICTC)*, Oct. 2015, pp. 977–980. doi: 10.1109/ICTC.2015.7354717.

[100] J. Yan, H. Hong, H. Zhao, Y. Li, C. Gu, and X. Zhu, “Through-Wall Multiple Targets Vital Signs Tracking Based on VMD Algorithm,” *Sensors*, vol. 16, no. 8, Aug. 2016, doi: 10.3390/s16081293.

[101] “Short-Range Vital Signs Sensing Based on EEMD and CWT Using IR-UWB Radar.” https://www.ncbi.nlm.nih.gov/pmc/articles/PMC5191006/ (accessed May 24, 2020).

[102] L. Ren, H. Wang, K. Naishadham, O. Kilic, and A. E. Fathy, “Phase-Based Methods for Heart Rate Detection Using UWB Impulse Doppler Radar,” *IEEE Trans. Microw. Theory Tech.*, vol. 64, no. 10, pp. 3319–3331, Oct. 2016, doi: 10.1109/TMTT.2016.2597824.

[103] W. Yin, X. Yang, L. Zhang, and E. Oki, “ECG Monitoring System Integrated With IR-UWB Radar Based on CNN,” *IEEE Access*, vol. 4, pp. 6344–6351, 2016, doi: 10.1109/ACCESS.2016.2608777.

[104] F. Khan and S. H. Cho, “A Detailed Algorithm for Vital Sign Monitoring of a Stationary/Non-Stationary Human through IR-UWB Radar,” *Sensors*, vol. 17, no. 2, Art. no. 2, Feb. 2017, doi: 10.3390/s17020290.

[105] “Vital Sign Monitoring and Mobile Phone Usage Detection Using IR-UWB Radar for Intended Use in Car Crash Prevention - PubMed.” https://pubmed.ncbi.nlm.nih.gov/28556818/ (accessed May 24, 2020).

[106] K.-K. Shyu, L.-J. Chiu, P.-L. Lee, T.-H. Tung, and S.-H. Yang, "Detection of Breathing and Heart Rates in UWB Radar Sensor Data Using FVPIEF-Based Two-Layer EEMD," *IEEE Sens. J.*, vol. 19, no. 2, pp. 774–784, Jan. 2019, doi: 10.1109/JSEN.2018.2878607.

[107] H. Shen *et al.*, "Respiration and Heartbeat Rates Measurement Based on Autocorrelation Using IR-UWB Radar," *IEEE Trans. Circuits Syst. II Express Briefs*, vol. 65, no. 10, pp. 1470–1474, Oct. 2018, doi: 10.1109/TCSII.2018.2860015.

[108] D. Yim *et al.*, "Quantified Activity Measurement for Medical Use in Movement Disorders through IR-UWB Radar Sensor," *Sensors*, vol. 19, no. 3, p. 688, Feb. 2019, doi: 10.3390/s19030688.

[109] "A Novel Human Respiration Pattern Recognition Using Signals of Ultra-Wideband Radar Sensor." https://www.ncbi.nlm.nih.gov/pmc/articles/PMC6696104/ (accessed May 24, 2020).

[110] C. Park and D. Lee, "Classification of Respiratory States Using Spectrogram with Convolutional Neural Network," *Appl. Sci.*, vol. 12, no. 4, Art. no. 4, Jan. 2022, doi: 10.3390/app12041895.

[111]Z. Xie, H. Wang, S. Han, E. Schoenfeld, and F. Ye, "DeepVS: a deep learning approach for RF-based vital signs sensing," in *Proceedings of the 13th ACM International Conference on Bioinformatics, Computational Biology and Health Informatics*, New York, NY, USA, Aug. 2022, pp. 1–5. doi: 10.1145/3535508.3545554.

[112] F. Khan, S. Azou, R. Youssef, P. Morel, and E. Radoi, "IR-UWB Radar-Based Robust Heart Rate Detection Using a Deep Learning Technique Intended for Vehicular Applications," *Electronics*, vol. 11, no. 16, p. 2505, Aug. 2022, doi: 10.3390/electronics11162505.

[113] M. Alekhin *et al.*, "A Novel Method for Recognition of Bioradiolocation Signal Breathing Patterns for Noncontact Screening of Sleep Apnea Syndrome," *Int. J. Antennas Propag.*, vol. 2013, pp. 1–8, Sep. 2013, doi: 10.1155/2013/969603.

[114] M. Kagawa, H. Tojima, and T. Matsui, "Non-contact screening system for sleep apnea-hypopnea syndrome using the time-varying baseline of radar amplitudes," in *2014 IEEE Healthcare Innovation Conference (HIC)*, Oct. 2014, pp. 99–102. doi: 10.1109/HIC.2014.7038884.

[115] H. Alshaer, G. R. Fernie, E. Sejdić, and T. D. Bradley, "Adaptive segmentation and normalization of breathing acoustic data of subjects with obstructive sleep apnea," in

2009 IEEE Toronto International Conference Science and Technology for Humanity (TIC-STH), Sep. 2009, pp. 279–284. doi: 10.1109/TIC-STH.2009.5444489.

[116] F. Qi, S. Wang, G. Lu, and J. Wang, "A novel detection method for obstructive sleep apnea based on wavelet information entropy spectrum," in *2017 IEEE 2nd Information Technology, Networking, Electronic and Automation Control Conference (ITNEC)*, Dec. 2017, pp. 1240–1243. doi: 10.1109/ITNEC.2017.8284974.

[117] R. El-Bardan, D. Malaviya, and A. Di Rienzo, "On the estimation of respiration and heart rates via an IR-UWB radar: An algorithmic perspective," in *2017 IEEE International Conference on Microwaves, Antennas, Communications and Electronic Systems (COMCAS)*, Nov. 2017, pp. 1–5. doi: 10.1109/COMCAS.2017.8244781.

[118] L. Walsh, E. Moloney, and S. McLoone, "Identification of nocturnal movements during sleep using the non-contact under mattress bed sensor," *Annu. Int. Conf. IEEE Eng. Med. Biol. Soc. IEEE Eng. Med. Biol. Soc. Annu. Int. Conf.*, vol. 2011, pp. 1660–1663, 2011, doi: 10.1109/IEMBS.2011.6090478.

[119] X. Long, J. Foussier, P. Fonseca, R. Haakma, and R. M. Aarts, "Analyzing respiratory effort amplitude for automated sleep stage classification," *Biomed. Signal Process. Control*, vol. 14, pp. 197–205, Nov. 2014, doi: 10.1016/j.bspc.2014.08.001.

[120] M. Halevi, E. Dafna, A. Tarasiuk, and Y. Zigel, "Can we discriminate between apnea and hypopnea using audio signals?," in *2016 38th Annual International Conference of the IEEE Engineering in Medicine and Biology Society (EMBC)*, Aug. 2016, pp. 3211–3214. doi: 10.1109/EMBC.2016.7591412.

[121] Y. Tian, G.-H. Lee, H. He, C.-Y. Hsu, and D. Katabi, "RF-Based Fall Monitoring Using Convolutional Neural Networks," *Proc. ACM Interact. Mob. Wearable Ubiquitous Technol.*, vol. 2, no. 3, p. 137:1-137:24, Sep. 2018, doi: 10.1145/3264947.

[122] M. Zhao *et al.*, "RF-based 3D skeletons," in *Proceedings of the 2018 Conference of the ACM Special Interest Group on Data Communication*, New York, NY, USA, Aug. 2018, pp. 267–281. doi: 10.1145/3230543.3230579.

[123] D. Vasisht, A. Jain, C.-Y. Hsu, Z. Kabelac, and D. Katabi, "Duet: Estimating User Position and Identity in Smart Homes Using Intermittent and Incomplete RF-Data," *Proc. ACM Interact. Mob. Wearable Ubiquitous Technol.*, vol. 2, no. 2, p. 84:1-84:21, Jul. 2018, doi: 10.1145/3214287.

[124] F. Adib, Z. Kabelac, and D. Katabi, "{Multi-Person} Localization via {RF} Body Reflections," presented at the 12th USENIX Symposium on Networked Systems Design

and Implementation (NSDI 15), 2015, pp. 279–292. Accessed: Nov. 11, 2022. [Online]. Available: https://www.usenix.org/conference/nsdi15/technical-sessions/presentation/adib

[125] S. Kumar, S. Gil, D. Katabi, and D. Rus, "Accurate indoor localization with zero start-up cost," in *Proceedings of the 20th annual international conference on Mobile computing and networking*, New York, NY, USA, Sep. 2014, pp. 483–494. doi: 10.1145/2639108.2639142.

[126] M. Zhao, S. Yue, D. Katabi, T. S. Jaakkola, and M. T. Bianchi, "Learning sleep stages from radio signals: a conditional adversarial architecture," in *Proceedings of the 34th International Conference on Machine Learning - Volume 70*, Sydney, NSW, Australia, Aug. 2017, pp. 4100–4109.

[127] S. Yue, Y. Yang, H. Wang, H. Rahul, and D. Katabi, "BodyCompass: Monitoring Sleep Posture with Wireless Signals," *Proc. ACM Interact. Mob. Wearable Ubiquitous Technol.*, vol. 4, no. 2, p. 66:1-66:25, Jun. 2020, doi: 10.1145/3397311.

[128] S. Yue, H. He, H. Wang, H. Rahul, and D. Katabi, "Extracting Multi-Person Respiration from Entangled RF Signals," *Proc. ACM Interact. Mob. Wearable Ubiquitous Technol.*, vol. 2, no. 2, p. 86:1-86:22, Jul. 2018, doi: 10.1145/3214289.

[129] C.-Y. Hsu, A. Ahuja, S. Yue, R. Hristov, Z. Kabelac, and D. Katabi, "Zero-Effort In-Home Sleep and Insomnia Monitoring using Radio Signals," *Proc. ACM Interact. Mob. Wearable Ubiquitous Technol.*, vol. 1, no. 3, p. 59:1-59:18, Sep. 2017, doi: 10.1145/3130924.

[130] M. Zhao, F. Adib, and D. Katabi, "Emotion recognition using wireless signals," in *Proceedings of the 22nd Annual International Conference on Mobile Computing and Networking*, New York, NY, USA, Oct. 2016, pp. 95–108. doi: 10.1145/2973750.2973762.

[131] Y. Yang *et al.*, "Artificial intelligence-enabled detection and assessment of Parkinson's disease using nocturnal breathing signals," *Nat. Med.*, vol. 28, no. 10, Art. no. 10, Oct. 2022, doi: 10.1038/s41591-022-01932-x.

[132] Y. Liu *et al.*, "Monitoring gait at home with radio waves in Parkinson's disease: A marker of severity, progression, and medication response," *Sci. Transl. Med.*, vol. 14, no. 663, p. eadc9669, Sep. 2022, doi: 10.1126/scitranslmed.adc9669.

[133] T. Li, L. Fan, Y. Yuan, and D. Katabi, "Unsupervised Learning for Human Sensing Using Radio Signals," in *2022 IEEE/CVF Winter Conference on Applications of*

Computer Vision (WACV), Jan. 2022, pp. 1091–1100. doi: 10.1109/WACV51458.2022.00116.

[134] G. Zhang *et al.*, "Contactless In-Home Monitoring of the Long-Term Respiratory and Behavioral Phenotypes in Older Adults With COVID-19: A Case Series," *Front. Psychiatry*, vol. 12, p. 754169, Oct. 2021, doi: 10.3389/fpsyt.2021.754169.

[135] S. Kang, Y. Lee, Y.-H. Lim, H.-K. Park, S. H. Cho, and S. H. Cho, "Validation of noncontact cardiorespiratory monitoring using impulse-radio ultra-wideband radar against nocturnal polysomnography," *Sleep Breath. Schlaf Atm.*, vol. 24, no. 3, pp. 841–848, Sep. 2020, doi: 10.1007/s11325-019-01908-1.

[136] S. Ahmed, Y. Lee, Y.-H. Lim, S.-H. Cho, H.-K. Park, and S. H. Cho, "Noncontact assessment for fatigue based on heart rate variability using IR-UWB radar," *Sci. Rep.*, vol. 12, no. 1, Art. no. 1, Aug. 2022, doi: 10.1038/s41598-022-18498-w.

[137] J.-Y. Park *et al.*, "Preclinical evaluation of noncontact vital signs monitoring using real-time IR-UWB radar and factors affecting its accuracy," *Sci. Rep.*, vol. 11, no. 1, Art. no. 1, Dec. 2021, doi: 10.1038/s41598-021-03069-2.

[138] D. Wang, S. Yoo, and S. H. Cho, "Experimental Comparison of IR-UWB Radar and FMCW Radar for Vital Signs," *Sensors*, vol. 20, no. 22, Art. no. 22, Jan. 2020, doi: 10.3390/s20226695.

[139] R. de Goederen *et al.*, "Radar-based sleep stage classification in children undergoing polysomnography: a pilot-study," *Sleep Med.*, vol. 82, pp. 1–8, Jun. 2021, doi: 10.1016/j.sleep.2021.03.022.

[140] H. B. Kwon *et al.*, "Hybrid CNN-LSTM Network for Real-Time Apnea-Hypopnea Event Detection Based on IR-UWB Radar," *IEEE Access*, vol. 10, pp. 17556–17564, 2022, doi: 10.1109/ACCESS.2021.3081747.

[141] "DW1000 User Manual Rev 2.18 – 2017 ; Accessed on: 15/10/2022." [Online]. Available: https://www.qorvo.com/products/p/DW1000

[142] "DW1000 - Qorvo; APH0007 Application Note; Antenna Selection/Design Guide for DW1000, Version 1.00." https://www.qorvo.com/products/p/https//www.qorvo.com/products/p/DW1000 (accessed Dec. 13, 2022).

[143] A. Tkac and V. Wieser, "Channel estimation using measurement of channel impulse response," *10th Int. Conf. ELEKTRO 2014 - Proc.*, no. 2, pp. 113–117, 2014, doi: 10.1109/ELEKTRO.2014.6847883.

[144] H. Hashemi, “Impulse Response Modeling of Indoor Radio Propagation Channels,” *IEEE J. Sel. Areas Commun.*, vol. 11, no. 7, pp. 967--978, 1993.

[145] C. Marrow, Gavin , Mclaughlin, Michael, Mcelroy, “Measuring angle of incidence in an ultrawideband communication system,” 2017

[146] “DWM1001-DEV - Qorvo.” https://www.qorvo.com/products/p/https//www.qorvo.com/products/p/DWM1001-DEV (accessed Mar. 13, 2023).

[147] I. Čuljak, H. Mihaldinec, H. Džapo, and M. Cifrek, “A Data-Fusion Algorithm for Respiration Rate Extraction Based on UWB Transversal Propagation Method,” in *2020 IEEE International Instrumentation and Measurement Technology Conference (I2MTC)*, May 2020, pp. 1–5. doi: 10.1109/I2MTC43012.2020.9128628.

[148] “Brain Products actiCHamp,” available on www.brainproducts.com/ (November, 2022)”.

[149] B. Großiwindhager, M. Stocker, M. Rath, C. A. Boano, and K. Römer, “SnapLoc: An Ultra-Fast UWB-Based Indoor Localization System for an Unlimited Number of Tags,” in *2019 18th ACM/IEEE International Conference on Information Processing in Sensor Networks (IPSN)*, Apr. 2019, pp. 61–72.

[150] “Alice 6 LDx.” Accessed: Oct. 25, 2022. [Online]. Available: https://www.usa.philips.com/healthcare/product/HC1063315/alice-6-ldx-diagnostic-sleep-system

[151] “Sleepware G3 Database Administration.” Accessed: Oct. 25, 2022. [Online]. Available: https://images.philips.com/is/content/PhilipsConsumer/Campaigns/HC20140401_DG/Documents/how-to-faqs-g3.pdf

[152] M. Stocker, M. Gallacher, C. A. Boano, and K. Römer, “Performance of support vector regression in correcting UWB ranging measurements under LOS/NLOS conditions,” in *Proceedings of the Workshop on Benchmarking Cyber-Physical Systems and Internet of Things*, New York, NY, USA, May 2021, pp. 6–11. doi: 10.1145/3458473.3458820.

[153] M. Schmidhammer and C. Gentner, “Multipath-Enhanced Device-Free Localization using Low-Cost Ultra-Wideband Devices,” in *2022 16th European Conference on Antennas and Propagation (EuCAP)*, Mar. 2022, pp. 1–5. doi: 10.23919/EuCAP53622.2022.9769046.

[154] P. Peterseil, D. Märzinger, B. Etzlinger, and A. Springer, “Labeling for UWB Ranging in Weak NLOS Conditions,” in *2022 International Conference on Localization and GNSS (ICL-GNSS)*, Jun. 2022, pp. 1–6. doi: 10.1109/ICL-GNSS54081.2022.9797024.

[155] M. De Sanctis, A. Conte, T. Rossi, S. Di Domenico, and E. Cianca, “CIR-Based Device-Free People Counting via UWB Signals,” *Sensors*, vol. 21, no. 9, Art. no. 9, Jan. 2021, doi: 10.3390/s21093296.

[156] M. Cimdins, S. O. Schmidt, and H. Hellbrück, “Comparison of I/Q- and Magnitude-based UWB Channel Impulse Responses for Device-free Localization,” in *2021 International Conference on Localization and GNSS (ICL-GNSS)*, Jun. 2021, pp. 1–7. doi: 10.1109/ICL-GNSS51451.2021.9452299.

[157] M. Piriyajitakonkij *et al.*, “SleepPoseNet: Multi-View Learning for Sleep Postural Transition Recognition Using UWB,” *IEEE J. Biomed. Health Inform.*, pp. 1–1, 2020, doi: 10.1109/JBHI.2020.3025900.

[158] S. Maranò, W. M. Gifford, H. Wymeersch, and M. Z. Win, “NLOS identification and mitigation for localization based on UWB experimental data,” *IEEE J. Sel. Areas Commun.*, vol. 28, no. 7, pp. 1026–1035, Sep. 2010, doi: 10.1109/JSAC.2010.100907.

[159] N. Kehtarnavaz, “CHAPTER 7 - Frequency Domain Processing,” in *Digital Signal Processing System Design (Second Edition)*, N. Kehtarnavaz, Ed. Burlington: Academic Press, 2008, pp. 175–196. doi: 10.1016/B978-0-12-374490-6.00007-6.

[160] P. Drakatos *et al.*, “Periodic limb movements during sleep: a narrative review,” *J. Thorac. Dis.*, vol. 13, no. 11, pp. 6476–6494, Nov. 2021, doi: 10.21037/jtd-21-1353.

[161] H. Akima, “A New Method of Interpolation and Smooth Curve Fitting Based on Local Procedures,” *J. ACM*, vol. 17, no. 4, pp. 589–602, Oct. 1970, doi: 10.1145/321607.321609.

[162] H. Alsolai *et al.*, “A Systematic Review of Literature on Automated Sleep Scoring,” *IEEE Access*, vol. 10, pp. 79419–79443, 2022, doi: 10.1109/ACCESS.2022.3194145.

[163] M. Hafezi, N. Montazeri, K. Zhu, H. Alshaer, A. Yadollahi, and B. Taati, “Sleep Apnea Severity Estimation from Respiratory Related Movements Using Deep Learning,” in *2019 41st Annual International Conference of the IEEE Engineering in Medicine and Biology Society (EMBC)*, Jul. 2019, pp. 1601–1604. doi: 10.1109/EMBC.2019.8857524.

[164] W. Gu, L. Shangguan, Z. Yang, and Y. Liu, “Sleep Hunter: Towards Fine Grained Sleep Stage Tracking with Smartphones,” *IEEE Trans. Mob. Comput.*, vol. 15, no. 6, pp. 1514–1527, Jun. 2016, doi: 10.1109/TMC.2015.2462812.

[165] H. Hong, L. Zhang, C. Gu, Y. Li, G. Zhou, and X. Zhu, "Noncontact Sleep Stage Estimation Using a CW Doppler Radar," *IEEE J. Emerg. Sel. Top. Circuits Syst.*, vol. 8, no. 2, pp. 260–270, Jun. 2018, doi: 10.1109/JETCAS.2017.2789278.

[166] C. Ding *et al.*, "Non-Contact Human Motion Recognition Based on UWB Radar," *IEEE J. Emerg. Sel. Top. Circuits Syst.*, vol. 8, no. 2, pp. 306–315, Jun. 2018, doi: 10.1109/JETCAS.2018.2797313.

[167] J. Andén and S. Mallat, "Deep Scattering Spectrum," *IEEE Trans. Signal Process.*, vol. 62, no. 16, pp. 4114–4128, Aug. 2014, doi: 10.1109/TSP.2014.2326991.

[168] T. Li and M. Zhou, "ECG Classification Using Wavelet Packet Entropy and Random Forests," *Entropy*, vol. 18, no. 8, Art. no. 8, Aug. 2016, doi: 10.3390/e18080285.

[169] A. Jović, "Feature selection (4th lecture); Course: Data Mining," University of Zagreb Faculty of Electrical Engineering and Compting, 2022. [Online]. Available: https://www.fer.unizg.hr/en/course/datmin_a

[170] Y. Zhang, A. Xiao, T. Zheng, H. Xiao, and R. Huang, "The Relationship between Sleeping Position and Sleep Quality: A Flexible Sensor-Based Study," *Sensors*, vol. 22, no. 16, p. 6220, Aug. 2022, doi: 10.3390/s22166220.

[171] Q. Xiao, F. Gu, N. Caporaso, and C. E. Matthews, "Relationship between sleep characteristics and measures of body size and composition in a nationally-representative sample," *BMC Obes.*, vol. 3, no. 1, p. 48, Nov. 2016, doi: 10.1186/s40608-016-0128-y.

[172] R. J. Thomas, S. Chen, U. T. Eden, and M. J. Prerau, "Quantifying statistical uncertainty in metrics of sleep disordered breathing," *Sleep Med.*, vol. 65, pp. 161–169, Jan. 2020, doi: 10.1016/j.sleep.2019.06.003.

[173] S. Chen, S. Redline, U. T. Eden, and M. J. Prerau, "Dynamic models of obstructive sleep apnea provide robust prediction of respiratory event timing and a statistical framework for phenotype exploration," *Sleep*, vol. 45, no. 12, p. zsac189, Dec. 2022, doi: 10.1093/sleep/zsac189.

[174] K. Hamill, R. Jumabhoy, P. Kahawage, M. de Zambotti, E. M. Walters, and S. P. A. Drummond, "Validity, potential clinical utility and comparison of a consumer activity tracker and a research-grade activity tracker in insomnia disorder II: Outside the laboratory," *J. Sleep Res.*, vol. 29, no. 1, p. e12944, Feb. 2020, doi: 10.1111/jsr.12944.

[175] P. Matos, F. Fradinho, A. Catarino, P. Lopes, and M. J. Matos, "Positional sleep apnea: An issue of therapeutic adherence," *Pulmonology*, vol. 21, no. 6, pp. 344–345, Nov. 2015, doi: 10.1016/j.rppnen.2015.07.005.

[176] P. R. Srijithesh, R. Aghoram, A. Goel, and J. Dhanya, “Positional therapy for obstructive sleep apnoea,” *Cochrane Database Syst. Rev.*, vol. 2019, no. 5, p. CD010990, May 2019, doi: 10.1002/14651858.CD010990.pub2.

[177] B. Mokhlesi and N. M. Punjabi, “‘REM-related’ Obstructive Sleep Apnea: An Epiphenomenon or a Clinically Important Entity?,” *Sleep*, vol. 35, no. 1, pp. 5–7, Jan. 2012, doi: 10.5665/sleep.1570.

[178] X. Chen *et al.*, “Racial/Ethnic Differences in Sleep Disturbances: The Multi-Ethnic Study of Atherosclerosis (MESA),” *Sleep*, vol. 38, no. 6, pp. 877–888, Jun. 2015, doi: 10.5665/sleep.4732.

[179] P. Brémaud, “Hawkes Point Processes,” in *Point Process Calculus in Time and Space*, vol. 98, Cham: Springer International Publishing, 2020, pp. 461–518. doi: 10.1007/978-3-030-62753-9_12.

[180] M. W. Johns, “A new method for measuring daytime sleepiness: the Epworth sleepiness scale,” *Sleep*, vol. 14, no. 6, pp. 540–545, Dec. 1991, doi: 10.1093/sleep/14.6.540.

Abbreviations

AASM	American Academy of Sleep Medicine
ABI	Abnormal Breathing Index
AF	Atrial Fibrillation
AHI	Apnea-Hypopnea Index
AI	Awakening Index
ANN	Artificial neural network
AUC	Area under the curve
BCWN	Body-centric wireless networks
BR	Breathing rate
BRI	Breathing Rhythmic Intensity
BRP	Breathing Rhythmic Periodic
CA	Central Apnea
CDF	Cumulative distribution function
CHF	Chronic heart failure
CIR	Channel impulse response
CNN	Convolutional neural network
COPD	Cronic obstructive pulmonary disease
CPAP	Continuous positive airway pressure
CSI	Channel State Information
CSS	Chirp spread spectrum
DAQ	Data acquisition
ECC	Electronic Communications Committee
ECG	Electrocardiogram

EEG	Electroencephalogram
EMG	Electromyogram
EOG	Electrooculogram
EIRP	Equivalent isotropically radiated power
ESS	Epworth Sleepiness Scale
FCC	Federal Communications Commission
FN	False Negative
FP	False Positive
HHT	Hilbert Huang Transform
HR	Heart Rate
IBC	Intra-body communication
IFI	Inter-frame interference
IR-UWB	UWB impulse radio
KNN	K-nearest neighbors
LOS	Line of sight
MA	Mixed apnea
MA	Moving average
MB-UWB	Multi-band UWB
ML	Machine Learning
ML	Maximum likelihood
MDACM	Modified differential and cross multiply
MPC	Multi-path components
MSE	Mean Square Error
NLOS	Non-line of sight
NREM	Non-rapid eye movement
OCST	Out-of-center sleep testing
ODWPA	One-dimensional wavelet packet analysis
OFDM	Orthogonal frequency division multiplexing
OSA	Obstructive sleep apnea
PAP	Positive airway pressure
PDP	Power delay profile
PL	Path loss
PRF	Pulse repetition frequency

PSD	Power spectral density
PSG	Polysomnography
PSQI	Pittsburgh Sleep Quality Index
RDI	Respiratory Disturbance Index
REM	Rapid eye movement
RF	Radio-Frequency
RIP	Respiratory inductance plethysmography
RSS	Received signal strength
RERA	Respiratory Event-Related Arousal
ROC	Receiver operating characteristic curve
RR	Respiration Rate
SDB	Sleep Disordered Breathing
SI	Snore Index
SNR	Signal-to-noise ratio
SS-TWR	Single-sided two way ranging
SVM	Support vector machine
TN	True Negative
TP	True Positive
TDA	Time difference of arrival
TOA	Time of arrival
TOF	Time of flight
TST	Total sleep time
TWR	Two way ranging
UBMS	Under-mattress bed sensor
UWB	Ultra-wideband
WASO	Wake time After Sleep Onset
WBAN	Wireless body area network

List of figures

List of tables

Appendix A:

Sleep questionnaires[3]

Name and surname _____ Year _____

Referral diagnosis _____ Sent from _____

Recording date _____ Recording performed_____

Questionnaire to the patient before sleep

1.	**Was today an unusual day? If yes, in what way (describe)?**	**Yes**	**No**
2.	How much sleep did you have last night?	_____ hours	
3.	Did you take a nap today?	Yes	No
	If yes, when _____ and how much _____ hours?		
4.	Have you had an alcoholic drink today?	Yes	No
	If yes, when _____, and which type of the alcohol _____, and how much_____		
5.	When was the last time of your meal _____		
6.	List the medicine you took today (including vitamins and aspirin)		

Medication	Dose	Medication	Dose

[3] **Note.** The original sleep questionnaires were in the Croatian language.
The translation was done following phrases given by AASM.

A) _____ C) _____

B) _____ D) _____

7. When was the last time you took a sleeping pill or medicine to stay awake? _____

Medication	Dose	Medication	Dose
A) _____		C) _____	
B) _____		D) _____	

8. Are you experiencing any physical difficulties right now? Yes No
9. Are you ready to go to sleep now? If not, describe why not. Yes No

10. Find a statement that best describes your current state. (circle the number)

1. Feeling active, alert, or wide awake
2. Functioning at high levels, but not fully alert
3. Awake, but relaxed: responsive but not fully alert
4. Somewhat foggy, let down
5. Foggy; losing interest in remaining awake; slowed down
6. Sleepy, woozy, fighting sleep; prefer to lie down
7. No longer fighting sleep, sleep onset soon; having dream-like thoughts

What time is it when you fill this out? _____

You are: (circle)

Right-handed Left-handed Ambidexter

Add any additional information or your comments:

The Epworth Sleepiness Scale [180]

Name and Surname: _____

Date of recording: _____

How likely are you to doze off or fall asleep in the following situations? You should rate your chances of dozing off, not just feeling tired. Even if you have not done some of these things recently try to determine how they would have affected you. For each situation, decide whether or not you would have:

- No chance of dozing =0
- Slight chance of dozing =1
- Moderate chance of dozing =2
- High chance of dozing =3

Write down the number corresponding to your choice in the right-hand column. Total your score below.

Situation	**Chance of dozing**
Sitting and reading	
Watching TV	
Sitting inactive in a public place (e.g., a theater or a meeting)	
As a passenger in a car for an hour without a break	
Lying down to rest in the afternoon when circumstances permit	
Sitting and talking to someone	
Sitting quietly after lunch without alcohol	
In a car, while stopped for a few minutes in traffic	
	Total score:

Analyze Your Score

Interpretation:

0-7: It is unlikely that you are abnormally sleepy.

8-9: You have an average amount of daytime sleepiness.

10-15: You may be excessively sleepy depending on the situation. You may want to consider seeking medical attention.

16-24: You are excessively sleepy and should consider seeking medical attention.

STOP-BANG Questionnaire

Name: _____ Surname: _____

Sex: Male Female

Height: _____ cm Weight: _____ kg Age: _____

Collar size of shirt: S, M, L, X, XL, or _____ cm

Neck circumference: _____ cm

1. **Snoring**

Do you snore loudly (louder than talking or loud enough to be heard through closed doors)?

Yes No

2. **Tired**

Do you often feel tired, fatigued, or sleepy during the daytime?

Yes No

3. **Observed**

Has anyone observed you stop breathing during your sleep?

Yes No

4. **Blood pressure**

Do you have or are you being treated for high blood pressure?

Yes No

5. **BMI**

BMI more than 35 kg/m^2?

Yes No

6. **Age**

Age over 50 years old?

Yes No

7. **Neck circumference**

Neck circumference greater than 40 cm?

Yes No

8. **Sex**

Gender male?

Yes No

Low risk: 0-2 *Yes* answers **Medium risk:** 3-4 *Yes* answers

High risk: 5-8 *Yes* answers or

2 answers *Yes* + male
2 answers *Yes* + BMI > 35 kg/m^2

2 answers *Yes* + neck circumference for males higher than 42 cm, and for females higher than 40 cm

Name and surname _____ Year _____

Referral diagnosis _____ Sent from _____

Recording date _____ Recording performed_____

Recording time from _____ to _____ hours

Awakened by himself or technician _____

Questionnaire to the patient after sleep

1. How long does it take to fall asleep? _____ hours and _____ minutes
2. How does that compare to the time it takes to fall asleep at home?

1	2	3	4	5	6	7
much shorter than usual			as usual			much longer than usual

3. How long do you think you slept last night? _____ hours _____ minutes
4. How does it in comparison to the sleeping duration at home?

1	2	3	4	5	6	7
much shorter than usual			as usual			much longer than usual

5. How many times did you wake up last night? _____ times
6. Did you get enough sleep last night? Yes No
7. Evaluate the quality of your sleep last night by circling a number in each of the 5 listed categories

A)	deep	1	2	3	4	5	6	7	shallow
B)	short	1	2	3	4	5	6	7	long
C)	intermittently	1	2	3	4	5	6	7	continuous
D)	dreamless	1	2	3	4	5	6	7	a lot of dreams
E)	restless	1	2	3	4	5	6	7	still

8. Find a statement that best describes your current state. (circle the number)

1. Feeling active, alert, or wide awake
2. Functioning at high levels but not fully alert
3. Awake, but relaxed: responsive but not fully alert
4. Somewhat foggy, let down
5. Foggy; losing interest in remaining awake; slowed down
6. Sleepy, woozy, fighting sleep; prefer to lie down
7. No longer fighting sleep, sleep onset soon; having dream-like thoughts

What time is it now as you fill this out? _____

9. What woke you up this morning?

Noise discomfort Don't know I woke up alone

Other circumstances (describe):

_____

10. Overall, how do you compare last night's sleep to your sleep at home?

1 2 3 4 5 6 7

worse than usual as usual much better than usual

11. Do you remember your dreams from last night? Yes No

If yes, describe

12. Are you having any physical difficulties this morning? Yes No

If yes, describe them

Add any additional information or your comments:

Appendix B:

UWB sleep study – data collection sheet

Segment circumference measurement - Start

Neck (cm)	
Chest (cm)	
Waist (cm)	
Hip (cm)	
Thigh (cm)	
Calf (cm)	
Ankle (cm)	

Length Measurement

Shoulder-Waist (cm)	
Waist-Hip (cm)	
Hip-Knee (cm)	
Knee-Ankle (cm)	
Chest height (cm)	
Chest length (cm)	

Segment circumference measurement - End

Neck (cm)	
Chest (cm)	
Thigh (cm)	
Calf (cm)	
Ankle (cm)	

Biography

Ivana Čuljak was born on October 29th, 1992 in Zagreb, Croatia. She received her bachelor's and master's degree in electrical engineering and information technology (electronic and computer engineering) in 2014 and 2016, respectively, from the University of Zagreb Faculty of Electrical Engineering and Computing.

She enrolled in a postgraduate study at the Faculty of Electrical Engineering and Computing in October 2017. She has been a teaching and research associate with the Department of Electronic Systems and Information Processing of the same Faculty since October 2016. She participated in a scientific project, "*Rotating magnetic field probe for NDT of safety-critical components of industrial facilities*," from October 2016 to June 2017. In addition, she was working as a young researcher in a project of The Centre of Researcher Excellence for Data Science and Advanced Cooperative Systems, and she participated in two bilateral Croatian Chinese scientific and technological projects entitled "*Body area networks for health applications based on intrabody communication*" and "*Body Area Network for Athlete Fatigue Monitoring*." Currently, she is working as a researcher on the industrial research & innovation (IRI) project "*Research and development of the Greyp Micromobility Platform – GMP*. "

From June to December 2021, she was visiting researcher at the University of Toronto, Institute of Biomedical Engineering, and a research trainee at University Hospital Network, KITE, Toronto, Canada.

Her professional and research activities are in the field of contactless measurements of vital signs, biomedical signal processing, and biomedical electronic instrumentation and measurement. She is co-author of several journal papers and international conference papers in the above-mentioned research areas.

Ivana Čuljak is a member of professional societies IEEE, IFMBE, and CROMBES. She served as a reviewer for the journals IEEE Sensors Journal and Automatika, and for the international conferences I2MTC2019, I2MTC2020, and I2MTC2022. She is or was a teaching assistant on the courses Biomedical Signals and Systems, Sensor Technology, Data Mining, and Introduction to Data Science, and she directly supervised several bachelor and master theses at the FER.

List of publications

Journal articles and review articles in CC journals

[1] **Čuljak, Ivana**, Željka Lučev Vasić, Hrvoje Mihaldinec, and Hrvoje Džapo. "Wireless Body Sensor Communication Systems Based on UWB and IBC Technologies: State-of-the-Art and Open Challenges" Sensors 20, no.12: 3587.https://doi.org/10.3390/s20123587

[2] Žilak, Matea, Željka Car, and **Ivana Čuljak**. 2022. "A Systematic Literature Review of Handheld Augmented Reality Solutions for People with Disabilities" Sensors 22, no. 20: 7719. https://doi.org/10.3390/s22207719

[3] B. Zhou, Y. Zhauang, Y. Gao, Ž. Lučev Vasić, **Čuljak, Ivana**, M. Cifrek, M. Du, "Electrical Impedance Myography for Evaluating Muscle Fatigue Induced by Neuromuscular Electrical Stimulation," in IEEE Journal of Electromagnetics, RF and Microwaves in Medicine and Biology, doi: 10.1109/JERM.2021.3092883.

[4] Xianghong Zhang, Ziqin Jiang, Xu Li, Pan Xu, Željka Lučev Vasić, **Ivana Čuljak**, Mario Cifrek, Min Du, Yue-ming Gao, "Dynamics Combined with Hill Model for Functional Electrical Stimulation Ankle Angle Prediction," IEEE Journal of Biomedical and Health Informatics, pp. 1–12, 2022, doi: 10.1109/JBHI.2022.3158426.

Scientific conference papers with international peer-review

[1] Antonio Stanešić, **Ivana Čuljak**, Luka Klaić, Patrik Šajinović, Ivan Vrhoci , Mario Cifrek, Hrvoje Džapo: "Noise Detection Level Analysis in Biomedical Signals Based on Capacitive Electrodes for Electric Bicycles", International Conference on Biomedical and Health Informatics (ICBHI 2022), 24-26 November, 2022, Concepción, Chile

[2] Luka Klaić, Antonio Stanešić, **Ivana Čuljak**, Hrvoje Džapo, Mario Cifrek: "Comparison of Simulated and Measured Results of Non-contact Capacitive Electrodes for Biomedical Applications", International Conference on Biomedical and Health Informatics (ICBHI 2022), 24-26 November, 2022, Concepción, Chile

[3] Luka Klaić, **Ivana Čuljak**, Antonio Stanešić, Ivan Vrhoci, Patrik Šajinović, Mario Cifrek, Hrvoje Džapo: "Wireless Device for Biomedical Signal Acquisition with Dry Electrodes on an e-Bike", 1st European Congress of Biomedical and Veterinary Engineering – Biomedvetmech, 20-22 October, 2022, Zagreb, Croatia

[4] **Čuljak, Ivana**; Mihaldinec, Hrvoje; Džapo, Hrvoje; Cifrek, Mario. A Data-Fusion Algorithm for Respiration Rate Extraction Based on UWB Transversal Propagation Method // 2020 IEEE International Instrumentation and Measurement Technology Conference Proceedings / Rapuano, Sergio; Van Moer, Wendy ; Vasic, Darko (editor). Piscataway, SAD: IEEE, 2020. page 1-5

[5] **Čuljak, Ivana**; Mihaldinec, Hrvoje; Lučev Vasić, Željka; Friganović, Krešimir; Džapo, Hrvoje; Cifrek, Mario. A Contactless Human Respiration Rate Measurement Using UWB Transversal Propagation Method. 2019 International Symposium on Antennas and Propagation (ISAP 2019), October 27-30, 2019, Xi'an, China

[6] Weikun Chen, Wenzhu Liu, **Čuljak, Ivana**, Xingguang Chen, Haibo Zheng, Yueming Gao, Željka Lučev Vasić, Mario Cifrek, Min Du, An Investigation on Phase Characteristics of Galvanic Coupling Human Body Communication, // Proceedings of the International Conference on Biomedical and Health Informatics (ICBHI 2019) / Lin, Kang-Ping ; Magjarevic, Ratko ; de Carvalho, Paulo (ur.).Cham, Switzerland : Springer, 2019. 335-341, Taipei, Taiwan, April 17.–20., 2019.

[7] **Čuljak, Ivana**; Mihaldinec, Hrvoje; Kovačić, Zrinka; Cifrek, Mario; Džapo, Hrvoje.UWB Platform for Vital Signs Detection and Monitoring//World Congress on Medical Physics and Biomedical Engineering 2018 / Lhotka, Lenka ; Sukupova, Lucie ; Lacković, Igor ; Ibbot, Geoffrey S., editor(s).Prague : Springer, 2018. 33-37

[8] **Čuljak, Ivana**; Ambruš, Davorin; Marušić, Marko; Špikić, Dorijan; Vasić, Darko; Bilas, Vedran. Eddy Current Probe for Inspection of Steel Tubes Based on Rotating Field Principle//2018 IEEE International Instrumentation and Measurement Technology Conference (I2MTC 2018) Proceedings / Baglio, Salvo; Karlovic, Steve, editor(s). Piscataway, USA: IEEE, 2018. 2079- 2084

[9] **Čuljak, Ivana**; Cifrek, Mario. Hilbert Transform Based Paroxysmal Tachycardia Detection Algorithm // Information and Communication Technology, Electronics and Microelectronics (MIPRO), 2017 40th International Convention on / Biljanović, Petar, editor(s).

Životopis

Ivana Čuljak rođena je 1992. godine u Zagrebu, Hrvatska. Diplomirala je i magistrirala elektrotehniku i informacijske tehnologije (elektroničko i računalno inženjerstvo) 2014. odnosno 2016. godine na Fakultetu elektrotehnike i računarstva Sveučilišta u Zagrebu.

Poslijediplomski studij elektrotehnike na Fakultetu elektrotehnike i računarstva upisala je u listopadu 2017. Nastavna i znanstvena suradnica je na Zavodu za elektroničke sustave i obradu informacija istog Fakulteta od listopada 2016. Sudjelovala je na znanstvenom projektu "*Rotating magnetic field probe for NDT of safety-critical components of industrial facilities*", od listopada 2016. do lipnja 2017. Osim toga, radila je kao mlađa istraživačica na projektu Znanstvenog centara izvrsnosti za znanost o podatcima i kooperativne sustave te je sudjelovala je na dva bilateralna hrvatsko-kineska znanstveno-tehnološka projekta pod nazivom „*Body area networks for health applications based on intrabody communication*" i "*Body Area Network for Athlete Fatigue Monitoring*". Trenutno radi kao istraživač na projektu industrijskog istraživanja i inovacija (IRI) "Istraživanje i razvoj Greyp Micromobility Platforme – GMP".

Od lipnja do prosinca 2021. bila je gostujuća istraživačica na Sveučilištu u Torontu, Institutu za biomedicinsko inženjerstvo i istraživačka pripravnica u *University Hospital Network – KITE*, Toronto Kanada.

Njezina stručna i istraživačka djelatnost je u području beskontaktnih mjerenja vitalnih funkcija, biomedicinske obrade signala te biomedicinske elektroničke instrumentacije i mjerenja. Koautorica je više časopisnih radova i međunarodnih skupova iz navedenih područja istraživanja.

Ivana Čuljak članica je stručnih društava IEEE, IFMBE i CROMBES. Radila je kao recenzent za časopise *IEEE Sensors Journal* i *Automatika*, te za međunarodnu konferencije I2MTC (2019-2022). Asistentica je ili je bila asistentica na kolegijima Biomedicinski signali i sustavi, Senzorska tehnologija, Dubinska analiza podataka te Uvod u znanost o podacima, a neposredno je mentorirala više diplomskih i završnih radova na FER-u.